AFAPL-TR-77-58

WIND TUNNEL MODEL STUDY OF THE HOT EXHAUST PLUME FROM THE COMPRESSOR RESEARCH FACILITY AT WRIGHT-PATTERSON AIR FORCE BASE, OHIO

CALSPAN CORPORATION
P. O. BOX 235
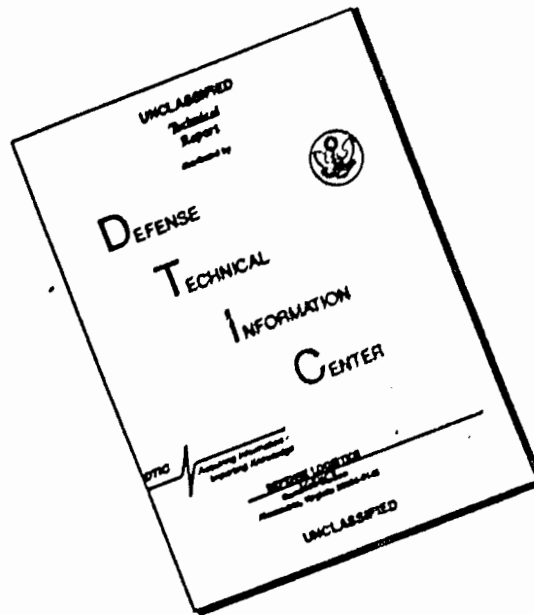*BUFFALO, NEW YORK 14221*

OCTOBER 1977

D D C
1977

DISCLAIMER NOTICE

THIS DOCUMENT IS BEST QUALITY AVAILABLE. THE COPY FURNISHED TO DTIC CONTAINED A SIGNIFICANT NUMBER OF PAGES WHICH DO NOT REPRODUCE LEGIBLY.

NOTICE

When Government drawings, specifications, or other data are used
for any purpose other than in connection with a definitely related
Government procurement operation, the United States Government
thereby incurs no responsibility nor any obligation whatsoever;
and the fact that the Government may have formulated, furnished,
or in any way supplied the said drawings, specifications, or other
data, is not to be regarded by implication or otherwise as in any
manner licensing the holder or any other person or corporation, or
conveying any rights or permission to manufacture, use, or sell any
patented invention that may in any way be related thereto.

This report has been reviewed by the Information Office,
ASD/OIP, and is releasable to the National Technical Information
Service (NTIS). At NTIS, it will be available to the general
public, including foreign nations.

This technical report has been reviewed and is approved for
publication.

Marvin A. Stibich

MARVIN A. STIBICH
Acting Chief
Components Branch
Turbine Engine Division

FOR THE COMMANDER

E.C.

E. C. SIMPSON
Director, Turbine Engine
   Division

Copies of this report should not be returned unless return is
required by security considerations, contractual obligations, or
notice on a specific document.

READ INSTRUCTIONS
BEFORE COMPLETING FORM

4. TITLE (and Subtitle) WIND TUNNEL MODEL STUDY OF THE HOT EXHAUST PLUME FROM THE COMPRESSOR RESEARCH FACILITY AT WRIGHT-PATTERSON AIR FORCE BASE, OHIO .	5. TYPE OF REPORT & PERIOD COVERED Phase V Final May 1976 — June 1977 on Phase 5
	6. PERFORMING ORG. REPORT NUMBER XE-5933-A-101
7. AUTHOR(s) Gary R. Ludwig	8. CONTRACT OR GRANT NUMBER(s) F33615-76-C-2092
9. PERFORMING ORGANIZATION NAME AND ADDRESS Calspan Corporation P. O. Box 235 Buffalo, New York 14221	10. PROGRAM ELEMENT, PROJECT, TASK AREA & WORK UNIT NUMBERS
11. CONTROLLING OFFICE NAME AND ADDRESS U.S. Air Force Aero-Propulsion Laboratory Air Force Systems Command Wright-Patterson AFB, OH 45433	12. REPORT DATE October 1977
	13. NUMBER OF PAGES 139
14. MONITORING AGENCY NAME & ADDRESS(If different from Controlling Office) CALSPAN-XE-5933-A-101	15. SECURITY CLASS. (of this report) Unclassified
	15a. DECLASSIFICATION/ DOWNGRADING SCHEDULE

16. DISTRIBUTION STATEMENT (of this Report)

Approved for public release; distribution unlimited.

155 p.

DDC
DEC 1 1977
F

17. DISTRIBUTION STATEMENT (of the abstract entered in Block 20, If different from Report)

18. SUPPLEMENTARY NOTES

19. KEY WORDS (Continue on reverse side if necessary and Identify by block number)

Dispersion of Pollutants
Emissions
Buoyant Plumes

Atmospheric Modeling
Compressor Test Facilities

20. ABSTRACT (Continue on reverse side if necessary and Identify by block number)

This report presents the results of a wind tunnel model study to determine temperatures at various locations generated by the hot exhaust air from the Compressor Research Facility (CRF) which is being built at Wright-Patterson Air Force Base, Ohio. The study was designed to provide data at the inlet to the CRF and at other nearby locations where pedestrians, building ventilation systems, and vegetation might be affected. The test program, which was conducted in the Calspan Atmospheric Simulation Facility, included flow visualization studies and quantitative concentration measurements of a tracer gas from which

DD FORM 1473 1 JAN 73   EDITION OF 1 NOV 65 IS OBSOLETE

20. Cont'd

full-scale temperatures could be calculated. The concentration measurements
were performed for a number of wind speeds at each of twelve different wind
directions. Two exhaust flows and two exhaust stack configurations were
studied.

FOREWORD

This is the final technical report prepared by Calspan Corporation
on one phase of a multi-phase program sponsored by the Air Force Aero-Propulsion
Laboratory, Air Force Systems Command, Wright-Patterson AFB, Ohio under Contract
F33615-76-C-2092. The work herein was accomplished under Phase V of Project
3066, "Investigation of Rotating Stall and Turbine Heat Transfer in Axial
Flow Turbomachinery; Phase V - Experimental Model Studies of Temperature In-
gestion in Compressor Research Facility", with Mr. Marvin A. Stibich, AFAPL/TBC,
as Project Engineer. Dr. Gary R. Ludwig of the Calspan Corporation was tech-
nically responsible for the work. Other Calspan personnel were Dr. George T.
Skinner, Dr. Joseph P. Nenni, and Mr. John Nemeth.

TABLE OF CONTENTS

ILLUSTRATIONS

ILLUSTRATIONS (Cont'd)

TABLES

SYMBOLS

A_i CRF inlet area (feet^2)

C_f Volume concentration of pollutant in full scale (dimensionless)

C_m Volume concentration of helium measured in model tests (dimensionless)

C_p Specific heat at constant pressure for air (= 6006 ft^2/sec^2 $^\circ$R)

g Acceleration of gravity (ft/sec^2)

h Stagnation enthalpy (= C_pT + ½ U^2 ft^2/sec^2)

h_A Stagnation enthalpy of ambient air and stack exhaust gas mixture at plume cross-section A(ft^2/sec^2)

h_a Stagnation enthalpy of ambient air (ft^2/sec^2)

h_s Stagnation enthalpy of stack exhaust gas (ft^2/sec^2)

ℓ Characteristic length (feet)

m_a Mass flux of ambient air (slugs/sec)

m_s Mass flux of stack exhaust gas (slugs/sec)

m_A Mass flux of ambient air and stack exhaust gas mixture at plume cross-section A (slugs/sec)

Q_f Mass flux of pollutant in full-scale stack (slugs/sec) (in this program the pollutant is hot air so $Q_f = W_f/g$)

T_{A_f} Absolute temperature of ambient air and stack exhaust gas mixture at point A in plume (deg. R)

T_{a_f} Absolute temperature of ambient air in full scale (deg. R)

T_{s_f} Absolute temperature of full-scale stack exhaust gas (deg. R)

ΔT_f Full-scale temperature rise above ambient at measuring point A (= $T_{A_f} - T_{a_f}$ deg F)

ΔT_{s_f} Full-scale temperature rise of exhaust gas at stack exit (= $T_{s_f} - T_{a_f}$ deg F)

t_s Sampling time in model tests (sec)

U_A Velocity in exhaust plume at measuring point A (ft/sec)

U_α Ambient wind velocity (ft/sec)

U_i Velocity at CRF Inlet (ft/sec)

$U_{f_{ref}}$ Full-scale reference wind velocity (ft/sec) corresponding to $U_{m_{ref}}$ (i.e., full-scale wind velocity at 2400 feet above ground level)

$U_{m_{ref}}$ Model reference wind velocity measured 4 feet above model ground

U_s Stack gas exit velocity (ft/sec)

U_w Full-scale wind velocity measured at weather station (ft/sec)

u_* Friction velocity (ft/sec); $u_* = (\tau_w / \rho)^{1/2}$

V_a Volume of entrained air in plume gas mixture at cross-section A

V_s Volume of stack gas in plume gas mixture at cross-section A

W_f Full-scale compressor weight flow (pounds/sec)

z_o Characteristic ground roughness length (feet)

δ Boundary layer thickness in ASF (feet)

θ Direction from which wind is approaching (deg.)

ν Kinematic viscosity (≈ 0.000157 ft^2/sec for air)

ρ_a Ambient air density (slugs/ft^3)

ρ_s Stack gas density (slugs/ft^3)

$\dot{\rho}_A$ Density of full-scale pollutant at plume cross-section A (slugs/ft^3)

SYMBOLS (Cont'd)

ρ_s^* Density of full-scale pollutant at stack exit ($slugs/ft^3$)

σ Fractional error in measurements (dimensionless)

τ_w Reynolds shear stress at the wall ($slugs/ft\ sec^2$)

ϕ_{He} Volume flux of helium from model stack (ft^3/sec)

ϕ_{H_2} Volume flux of hydrogen from model stack (ft^3/sec)

ϕ_i Volume flux of air in CRF inlet

ϕ_{N_2} Volume flux of nitrogen from model stack (ft^3/sec)

General Subscripts:

$(\ )_a$ In ambient air

$(\ )_f$ Full-scale

$(\ )_m$ Model

$(\ )_s$ At stack exit

SECTION I

INTRODUCTION

The U.S. Air Force is building a Compressor Research Facility (CRF) at Wright-Patterson Air Force Base, Ohio. The CRF is being built in an existing structure, a building which formerly served as a propeller test facility. The compressors are to be driven through a shaft powered by electric drive motors; both the compressor being tested and the motors will be housed in the building. This will be an open-circuit flow, with the inlet air being ingested directly from the ambient atmosphere through the building walls, which are of a porous or honeycomb structure. Outlet air from the compressor, which will have been considerably heated above the ambient temperature, is t be ducted outside the building to an exhaust stack located approximately 60 ft. from the nearest wall, and rising to a height 13 ft. below the roof of the building. This is believed to be a sufficient distance away so that the hot exhaust air will not be reingested by the compressor inlet flow. This report presents the results of an experimental model study of the CRF exhaust plume to determine if exhaust reingestion is a problem at the inlet, and also to assess the effect of the hot exhaust plume on temperatures at other locations in the area.

A 1:600 scale model of the CRF and surrounding portions of Area B, Wright-Patterson Air Force Base, was constructed and tested in the Calspan Atmospheric Simulation Facility (ASF). This specialized wind tunnel, which is described in the text, was designed for the specific purpose of modeling the wind in the lower atmosphere. The CRF model included provision for supplying properly scaled flows at the exhaust stack and at the inlet. The exhaust from the CRF was modeled by a mixture of hydrogen, helium and nitrogen mixed to the proper density. The helium in the gas mixture was the temperature simulant, that is, the full-scale temperature rise could be directly proportioned to the local concentration of helium which was measured at various locations on the model. In this fashion the full-scale temperature rise at the CRF inlet and surrounding areas was determined.

1

The test program included flow visualization studies and quantitative measurements to determine the temperature rise above ambient which is generated by the exhaust plume. Two model exhaust gas mixtures were used to simulate full-scale compressors operating at weight flows of 90 and 150 pounds per second while absorbing the full 30,000 horsepower available in the CRF drive system. Two different exhaust stacks were used in the test program, the standard stack design intended for the CRF and an extended version of this stack which is 15 feet higher and has a smaller exit area. The tests were performed for a number of wind speeds at each of 12 different wind directions. The results are presented in terms of full-scale temperature rise above ambient at various locations on the model.

In the sections that follow, the scaling criteria for the model tests are presented first. This is followed by descriptions of the test facilities and of the wind tunnel model. Next, the experimental results are presented in three parts. First, mean velocity profiles measured in the flow approaching the model and in the flow above the CRF model building are presented. Next the results of the flow visualization studies are presented in some detail. Finally quantitative values of the full-scale temperature rise calculated from the model concentration measurements are presented. A summary of the results and of the conclusions reached are presented in the last section.

SECTION II
SCALING CRITERIA

In conducting small-scale modeling of flows in the atmospheric bound-
ary layer, care must be taken to ensure that all important features of the
full-scale situation are represented in the model. Broadly speaking, these in-
clude the ambient wind environment, including both the mean and turbulent
characteristics, as well as the local terrain. In stack and vent emission
studies one must also model the relevant features of the exhaust gases, namely,
exit momentum, buoyancy and pollutant concentration. The dynamics of such
flows involve inertial, viscous and buoyancy forces, as well as turbulent
transport. The scaling criteria presented below are mathematical statements
of the requirement that each of these forces be present in the same relative
degree in the model as in full-scale. Most of the criteria are discussed at
some length in References 1 through 5, and here we will only list them, along
with a brief description of what they represent.

The most obvious requirement is that of geometric scaling between
the full-scale and model flows, with regard to buildings and local topography.
This also implies that one should hold the ratio of some characteristic geo-
metric length, say ℓ , to a length characteristic of the local ground rough-
ness, say Z_o , constant between full-scale and the model:

$$\left(\frac{\ell}{Z_o}\right)_m = \left(\frac{\ell}{Z_o}\right)_f$$

(1)

where $()_m$ refers to the model, and $()_f$ to full scale. Since Z_o essentially
determines the scale of the turbulent eddies near the ground, this ensures that
the relative size of the structures and the eddies is maintained.

The majority of flows very near the ground are "aerodynamically
rough", i.e., no laminar sublayer exists, and the flow is fully turbulent.
In such cases, molecular diffusion is negligible in comparison with that re-
sulting from turbulent transport. For this reason, matching between model
and full scale of the usual Reynolds number, based on free-stream conditions
and a characteristic length, is generally not required. Experience has shown

3

that the flow will be aerodynamically rough when a Reynolds number based on surface conditions is sufficiently large, i.e.,

$$\frac{u_* z_o}{\nu} \gtrsim 3$$

(2)

where u_* , the friction velocity, is related to the shear stress at the ground, τ_w by $u_* = \sqrt{\tau_w/\rho}$. Here ν is the kinematic viscosity and ρ the air density. Of the two conditions, (1) and (2), it is more important to satisfy condition (2).

The problem of actually generating the required flow in a laboratory facility is one that has received a great deal of attention in recent years. A wide variety of approaches is available for the development of the proper flow; these involve the use of various types of roughness elements, fences, spires, and jet transverse to the flow. At Calspan, the approach that has been used is that of a matched fence/rough-floor combination.[2,3,4] With this technique, the appropriate logarithmic mean velocity profile, as well as turbulence spectrum representative of that in the neutral atmosphere, is generated.

There are additional scaling criteria which must be satisfied when modeling buoyant flows such as stack emissions or thermally stratified atmospheric flows. A relatively comprehensive summary of these is presented in Reference 5. In the current study, stratified flows were not studied. Thus, the remaining scaling criteria are concerned with the stack emissions.

Intuitively, one expects that near the stack exit the shape of the exhaust plume is determined primarily by its exit momentum relative to that of the ambient wind, i.e., that inertial forces are dominant. Accordingly, we require that the ratio of vertical momentum flux issuing from the stack exit to the horizontal momentum flux in the ambient wind be the same in the model as it is in full-scale.

$$\left(\frac{\rho_s U_s^2}{\rho_a U_a^2}\right)_m = \left(\frac{\rho_s U_s^2}{\rho_a U_a^2}\right)_f$$

(3)

where ρ_s and U_s denote the density and vertical exhaust velocity of the emissions at the stack exit, and ρ_a and U_a are the ambient air density and wind speed. For neutrally stable thermal equilibrium of the atmosphere, which is assumed here, the ambient density, ρ_a , is the same in model and full-scale.

At large distances downstream of the stack, the plume rise will be determined by the buoyant forces arising from its temperature (or density) deviation from ambient, as well as by inertial forces. The ratio of inertial to buoyant forces must be held constant between model and full scale resulting in the buoyancy-scaling law,[5]

$$\left[\frac{\rho_a U_a^3}{(\rho_s - \rho_a) U_s g l} \right]_m = \left[\frac{\rho_a U_a^3}{(\rho_s - \rho_a) U_s g l} \right]_f \tag{4}$$

where g is acceleration of gravity.

By making use of Equation (3), it is possible to re-write this equation in a more convenient form:

$$\frac{U_{am}}{U_{af}} = \left[\frac{\rho_a - \rho_{sm}}{\rho_a - \rho_{sf}} \frac{l_m}{l_f} \left(\frac{\rho_{sf}}{\rho_{sm}} \right)^{1/2} \right]^{1/2} \tag{5}$$

where g and ρ_a are assumed to be the same in the model and in full scale.

Ordinarily, it is not necessary to scale the volumetric (or mass) flux at the stack exit, and no further restriction need be imposed on the scaling of the dynamics of the plume. If it were necessary to scale mass flux, the model and full-scale stack densities in Equation (5) would be equal with the result that the wind velocity over the model would be reduced in proportion to the square root of the geometric scale ratio between the model and full-scale. In many situations, it is necessary to model relatively large areas and the geometric scale ratio must be chosen so that the area will fit in the wind tunnel. This may require values of l_m/l_f which are small. Then, it becomes desirable to increase the values of the other terms in Equation (5) so that the required model wind velocities do not become so small that Equation (2) cannot be satisfied. This is done using highly

5

buoyant gas mixtures for the model stack effluents. It can readily be seen from Equation (5) that a decrease in ρ_{sm} will increase U_{am} for given values of the other variables. In other words, the buoyancy and inertial forces must not only be in the proper ratio, but must be large enough in absolute terms to keep the influence of molecular viscosity negligible, and satisfy Equation (2). This results in an envelope or "window" of experimental conditions within which one must operate to simulate the full-scale flow properly.

Equations (3) and (4) are the scaling criteria used to ensure similarity in the dynamic behaviors of the model and full-scale plumes. In most pollution studies, one wants to determine full-scale concentrations of pollutants at various full-scale locations. This is generally done by placing a tracer gas (helium in this program) into the model stack gas mixtures. Samples of the air at various points on the model are collected and analyzed for helium concentration. A scaling law relating helium concentration in the model to pollutant concentration in full-scale is used to obtain the desired results. In the current study, the interest is centered on determining full-scale temperatures rather than pollutant concentrations. These temperatures are directly related to the full-scale concentrations of stack exhaust gas. Thus, the model concentration levels of helium can be converted to equivalent full-scale temperatures. In the following paragraphs, the relationship between full-scale temperature and full-scale concentration of stack exhaust gas is developed. This is then combined with the scaling law relating model and full-scale concentration levels to obtain the relationship between full-scale temperatures and concentration levels of helium measured in the model tests.

The relationship between full-scale temperature and full-scale concentration of stack exhaust gas can be obtained by considering the flux of enthalpy through a cross-section of the plume at measuring station A. The total enthalpy flux through the cross section at A is equal to the sum of the total enthalpy flux of stack gas and of entrained air. That is

6

$$m_a h_a + m_s h_s = m_A h_A \tag{6}$$

where h = stagnation enthalpy = $C_p T + \frac{1}{2} U^2$

C_p = specific heat at constant pressure for air
($= 6006 \text{ ft}^2/\text{sec}^2 \text{ °R}$)

m = mass flux

T = absolute temperature

U = velocity

and subscripts

a = ambient air

s = stack exhaust

A = ambient air and stack exhaust mixture at cross section A

The total mass flux, m_A, is equal to the sum of the mass fluxes of entrained ambient air, m_a and stack exhaust, m_s. Thus, Equation (6) can be rewritten as

$$h_A = \frac{m_a}{m_a + m_s} h_a + \frac{m_s}{m_a + m_s} h_s \tag{7}$$

It is assumed that the stack exhaust gas and entrained ambient air are completely mixed at plume cross-section A. Then, since the CRF exhaust is air, the entrained air and the stack exhaust in the mixture at A will have equal temperatures, T_{A_f} and densities, ρ_{A_f}. Thus, the mass flow fraction and volume fraction of the mixture at A will be equal. That is

$$\frac{m_s}{m_a + m_s} = \frac{V_s}{V_a + V_s} \equiv C_f$$

where V_a = volume of entrained air in mixture at A

V_s = volume of stack gas in mixture at A

Similarily

$$\frac{m_a}{m_a + m_s} = 1 - C_f$$

7

Using the above relations for C_f in Equation (7) gives

$$h_A = (1 - C_f) h_a + C_f h_s$$

Substituting for the stagnation enthalpies, h_A , h_a and h_s

$$C_p T_{A_f} + \frac{1}{2} U_{A_f}^2 = (1 - C_f)(C_p T_{a_f} + \frac{1}{2} U_{a_f}^2) + C_f (C_p T_{S_f} + \frac{1}{2} U_{S_f}^2)$$

Rearranging

$$T_{A_f} - T_{a_f} = C_f (T_{s_f} - T_{a_f}) + \frac{C_f}{2 C_p} (U_{s_f}^2 - U_{a_f}^2) + \frac{1}{2 C_p} (U_{a_f}^2 - U_{A_f}^2)$$

$$(8)$$

Equation (8) is a general expression relating full-scale temperature to full-scale volume concentration level in the plume. It can be simplified by noting that $U_{A_f} \approx U_{a_f}$ except very close to the stack exit and that

$$\frac{U_{s_f}^2 - U_{a_f}^2}{2 C_p} << (T_s - T_a)$$

for almost all real plumes includ.ng the CRF plume. Thus, for the CRF tests

$$(T_A - T_a)_f = C_f (T_s - T_a)_f$$

$$(9)$$

The concentration scaling law relating helium concentration in the model to pollutant concentration in full scale is as follows.[5]

$$\frac{C_f}{C_m} = \frac{Q_f}{\rho_A^* \phi_{He}} \frac{l_m^2}{l_f^2} \frac{U_{A_m}}{U_{A_f}}$$

$$(10)$$

where C_f = volume concentration of pollutant in full-scale

C_m = volume concentration of helium measured in model tests

Q_f = mass flux of pollutant in full-scale stack

U_{A_f} = velocity in plume at measuring point, A, in full scale

U_{A_m} = velocity in plume at measuring point, A, on model

ρ_A^* = density of full scale pollutant at measuring point, A

ϕ_{He} = volume flux of helium from model stack

8

Most measurement locations used in pollution studies are far enough from the stack exit that it is sufficient to assume that ambient conditions of temperature and velocity prevail in the plume at A. Quite close to the stack exit, the plume will have dissipated most of its initial vertical velocity (i.e., after it has bent over) so that the velocity in the plume, U_A, can be taken as the ambient wind velocity, U_a. However, in the current study, the plume is initially very hot and the interest is centered on determining temperatures in the bent-over plume at locations where they may be significantly above ambient. Thus, it is not permissible to assume ambient temperature for estimating ρ_A^* in Equation (10). Since the exhaust plume behavior is a constant pressure process, we have

$$\rho_A^* = \rho_s^* \frac{T_{s_f}}{T_{A_f}}$$

(11)

where ρ_s^* = pollutant density at stack exit in full scale

T_{s_f} = absolute temperature in plume at stack exit in full scale

T_{A_f} = absolute temperature in plume at measuring point A in full scale.

Using Equation (11) and assuming all measurements are made at points far enough from the stack that the plume is convected at ambient wind velocity, Equation (10) becomes

$$\frac{C_f}{C_m} = \frac{Q_f}{\rho_s^* \phi_{\mu_e}} \frac{T_{A_f}}{T_{s_f}} \frac{\ell_m^2}{\ell_f^2} \frac{U_{a_m}}{U_{a_f}}$$

(12)

Combining Equations (9) and (12) and noting that in this model study the pollutant is the hot exhaust air from the CRF stack, so that $\rho_s^* = \rho_{s_f}$, one obtains

$$(T_A - T_a)_f = \frac{\left[\frac{Q_f}{\rho_{s_f} \phi_{\mu_e}} \left(\frac{\ell_m}{\ell_f} \right)^2 \left(\frac{U_{a_m}}{U_{a_f}} \right) \right] \frac{T_{a_f}}{T_{s_f}} (T_{s_f} - T_{a_f}) C_m}{1 - \left(1 - \frac{T_{a_f}}{T_{s_f}} \right) \left[\frac{Q_f}{\rho_{s_f} \phi_{\mu_e}} \left(\frac{\ell_m}{\ell_f} \right)^2 \left(\frac{U_{a_m}}{U_{a_f}} \right) \right] C_m}$$

(13)

Equation (13) is the final relation between the full-scale temperature at any measuring point, A, and the helium concentration levels, C_m, measured in the model tests.

Equations (1) through (13) deal with the scaling criteria for the flow over the model and the stack emissions. In the CRF model study, it is necessary also to scale the flow into the CRF model inlet. This is done by noting that the ratio of the local velocity at the inlet to the ambient wind velocity must be the same in the model and in full-scale. That is

$$\left(\frac{U_i}{U_a}\right)_m = \left(\frac{U_i}{U_a}\right)_f$$

(14)

where U_i is the mean velocity at the CRF inlet. The inlet volume flow rate in the model, $Q_{i_m} = U_{i_m} A_{i_m}$ where A_{i_m} is model inlet area. The full-scale volume flow rate $Q_{i_f} = U_{i_f} A_{i_f} = \frac{W_f}{g \rho_{a_f}}$ where A_{i_f} is the full scale inlet area, W_f is the weight flow of the compressor being tested in the CRF and g is the acceleration of gravity.

Thus
$$U_{i_m} = \frac{Q_{i_m}}{A_{i_m}} \qquad \text{and} \qquad U_{i_f} = \frac{W_f}{g \rho_{a_f} A_{i_f}} .$$

Substituting the U_i expressions in Equation (14) and rearranging, one obtains

$$Q_{i_m} = \frac{W_f}{g \rho_{a_f}} \frac{A_{i_m}}{A_{i_f}} \frac{U_{a_m}}{U_{a_f}} = \frac{W_f}{g \rho_{a_f}} \left(\frac{\ell_m}{\ell_f}\right)^2 \frac{U_{a_m}}{U_{a_f}}$$

(15)

as the volume flow rate required at the model CRF inlet.

A final discussion, regarding the comparison of model results with full-scale, relates to the well-known fact that in full-scale, the averaging time has a distinct effect on the measurements. This is not the case in model tests in the ASF. The model results correspond to short-time averaged full-scale measurements, taken over not more than 10 or 15 minutes in most cases. Briefly, what is involved here is the following. The frequency spectrum of wind gusts in full-scale always shows a null, or near null, in the range 1 to 3

10

cycles per hour.[6] Thus, it is theoretically correct to separate the spectrum into two parts at a frequency in that range, and deal with phenomena associated with each part separately. In the ASF, th. high-frequency portion related to the ground-induced turbulence is fully simulated. The low-frequency portion related to meandering of the wind, diurnal fluctuations, passage of weather systems, annual changes, and so on, must be considered separately if they are important to the study. In the current program, these very low frequency effects are not important.

Since the effective full-scale averaging time is independent of model averaging times, one can choose the model averaging time to provide data which are repeatable to within a specified accuracy. The model averaging times required to obtain a given accuracy can be estimated from statistical considerations as described in Reference 5. The result is:

$$t_s = \frac{\delta}{U_{m_{ref}} \sigma^2}$$

(16)

where

t_s = model sampling time (seconds)

δ = ASF boundary layer thickness (≈ 4 feet)

$U_{m_{ref}}$ = ASF reference velocity at top of boundary layer (feet/sec.)

σ = fractional error in measurements (% error/100)

It should be noted that, in the case of turbulence measurements, high frequency components require the same averaging time as discussed above because they are products of the breakdown of the large (low frequency) eddies. Therefore, they are subject to the same statistical considerations.

It is not generally appreciated how long an averaging time is required for ASF data processing. This can be illustrated by application of Equation (16). Typical accuracies expected in pollution studies are about 10% and the majority of quantitative tests in the current progrem were performed at reference velocities of 3,5, and 7 ft/sec. For ten percent accuracy, (σ = 0.1), Equation (16) gives t_s = 133, 80, and 57 seconds. These results are only approximate. In practice, it has usually been found that somewhat shorter averaging times provide the required accuracy. To establish

11

a suitable value at the start of any program, a few averages are generally checked as a function of integration period. An integration period of 90 seconds for all quantitative testing was used in this study.

The basic scaling criteria used in this investigation can be summarized as follows.

Ground Roughness Reynolds Number	-	Equation (2)
Stack Exit Momentum	-	Equation (3)
Stack Emission Buoyancy	-	Equation (5)
Full-Scale Temperature	-	Equation (13)
CRF Inlet Volume Flow	-	Equation (15)
Approximate Sampling Time Required	-	Equation (16)

In addition, Equation (1) which relates a typical length scale to the characteristic roughness length of the ground is satisfied approximately in the ASF in that (i) geometric scaling for the model is used, and (ii) the approach flow to the model is developed over a considerable length of random roughness elements whose mean height is scaled to full-scale terrain upwind of the modeled area.

SECTION III
TEST FACILITIES

A.   THE ATMOSPHERIC SIMULATION FACILITY

The Calspan Atmospheric Simulation Facility (ASF), is designed mainly mainly for studying atmospheric flow phenomena. This wind tunnel differs from the conventional aeronautical wind tunnel in two important respects, namely, the wind shear and the degree of turbulence. Every effort is made in a conventional aeronautical wind tunnel to assure a smooth, uniform flow, free from turbulent gusts. In contrast to this, a wind tunnel for simulating the lower atmospheric flow requires a relatively thick turbulent boundary layer within which the mean and turbulent properties are similar to those in the atmosphere.

In order to simulate these effects properly, a wind tunnel must be constructed in a very unconventional way. The particular method developed at Calspan for this purpose[2-4] is to use a fence, protruding from the floor of the tunnel, followed by a length of floor that is covered with roughness elements. This combination assures both the desired shear, and the associated turbulent gust spectrum as well. Figure 1 shows an exterior view of the facility. The rough floor, consisting of wooden blocks in this case, can be seen upstream of the model in Figure 2. The fence, which is a solid aluminum plate, protruding from the floor at the beginning of the flow development region, is also visible in this figure.

The facility is 119 feet long. The test flow is developed generally over a 50-foot length downwind of the intake, leaving approximately 30 feet available as a test section. The tunnel is 8 feet wide by approximately 7 feet high. The tunnel ceiling is adjustable to allow the axial pressure gradient to be set near zero. The turbulent shear layer occupies roughly the lower 5 feet in the ASF. A variable-pitch fan powered by a two-speed motor pulls air through the tunnel at speeds from less than 1 mph to 55 mph. Sound attenuators upstream and downstream of the fan system are included in power package. Even at very low free-stream velocities, the mean flow in the tunnel is quite steady. The wind tunnel is situated in a very large room which forms the

13

return circuit between the tunnel inlet and exhaust. This probably accounts for the excellent wind-speed control at very low flows.

Two mechanical turntables are incorporated into the floor of the ASF. Both of them have a diameter of 88 inches. These turntables can be placed at various axial locations, depending on the program requirements. Models to be tested are mounted on one of the turntables. In this way, when upstream details are not sufficiently unique to require specific modeling, the general rough ground can be continued up to turntable, which can then be rotated to change wind direction. The floor of the ASF can be warped both upstream and downstream of a model placed on either of the turntables in order to match the terrain contours at the edge of the model.

Various rough grounds are used depending on the scale of the model and the upwind terrain. The latter may change as the wind direction is changed; for example, a building located near a shore line will require an over-water approach for on-shore winds and perhaps a suburban approach for other wind directions. Close to the actual model under test, greater detail is incorporated. For example, a city building will be surrounded by several blocks of accurately modeled city.

B.   POLLUTANT-CONCENTRATION MEASURING SYSTEM

The most common application of the ASF to pollution dispersion is related to the emission from multiple sources (stacks) in an industrial area. These emissions are generally hot and have reasonably high exit velocities. As discussed in Section 11, it is necessary to simulate the proper stack emission buoyancy, exit momentum, and pollution content. This is done by using gas mixtures to simulate the emission from each stack. The mixtures are made up of nitrogen, helium, and hydrogen. The helium in the gas mixtures is the pollutant simulant and the mass flow of helium is made proportional to the mass flow of pollutant (hot air in this program). The nitrogen and hydrogen components in the gas mixtures are adjusted to provide the correct buoyancy and exit momentum for the stack emissions.

14

The Calspan concentration sampling system is illustrated in Figure 3, where it is shown connected to a helium leak detector for quantitative analysis. As noted above, the system uses helium as the pollution simulant gas. The sensitivity in terms of most full-scale pollutants is much greater than the actual sensitivity to He at model scale. An advantage of using He as the simulant is that the background concentration in normal air is low, generally about 5 ppm.

Briefly, the sampling system consists of a ring of 24 chambers (the numbered cylinders on the left of Figure 3), which are initially pumped down to a hard vacuum, into which the samples are drawn through 12-foot long capillaries. Three of these capillaries are taken to calibration gases. The other capillaries are exposed to the mixtures drawn from the 20 sampling points on the model and one upstream reference to determine background level. The samples are drawn from the tunnel locations, through plastic tubing by a jet pump. Each capillary is aligned with a sample tube at the connection to the jet-pump plenum in such a way that it can receive gas only from that sample tube.

Each capillary is connected to the top of a sample collection chamber through a solenoid valve electrically driven so that all 24 solenoids can be opened or closed simultaneously. The bottom of each collection chamber is open to a vacuum plenum, which is held ar toughly 10^{-5} torr by a diffusion pump backed by a large mechanical pump. A single plate valve is used to seal off all 24 chamhers from the vacuum plenum at the start of sample collection in the chamhers.

The method of collecting the samples is as follows. The collection chambers are pumped down to a hard vacuum (10^{-5} torr) with the capillary end of the chamhers closed by the solenoid valves. Then, with the conditions for a test established (model operating and capillaries exposed to the proper calibration gases and flows to he sampled), the capillaries are flushed for 15 seconds by opening the solenoid valves. This is sufficient time to draw legitimate samples into the full lengths of the capillaries. The solenoid

15

valves are then closed and the chambers are pumped down to a hard vacuum.
This takes about 10 seconds. During this time the capillaries return to
atmospheric pressure but they now contain legitimate samples. Once the hard
vacuum is attained in the chambers, the large plate valve at the bottom of
the chambers is closed to seal off all 24 chambers from the vacuum plenum.
Finally, the solenoid valves are reopened for, generally, 90 seconds to allow
samples into the chambers. The solenoid valves are then closed to seal the
collection chambers, which now contain the collected samples at a final pres-
sure of 1 or 2 torr.

At the end of sampling, each chamber is analyzed for helium concen-
tration by connecting it, in turn, to the measuring system through an elec-
trically driven scanning valve. The measurement is made on a modified helium
leak detector in which the pressure is regulated by the fixed geometrical (area)
relationship between an inlet pinhole at the scanning valve and the outlet
restriction of a butterfly valve which is part of the leak detector. Since
each sample chamber is at the same pressure, the leak detector provides a
direct reading of the concentration level. Calibration mixtures in the three
calibration channels allow direct standardization on each scan. The system
has been trimmed so that, when all channels are exposed to the same source,
the readouts lie within 5% of the mean, down to concentrations of about
5 ppm helium. A complete scan of the 24 channels takes about 10 minutes.

The output of the leak detector is normally read on a meter driven
by the built-in electrometer. This has been modified to provide an output
voltage which can be taken directly, or integrated for a few seconds, and
converted to BCD code which is then processed by a Hewlett-Packard 9825A cal-
culator system. The data are stored on tape cassette, processed, and plotted
as required.

C.   AUXILIARY EQUIPMENT

Mean velocity profiles above the model and above the rough ground upstream of the turntable were measured with a heat-pulse anemometer. This instrument was developed at Calspan as an alternative to the hot-wire anemometer for measuring low velocity flows. It has the advantage that its calibration is insensitive to variations in temperature. The heat-pulse anemometer operates as follows.

A hot-wire, similar to a conventional hot-wire anemometer, is raised in temperature step-wise 100 times per second. It is maintained at a constant elevated temperature for 0.5 millisec. It can be shown theoretically[7] that if the heat transport is mainly by convection rather than conduction (large Peclet number), then the temperature jump at any point downstream is affected symmetrically by the diffusion process, and the mid-point of the jump occurs at a time determined by fluid velocity and the distance from the heated wire to the point. That is, the mid-point, or point of inflection, is independent of the thermal properties of the fluid.

The Calspan heat-pulse anemometer consists of two fine wires at right-angles to each other, and to the mean flow velocity. The upstream wire is pulsed electrically and the downstream wire acts as the temperature sensor. A signal-processing circuit determines each transit time as described above, rejecting any unsatisfactory measurements, and integrates over 1,000 samples (i.e., for approximately 10 seconds) to produce a voltage proportional to the average velocity. Lacking a longer-term integration period we have generally summed about 5 or 6 readings to obtain a more useful average.

Calibration of the heat-pulse anemometer was accomplished by placing it in a uniform flow and comparing its output with the flow velocity. The flow velocity was determined from the measured time of passage of a smoke puff between two streamwise locations in the flow. The smoke puff technique was also used during the tests to measure the model reference wind speed in the approximately uniform flow 4 feet above the model.

17

SECTION IV

WIND TUNNEL MODEL

A.   PHYSICAL MODEL

The model of the CRF building and the surrounding vicinity of Area B
is shown in Figure 2 installed on the turntable in the ASF. A plan view of the
area modeled is presented in Figure 4. At the 1:600 scale selected for the model,
the 88-inch diameter turntable in the ASF encompasses a circle with a full-scale
diameter of 4400 feet. The base of the model is contoured to simulate the ground
elevations of the full-scale terrain. The model elevations are particularly
evident in Figure 2 near the left edge of the turntable and near the CRF building.

Modeling of the ground elevations incurred changes in height at the
edge of the turntable which made it necessary to provide for a smooth junction
between the upstream edge of the turntable and the ground upstream of the turn-
table. This was accomplished by mounting the upstream ground on an adjustable
ramp frame which can be warped to match the edge of the turntable. In Figure 2,
the ramp has been adjusted to provide a good match between the upstream ground
and the front edge of the turntable. For other orientations of the turntable,
the upstream ground is readjusted to provide a similar match. The downstream
edge of the turntable is not matched to the ASF flooring since a small dis-
continuity at this location will have a negligible effect on the behavior of
the CRF exhaust plume over the main body of the turntable.

The flow approaching the turntable model is developed over a length
of rough floor which is preceded by a fence protruding from the floor of the
ASF at the inlet. The rough floor consists of randomly spaced wooden blocks
whose heights are scaled to match the approximate mean height of the roughness
elements (trees, building, etc.) in the full-scale approaching fetch. The
fence and the wooden block rough ground which were used for most wind directions
are visible in Figure 2. However, for winds approaching from approximately
200 to 270 degrees, the full-scale terrain is very flat with few buildings in
the region upstream of the turntable. For these wind directions, two sets of
quantitative data were taken, one with the wooden block ground shown in Figure 2,

18

and one in which the 12 feet of model ground (7200 feet in full-scale) closest to the turntable was replaced by small gravel elements similar to those visible near the corners of the turntable in Figure 2. The two sets of quantitative data were used to determine if the local temperature rises from the CRF exhaust plume are affected by the change in upstream roughness.

Two versions of the CRF exhaust stack were tested in this study. The first or standard version, has a rectangular exit configuration with internal full-scale dimensions of 13-1/2 x 17-1/2 feet and an exit elevation of 865 feet in full-scale (Figure 5). This is 13 feet below the 878 foot roof elevation of the CRF building. The second or extended version of the stack (Figure 6) converts the stack exit to a circle with 10 foot ID in full-scale and raises the stack exit to a full-scale elevation of 880 feet.

The model of the CRF building incorporates openings in the walls which are scaled to the full-scale building from drawings supplied by the Aero Propulsion Laboratory. In some cases, existing openings in the building will be blocked off after modification to the CRF configuration. These particular openings were eliminated in the model. The openings in the north wall and a portion of the west wall can be seen in Figures 5 and 6.

The inside of the CRF model is shown in Figure 7. The model of the inlet filter box and the inlet ducting is visible in this figure. The front and two side faces of the inlet filter are modeled with fine mesh screen. The top, bottom and back of the filter box are made from brass shim stock. The 20-foot diameter settling chamber of the CRF is modeled with brass tubing which is connected to an air ejector system below the floor of the model. The ejector is used to provide suction for inducing air flow through the model inlet ducting. A precision flow meter and metering valve between the inlet ducting and the ejector are used to provide properly scaled inlet mass flows during the tests. The hole in the floor of the CRF model is used to provide an exit for tubing from sampling probes within the CRF building and on the roof of the CRF building. When this tubing is installed, the hole is sealed to prevent air flow from entering the model from outside the ASF. (When operating, the test section of the ASF is at a static pressure slightly below that of the surrounding room.)

19

B. STACK EMISSION MODEL

The model exhaust stack is provided with a gas mixture composed of hydrogen, helium and nitrogen. The helium in the gas mixture is the temperature simulant in the model tests. The nitrogen and hydrogen components in the gas mixture are used to provide the correct buoyancy and momentum for the stack emission. In the quantitative tests, the volume concentration of helium was measured in the CRF inlet ducting and at various other sampling locations. The measured He concentration data were then converted to equivalent temperature rise data for the full-scale situation.

Two different exhaust gas mixtures were used in this study. The first mixture was scaled to represent a compressor weight flow of 90 pounds/second and a temperature rise of 950 degrees Fahrenheit. This temperature is approximately the maximum allowed in the stack; higher values would require cooling, probably by injecting water spray. The second mixture corresponds to 150 pounds/second weight flow with a temperature rise of 570 degrees Fahrenheit. Both mixtures correspond to converting all the 30,000 horsepower available in the CRF compressor drive system into heat (21,200 BTU/sec) in the CRF exhaust. It is believed that the 90 pounds/second represents a "worst case" from a thermal pollution viewpoint. It has high heat flux in combination with low exhaust momentum. The 150 pounds/second case has the same heat flux but lower initial temperature and higher momentum at the stack exit. The 150 pounds/second case was used for comparison with the estimated "worst case" exhaust mixture.

The scaling laws presented in Section II were used to calculate the various model flow quantities and conversion factors. The quantitative results for the two exhaust gas mixtures are listed in Table 1. The scale quantities were chosen to maximize the ratio of model to full-scale wind velocity (Section II-Equation 5). This was accomplished by using the most buoyant model gas mixture possible to simulate the hottest full-scale emission while at the same time including sufficient helium for adequate sensitivity in the concentration measurements.

20

Locations for the measurement of helium concentrations in the model tests are shown in Figures 8 and 9. These sampling point locations are divided into two groups, a set of fifteen fixed locations in the near field (Figure 8) and a set of five variable locations in the far field (Figure 9).

The fixed locations shown in Figure 8 are numbered for reference purposes. They are located as follows: one sampling probe (No. 1) inside the CRF inlet ducting, one probe (No. 2) inside the CRF building, three probes (Nos. 3,4,5) on the roof of the CRF building near the exhaust stack, and ten (Nos. 6-13, 14(a), 15(a)) at the locations of ventilation intakes on the surrounding buildings. The locations for the ventilation intakes were taken from drawings supplied by the Aero Propulsion Lab. The vertical heights of these intakes as well as the horizontal locations are scaled in the model. Two ground-level probes, 14(b) and 15(b), were used in place of ventilation intakes, 14(a) and 15(a), when the wind was from the southern half of the compass. The reason for this replacement is discussed in Section V-B.

Five sampling probes were used to determine ground level temperature rise in the far field. The locations of these probes vary with wind direction. The locations of the probes relative to a given wind direction are shown in Figure 9. The probes lie on a circle whose center is the CRF exhaust stack and whose radius is 1600 feet in full-scale. The middle probe in the five-probe array is directly downwind of the CRF exhaust stack and the remaining four probes are spaced at 15 degree intervals. The 1600 foot radius for the circle was chosen so that the circle intersects a small park area east of the exhaust stack between "L" Street and Skyline Drive. Thus, temperature rise data in the park area was obtained when the wind direction is such that the exhaust plume passes over the park. Moreover, similar far field data were also obtained for all other wind directions.

Since the location of the CRF exhaust stack is not coincident with the center of the turntable in the ASF (see Figure 9), it was necessary to mount the far field sampling probe array on the traversing system in the ASF. The traverse system was used to reposition the sampling probe array each time

21

a new wind direction was tested. The probe array is constructed so that the probes automatically adjust for variations in terrain elevation or building contours which intersect the desired positions of the probes. In each instance, the sampling probes take vertical positions slightly above (about 6 feet in full-scale) the local terrain or building elevations.

SECTION V
EXPERIMENTAL RESULTS AND DISCUSSION

The experimental results are presented in three parts. Mean velocity profiles in the flow over the model are presented in V-A. Flow visualization studies are discussed in V-B. Finally, full-scale temperatures calculated from helium concentrations measured on the model are presented in V-C.

A.   MEAN VELOCITY PROFILES

One of the problems encountered in interpreting model test data, or for that matter full scale data, is the selection of a location for measuring the mean wind velocity. In full scale these are usually measured at meteorological stations which may be remote from the area of interest. Moreover, the anemometers are located at low altitudes, typically about 100 feet or less above local ground level. The measured wind velocities can be influenced by the local terrain as well as the height above ground. In the ASF, the possibility of local terrain influences on the reference wind velocity is avoided by selecting a measuring location well above the terrain, in this case at a model height of 4 feet or an effective full scale height of 2400 feet above the ground. However, this reference velocity is still required to have a known relationship with some full-scale meteorological station. Such a relationship can be found from mean velocity profiles measured above the model.

Mean velocity profiles in the flow approaching the model are shown in Figure 10 for the two rough ground configurations used in this program. As explained in Section IV-A, the all wooden block ground was used upstream for quantitative tests with all wind directions. The wooden block plus gravel ground was used for repeat tests with wind directions between 200 and 270 degrees. The low and the high velocity portions of each profile in Figure 10 were measured with two different sensing probes on the heat-pulse anemometer in order to cover the complete velocity range. Data taken with each sensing probe are noted in Figure 10.

23

The roughness of the terrain has considerable effect on the wind velocities close to the ground. Figure 10 shows that the mean velocities over the gravel ground are significantly higher than those over the wooden blocks. This, of course, is the expected result, but it leads to difficulty in providing an exact relationship between the reference velocity used in the ASF and the full-scale wind velocities measured at much lower heights. For example, the velocity ratio at 100 feet in full-scale is 0.39 above the rough (wooden block) terrain and 0.57 above the flat unobstructed (gravel) terrain. Meteorological stations in the area are probably situated in terrain which corresponds more closely to the gravel ground in the model and the anemometer is likely at a height less 100 feet. Thus, a reasonable approximation to the velocity ratio for typical full-scale wind velocity (U_w) measurements would appear to be $U_w / U_{ref} \approx 0.5$.

As mentioned previously, in the model tests the reference wind veloc-ity, $U_{m_{ref}}$, is measured approximately four feet above the ground in the ASF where the velocity variation with height is negligible. In full-scale, this would correspond to measuring the wind speed, $U_{f_{ref}}$, at a height of 2400 feet above the ground. With the scaling parameters selected for this program (see Table 1) the relationship between model and full-scale reference velocities is $U_{f_{ref}} = 13.9\ U_{m_{ref}}$. Thus, if $U_{m_{ref}}$ is 3 feet/second, then the equivalent full-scale reference velocity at 2400 feet above ground level would be 41.7 feet/second. Using the estimate developed above to relate the full-scale wind velocity, U_w , measured at a weather station, to the full-scale reference velocity, $U_{f_{ref}}$, one obtains finally

$$U_w \approx 0.5\ U_{f_{ref}} \approx 7 U_{m_{ref}}$$

(17)

This relation may be used to convert the model reference wind velocities noted in the presentation of the data to approximate full-scale wind velocities measured at a local weather station.

Mean velocity profiles measured above the roof of the CRF model are shown in Figure 11. Data were measured for four different wind directions and

for both configurations of upstream terrain. As can be seen, there are only small differences in the velocities measured for the different conditions. Apparently the terrain roughness presented by the ground elevations and the structures in Area B near the CRF building are sufficiently homogeneous that wind direction and far upstream terrain features have little effect on the mean velocity profile above the CRF building. This suggests that differences in the far upstream terrain will have little effect on the exhaust plume dispersion near the CRF. As will be seen, this suggestion is corroborated by the quantitative temperature data.

B.   FLOW VISUALIZATION STUDIES

A flow visualization study was made at the start of the model tests to assist in the selection of a test schedule for the quantitative measurements. In this study, smoke was generated in the model exhaust plume by passing the exhaust gas mixture of He, H_2 and N_2 through a flask containing a small amount of Titanium Tetroachloride prior to introducing the mixture into the stack. The small amount of $TiCl_4$ vapor picked up by the gas mixture as it passes through the flask produces a white smoke when it encounters moisture in the air in the ASF test section.

Prior to photographing the exhaust plume from the CRF, a preliminary visual study was made to determine which wind directions caused the most downwash of the plume in the vicinity of the CRF building. It was found that for winds approaching from angles between about 0 and 45 degrees, the plume often was swept by the west face of the CRF building near the inlet ducting. The frequency with which this occurred increased with increasing wind velocity and the worst downwash appeared to occur at a wind angle of 30 degrees. Moreover, with the wind approaching from the southerly directions, substantial plume downwash was observed in the vicinity of the nearby rotor whirl tower. In this case, the worst downwash occurred for wind directions near 200 degrees. Thus, the majority of the photographs were taken with northerly and southerly winds (i.e., 0°, 30°, 180° and 200°). In addition, a series of photographs were taken with a west (270°) wind to show the plume behavior in the park area east of the CRF stack.

Once the problem wind directions were found, the wind velocity was varied for each of these directions. The lowest velocity at which the plume touches down frequently in the area of interest was determined. This wind velocity usually represents the most critical condition. At lower wind velocities the plume is infrequently in the area of interest, and at higher wind velocities the concentration of plume gas will decrease because of increased dilution by the ambient air. The wind velocities at which the smoke pictures were taken were selected to bracket this critical wind velocity.

Photographic results from the smoke flow visualization studies are presented in Figures 12 through 21. It is worth noting at the outset of this discussion that the smoke studies provided no distinguishable differences between the exhaust plumes for the two gas mixtures (90 pounds/second and 150/pounds/second) described in Section IV-B; evidence of differences in the two plumes (if any) must await the results of the quantitative test program. Thus, in the following presentation, the most illustrative photographs were selected without discrimating between stack gas mixtures. The smoke photographs will be presented in groups according to wind direction, with model reference wind speed, $U_{m_{ref}}$, as a variable.

Figure 12 illustrates the exhaust plume behavior with the wind approaching from due north. Parts a, b and c of Figure 12 are for different model reference wind velocities, $U_{m_{ref}}$. Each part of this figure (and of Figures 13 through 20) contain two pictures to illustrate the highest (upper picture) and the lowest (lower picture) plume trajectories which were photographed for the wind conditions cited in the title of the figure. Since the plume was usually unsteady in time, it was felt that two photographs were necessary to illustrate its general behavior. The lower picture in Figure 12(c), $U_{m_{ref}}$ = 7 feet/second, shows a condition where part of the exhaust plume was swept by the west face of the CRF building near the inlet ducting. A similar condition occurred occasionally with $U_{m_{ref}}$ = 5 feet/second but we did not manage to capture it in the photographs.

26

Figures 13(a) through 13(c) show the results obtained for a wind direction of 30 degrees. This particular wind direction caused the severest plume downwash in the vicinity of the CRF inlet ducting. The lower pictures in Figures 13(b) and 13(c) illustrate this phenomenon. It occurred fairly regularly at model reference wind velocities as low as 5 feet/second but not very often at 3 feet/second.

Since the 30 degree wind direction appeared to provide the greatest potential for ingestion of the hot exhaust plume into the CRF inlet ducting, additional smoke studies were made with the CRF stack extended as described in Section IV, and also with the rotor whirl tower removed from the model. The results are illustrated in Figures 14, 15 and 16. Figure 14 shows the extended stack with the whirl tower intact. Figures 15 and 16 show the standard and the extended stack respectively with the whirl tower removed. Extending the stack in the presence of the whirl tower slighly decreased the frequency with which plume downwash occurred near the CRF inlet. However, the effect was not large at $U_{m_{ref}}$ = 5 feet/sec (Figures 13(b) and 14(b)) and nonexistent at $U_{m_{ref}}$ = 7 feet/second (Figures 13(c) and 14(c)). Removal of the rotor whirl tower (Figures 15 and 16) provided little or no improvement in the exhaust plume behavior. (Note that Figure 16 illustrates the plume only for $U_{m_{ref}}$ = 5 and 7 feet/second. No photographs were taken with $U_{m_{ref}}$ = 3 feet/sec since the plume was always clear of the CRF inlet in a fashion similar to Figures 13(a), 14(a) and 15(a)).

Figures 17 and 18 show the plume from the standard stack and the extended stack respectively for a wind from 180 degrees. With the standard stack, there is considerable downwash of the plume for model reference wind velocities of 5 and 7 feet sec (Figures 17(b) and (c)). In fact, the plume touched ground almost continuously in the vicinity of the whirl tower for $U_{m_{ref}}$ = 7 feet/second (Figure 17(c)). Extending the stack helped the plume to clear the whirl tower for $U_{m_{ref}}$ ≤ 5 feet/second (Figures 18(a) and (b)), but it still touched ground frequently with $U_{m_{ref}}$ = 7 feet/second (Figure 18(c)). The area near the whirl tower where the plume touches ground is near an entrance to Building 62 and is also just upwind of ventilation intakes for Buildings 62 and 23 (see Figure 8). Thus, it is possible that this area may be of some concern for pedestrian traffic and for building ventilation, especially since we understand that the prevailing wind is from the southwest.

27

Further smoke studies with the wind approaching from the southwest quadrant showed that the greatest plume downwash occurs with a wind direction of approximately 200 degrees. Plume trajectories for this wind direction are shown in Figure 19 for the standard stack and in Figure 20 for the extended stack. With the standard stack, the plume frequently touches ground near the whirl tower for model reference wind velocities as low as $U_{m_{ref}}$ = 3 feet/second (Figure 19(b)). Extending the stack kept the plume clear of the ground most of the time for this wind velocity, but it still touched ground for $U_{m_{ref}}$ = 5 feet/second (Figure 20(c)).

A model reference wind velocity, $U_{m_{ref}}$, of 3 feet/second is not particularly high in terms of full-scale wind velocities measured at typical heights above ground. As explained previously (see Equation 17), the corresponding full-scale wind quoted by a weather station would be approximately 21 feet/second or about 14 miles per hour. Thus, the situation depicted in the lower picture of Figure 19(b) could occur enough times to warrant further investigation in the quantitative model test program. In view of this, we repositioned the two most southern sampling probes (Nos. 14(a) and 15(a)) in Figure 8 when the wind was from the southern half of the compass. The two sampling probes were repositioned to ground-level locations 25 feet due east and 25 feet due west of the whirl tower exterior faces. These two probes (Nos. 14(b) and 15(b)) provided ground-level temperature rise data under plume downwash conditions near the whirl tower.

The final series of photographs (Figures 21(a) through 21(d) are for a wind direction of 270 degrees. With this wind direction, the exhaust plume is swept over the park area east of the CRF stack. The format of the pictures in these figures is different from that used for Figures 12 through 20. Here, we are interested in observing the plume for larger distances downwind of the exhaust stack, in the vicinity of the park area. (This area is distinguished by the presence of model trees in the photographs.) With a 270 degree wind, the far field plume behavior was more steady in time than in the previous near field studies. Thus, it was possible to select single photographs to illustrate typical plume behavior. This has been done in Figures 21(a) through 21(d). In these figures, the upper picture shows a typical plume from the extended stack and the lower picture shows a typical plume from the standard stack.

28

The photographs in Figure 21 show that there is very little difference in far field plume behavior from the standard and the extended stack. Plumes from both the standard and extended stacks begin to touch ground in the park area for model reference wind velocities as low as 3 feet/second (Figure 21(b)) and are swept progressively lower as wind velocity is increased (Figures 21(c) and 21(d)). The photographs suggest that the maximum temperature rise in the park area should occur for values of $U_{m_{ref}}$ in the vicinity of 3 to 5 feet/second. This is the velocity range where the plume first touches ground continuously in the park area.

C.   FULL-SCALE TEMPERATURE RISE

The smoke flow visualization studies described above were used to select a test schedule for the quantitative measurements. The model conditions tested are given in Table 2. The schedule consists of 94 tests in which temperature rise data were obtained simultaneously from 20 different sampling probes. Wind directions were varied in 30 degree increments (0°, 30°, 60°, etc.) and model reference wind velocities covered the range between 2 and 7 feet/second. The standard stack was tested with gas mixtures corresponding to full-scale compressor weight flows of 90 and 150 pounds/second and the extended stack was tested for conditions corresponding to a compressor weight flow of 90 pounds/second. Finally, for wind directions of 210 and 270 degrees, tests were performed both with the wooden block rough ground in the flow development region (as shown in Figure 2), and also with smaller gravel elements for 12 feet upstream of the turntahle model. The reason for the two types of ground roughness in the flow development region has been discussed in Section IV-A.

In these tests, the measured concentrations of helium were converted by an on-line minicomputer to equivalent full-scale temperature rise, ΔT_f , in degrees Fahrenheit above local amhient temperature. At the end of each test, the ΔT_f data were plotted by the computer on "near-field" and "far-field" background maps similar to Figures 8 and 9 respectively. Thus there are two maps for each test run for a total of 188. A representative sample of these maps is presented in the following discussion.

29

A complete set of near-field maps for the standard stack configuration with condition 1 exhaust $(W_f = 90^\#/sec , \Delta T_{s_f} = 950^\circ F)$ is presented in Figures 22 through 33. Selected far-field maps for the same conditions are presented in Figures 34 through 37. The data maps are presented in groups according to wind direction, with model reference speed, $U_{m_{ref}}$ as a variable. The numbers beside the points are temperature rise above local ambient in degrees Fahrenheit rounded off to the first decimal place. In some cases -0.0 is indicated as a temperature rise. The negative signs have no significance. They arise from very small inaccuracies in calibration of the sampling channels.

The extended stack was tested for many of the wind conditions tested with the standard stack (see Table 2). In cases where both sets of data are available, the data for the extended stack have been added in brackets along with an explanatory note on the appropriate near-field figures. When ΔT_f equals 0.0 for both the standard and extended stack, the bracketed value (0.0) is omitted on these figures.

As mentioned near the beginning of Section V-B, for any given sampling location there will be a critical wind direction and wind speed at which the temperature rise will be a maximum. For wind directions different from the critical direction, the plume will not pass over the sampling location. Moreover at the critical wind direction but at wind speeds lower than the critical speed the plume will pass above the sampling location most of the time. At wind speeds higher than the critical speed the concentration of plume gas (and hence the temperature) will decrease because of increased dilution by the ambient air.

Inspection of the data shown in Figures 22 through 33 show that the highest temperature rise observed in the CRF inlet occurred with the standard stack for wind conditions of $U_{m_{ref}}$ = 5 ft/sec. and θ = 30 deg. (Figure 23c). The inlet data are summarized in Table 3 along with data measured inside the CRF building. The variation of inlet temperature rise with wind direction for $U_{m_{ref}}$ = 5 ft/sec is shown in Figure 38 along with data from other sampling points in the near-field. The peak in inlet temperature rise at θ = 30 degrees is

evident in this figure. The variation in temperature rise with wind speed for θ = 30 degrees is shown in Figure 39 for the CRF inlet and for sampling point No. 3 on the CRF roof. The temperature rise at the latter location also peaked for θ = 30 degrees (see Figure 38). The critical wind speed for the CRF inlet appears to be $5 \lesssim U_{m_{ref}} \lesssim 6$ ft/sec for both the standard stack and the extended stack. In contrast the critical wind speed for sampling point No. 3 on the roof depends on the stack configuration. With the standard stack this speed is $U_{m_{ref}} \approx 4$ ft/sec and with the extended stack it is $U_{m_{ref}} \approx 6$ ft/sec.

As discussed in Section II, the temperature rise data presented here correspond to full-scale data which have been averaged over a time period of 10 to 15 minutes. This means that instantaneous temperatures could reach substantially larger values, especially at sampling points very close to the stacks. Thus, instantaneous temperature rise peaks as large as 10 to 20 times the maximum average temperature rise data can be expected on the CRF roof (sampling points No. 3,4 and 6). All other sampling points are either farther from the stack or else located such that the plume trajectory must be influenced by the wake of the CRF building in order for the plume to reach the sampling point. Both distance and building wake effects increase the plume diffusion and decrease the timewise intermittency of plume gas concentration at the sampling points. In these cases it is expected that the instantaneous temperature rise would exceed the average only by a factor on the order of 5 or less.

The temperature rise data for the CRF inlet show a maximum value of $\Delta T_t \approx 1.2$ degrees Fahrenheit for the standard stack at the critical wind conditions (Figure 39). If this maximum is increased by a factor of 5 to estimate short term temperature fluctuations one obtains instantaneous temperature peaks of 6 degrees Fahrenheit above ambient. This value is probably acceptable when one considers that it occurs only over a very limited range of wind conditions. Stated conservatively these wind conditions are $0 \lesssim \theta \lesssim 60$ degrees and $U_{m_{ref}} \gtrsim 3$ ft/sec. In terms of full-scale weather station forecasts these are winds from the north to east-northeast direction at speeds in excess of 15 miles per hour. We understand that the prevailing wind direction for the area is from the southwest. For wind directions in this range, the exhaust plume never enters

31

the inlet. Thus, ingestion of high temperature exhaust gas into the CRF inlet would not appear to be a problem with the standard stack design. With the extended stack the data (Figure 39) indicate that the inlet temperatures are reduced even more, down to about one-half the values found for the standard stack.

The temperature rise observed at sampling point No. 2 inside the CRF building is similar in magnitude to that found in the CRF inlet. The variation of temperature rise with wind direction for $U_{m_{ref}}$ = 5 ft/sec is included in Figure 38. However, in this case the maximum value $(\Delta T_f = 1.2\,^\circ F)$ occurred at a reference wind velocity of 7 ft/sec. instead of 5 ft/sec. and the critical wind direction was 330 deg. (see Table 3 and Figure 33(c)). As with the CRF inlet, the temperature rise inside the building is not excessive and non-zero values occur only for winds from the northwest quadrant at full-scale wind speeds, U_w , in excess of approximately 15 miles per hour $(U_{m_{ref}} \approx 3 \text{ ft/sec.})$. The extended stack was very effective in reducing the temperature rise inside the CRF building. The temperature rise was reduced by a factor of at least 3 in all cases measured (Figures 31, 32, and 33).

The maximum temperature rise, $\Delta T_{f\,max}$, found anywhere during a test is listed in Table 4 for both the standard and the extended stacks with condition 1 exhaust gas ($W_f = 90''/sec$, $\Delta T_{s_f} = 950\,^\circ F$). The sampling point at which the maximum occurred is listed in parentheses beside the magnitude of the maximum temperature rise. In some cases, the location of the maximum temperature was different for the standard and the extended stack. In these cases, temperature rise data have been added in square brackets to allow comparison of data at identical sampling point locations.

Inspection of Table 4 shows that the highest temperatures occur on the CRF roof at sampling points No. 3 and 5 for wind directions of 30 degrees and 300 degrees respectively and $U_{m_{ref}}$ = 5 ft/sec. In almost all cases the maximum temperature was found to occur at a model reference velocity, $U_{m_{ref}} \approx 5$ ft/sec. Temperature rise data for sampling points No. 3 and 5 with $U_{m_{ref}} = 5$ ft/sec. have been plotted in Figure 38 as a function of wind direction.

The large peaks for the rooftop sampling points (3 and 5) are obvious in Figure 38. The variation of temperature rise with wind speed for sampling point No. 3 is shown in Figure 39 for both the standard stack and the extended stack. As discussed previously, the critical wind speed for this location is $U_{m_{ref}} \approx 4$ ft/sec. for the standard stack and $U_{m_{ref}} \approx 6$ ft/sec. for the extended stack. The maximum temperature rise with the standard stack approaches $\Delta T_f \approx 8$ degrees Fahrenheit at the critical wind speed. If this value is increased by a factor of 20, as discussed previously, one obtains 160°F as an estimate of the maximum instantaneous temperature rise on the roof. This would not appear to be high enough to cause concern about ignition of the roofing material. In addition, the maximum average temperature rise of 8 degrees occurs only for non-prevailing northerly wind directions. Moreover the rooftop temperature drops rapidly for wind speeds $U_{m_{ref}} < 3$ ft/sec. (full-scale winds $U_w < 15$ mph). The fact that the highest temperature rise generated by the exhaust plume impinging on the roof occurs only under moderately windy conditions is an advantage since the presence of the wind tends to dissipate heat generated by solar radiation on the roofing material.

The above discussion of the CRF rooftop temperatures is based on data from sampling point No. 3. Data measured at sampling point No. 5 are quite similar except that the critical wind direction is 300 degrees rather than 30 degrees. Measurements at sampling point No. 4 on the roof indicated substantially smaller maximum temperatures ($\Delta T_f = 1.7$ °F at $\theta = 330$ deg.) than those obtained at locations 3 and 5. In the two worst cases (locations 3 and 5) extending the stacks reduced the maximum temperature rise on the roof by at least 40 percent.

Following the rooftop temperature data, the next largest temperatures observed occurred at ground level beside the whirl tower (sampling point locations 14(b) and 15(b) in Figure 8). The variation of ΔT_f with wind direction for these points is shown in Figure 38 for $U_{m_{ref}} = 5$ ft/sec. In each case the temperature peaks for wind directions which place the sampling points approximately downwind of the stack. The variation of temperature with wind speed is shown in Figure 40 for sampling points No. 14(b) and 15(b) for a

33

wind direction of 180 degrees. This wind direction is near the critical value
for both sampling locations. Figure 40 indicates that the critical wind speed
is near $U_{m_{ref}}$ = 5 ft/sec. for locations 14(b) and 15(b) with the standard stack
and Figure 38 shows that at this wind speed, the maximum temperature, rise is
$\Delta T_f \simeq$ 5 1/2 degrees Fahrenheit at location 15(b) and a wind direction of about
200 degrees. Extending the stack reduces the maximum values of ΔT_f at these
locations but the reduction is not as great as in the CRF inlet or on the CRF
roof.

As discussed previously, the influence of the CRF building wake on
plume dispersion will probably keep the instantaneous peak temperature rise
from exceeding the measured ΔT_f values by more than a factor of 5. Using
this value gives instantaneous temperature peaks of 25 to 30 °F above ambient
near the base of the whirl tower. These temperatures would be very uncomfortable
to pedestrians on a hot day. The wind directions which induce these temper-
atures are near the prevailing southwest wind direction.   Thus, it is recom-
mended that the area near the whirl tower be closed to pedestrian traffic
when the CRF is operated. If this is not feasible as a general rule, the area
should be closed at least when the CRF is operated under southerly wind con-
ditions at full-scale wind speeds, U_w in excess of 10 miles per hour ($U_{m_{ref}} \approx$
2 ft/sec.).

Thus far, the temperature rise observed in the CRF inlet, inside the
CRF building, on the CRF roof, and at ground level near the whirl tower has
been discussed. In addition to these locations, data were measured at various
ventilation intakes on nearby buildings (sampling points No. 6 through 13,
14(a) and 15(a)). The majority of these data can be seen in Figures 22 through
33. Inspection of these figures shows that the largest temperature rise occurs
at sampling points 6, 7 and 8 at a wind direction of 150 degrees. The tempera-
ture rise observed here is more than twice as large as that obtained at any
other ventilation intake. The largest value of ΔT_f occurred at sampling
point No. 6 with $U_{m_{ref}}$ = 5 ft/sec. and θ = 150 degrees. The variation of
ΔT_f with wind direction for this location is included in Figure 38 for

$U_{m_{ref}}$ = 5 ft/sec. The variation of ΔT_f with wind speed for θ = 150 degrees is shown in Figure 41 for sampling points No. 6 and 8. Data obtained at sampling point No. 7 fall between the data at points 6 and 8.

Combined inspection of Figures 38 and 41 suggests that the maximum value of ΔT_f is close to 3 deg. F for sampling point No. 6 and that it occurs for wind conditions close to $U_{m_{ref}} \approx 5$ ft/sec. and θ = 150 degrees. Here again it is estimated that the instantaneous peak temperature rise will exceed the time averaged ΔT_f values by less than a factor of 5. Thus, the instantaneous peak temperature rise should not exceed 15°F for sampling point No. 6 and will be substantially less for all other intakes except nearby intakes 7 and 8. This indicates that there are no serious temperature problems at the ventilation intakes. However, an average temperature rise of 3 °F for the intake at location 6 and nearly similar values for locations 7 and 8 suggest that the buildings these intakes service (presumably buildings 62 and 23 in Figure 8) may become slightly uncomfortable on a hot day with winds blowing from the south to southeast. The extended stack does little to improve this situation. Note however that the most uncomfortable day is usually hot with little or no wind. Under low wind conditions, that is $U_{m_{ref}} \lesssim 2$ ft/sec. or $U_w \lesssim 10$ miles per hour, the exhaust plume will have negligible effect on the ventilation intakes.

In addition to determining the temperature rise induced by the CRF exhaust in the immediate vicinity of the exhaust stack, the rise in temperature at greater distances was of some concern because of possible effects on local trees and other plants. Specifically the temperature rise in a small park area directly east of the CRF between "L" Street and Skyline Drive was of interest. This area can be seen on the map in Figure 9 on which a five point sampling array is overlaid. As described in Section IV-B, "far-field" temperature rise data were obtained on a circular arc segment 1600 full-scale feet downwind of the exhaust stack. The 1600 foot radius circle intersects the park area between "L" Street and Skyline Drive.

The far-field temperature rise data are shown in Figures 34 through 37 for wind directions of 0, 90, 180 and 270 degrees. Parts a, b and c of each figure show data obtained at different reference wind velociti.s. As can be seen, the maximum temperature rise observed for any wind condition is 0.3 deg. Fahrenheit. The data shown are for the standard stack with exhaust condition 1 ($W_f = 90^\#/sec$, $\Delta T_{s_f} = 950°F$) . Tests for all other conditions (wind direction, extended stack, exhaust condition 2, change in upstream ground) provided essentially the same results as Figures 34 through 37. Thus the maximum time-averaged temperature rise near ground level 1600 feet from the CRF exhaust stack does not exceed 0.3 deg. Fahrenheit. This is a very low value and should have no effect on trees and other vegetation. Instantaneous peak temperature rises can be expected to reach one or two degrees Fahrenheit in the park area. These values may be noticeable but they should not cause discomfort.

The data presented and discussed thus far were obtained with a model exhaust gas mixture (condition 1) which simulated a compressor absorbing 30,000 horsepower operating at a weight flow of 90 pounds per second to give a temperature rise of 950 degrees Fahrenehit. The 30,000 horsepower is the maximum available in the CRF drive. As noted in Section IV-B, this exhaust condition is believed to be the "worst case" from a thermal pollution viewpoint. To verify that this is indeed a "worst case", a series of tests were performed with a second model gas mixture (condition 2) simulating a compressor weight flow of 150 pounds per second and absorbing the same horsepower. The test schedule in Table 2 lists those tests which were performed with the condition 2 exhaust gas mixture.

Temperature rise data obtained with both exhaust gas mixtures are compared in Table 5 for all tests performed at a model reference velocity $U_{m_{ref}}$ = 5 ft/sec. These data are representative also of data measured with $U_{m_{ref}}$ = 7 ft/sec. Inspection of Table 5 shows that both exhaust gas conditions gave nearly identical temperature rise data at most points. In those cases where there was a difference, exhaust condition 1 usually provided the highest temperature rise.. The largest deviation from this trend can be seen

36

for sampling point 15(b) for a 180 deg. wind. Here the condition 1 exhaust gave ΔT_f = 4.7 deg. while the condition 2 exhaust gave ΔT_f = 5.1 deg. The difference in these two values is within the repeatability of the measurements for this location. Thus it is concluded that the data obtained with the condition 1 exhaust is representative of the worst case from a thermal pollution viewpoint.

The final series of tests performed on the CRF model were designed to study the effect of changing the upstream terrain on the measured data. Up to this point, all of the temperature rise data were obtained with an upstream terrain composed of wooden blocks (Figure 2) whose heights are scaled to match the approximate mean height of trees and buildings in the full-scale approaching fetch. However, as discussed in Section IV-A, the full-scale upstream terrain is very flat with few buildings or trees for winds approaching from about 200 to 270 degrees. Thus it is of interest to determine if a smoother approaching fetch changes the temperature rise data. For this purpose, additional tests were performed with the 12 feet of model ground (7200 feet in full-scale) closest to the turntable replaced by small gravel elements to simulate the smooth full-scale terrain. As noted in Section V-A, velocity measurements above the CRF model building suggested that the change in upstream ground would have little effect on the temperature measurements.

The tests with the gravel ground upstream were performed for wind directions of 210 and 270 degrees. The original data obtained with the wooden-block ground showed that it was not worthwhile to repeat these tests with a 240 deg. wind. For this wind direction there was a negligible temperature rise at all of the sampling points in the near field (see Figure 30). The data obtained with the gravel ground are compared to that obtained with the wooden blocks in Table 6. Note that sampling point locations in the near field which are not listed in this table gave ΔT_f = 0 for both upstream grounds. In general, the data obtained with the two upstream grounds are nearly identical. Differences are within the repeatability of measurements for identical test conditions. Thus it is concluded that the data obtained

with the wooden block ground are representative of full-scale for the wind approaching from any direction. Full-scale differences in upstream terrain for different wind directions will not significantly effect the test results or conclusions presented previously.

SECTION VI

SUMMARY AND CONCLUSIONS

An experimental study has been conducted on a 1:600 scale model of the Compressor Research Facility (CRF) and surrounding vicinity of Area B at Wright-Patterson Air Force Base, Ohio. The primary purpose of this study was to determine the conditions under which hot air from the exhaust stack of the facility might be recirculated back into the inlet and the severity of the inlet temperature rise when such recirculation occurs. Secondary objectives were to determine the temperature rise at ventilation intakes on nearby buildings and to assess the effect of the hot exhaust plume on trees and vegetation in a park area east of the CRF.

The tests were performed in the Calspan Atmospheric Simulation Facility which is a low speed wind tunnel specifically designed to model both the mean and turbulent flow properties in the earth's boundary layer. The tests included qualitative flow visualization studies and quantitative measurements to determine temperatures at twenty different locations on the model. The schedule for the quantitative measurements included 94 tests. Primary variables in the tests were wind speed and wind direction. In addition, two exhaust stack configurations, a standard design and a slightly higher or extended design, were studied. Finally, two exhaust gas mixtures were used to simulate compressors operating at full-scale weight flows of 90 pounds/second and 150 pounds/second and converting into heat the full 30,000 horsepower available in the CRF drive system.

The data measured in the CRF inlet indicate that recirculation of the hot exhaust back into the inlet is not a problem. With the standard stack, the maximum time-averaged temperature rise observed in the inlet was only 1.2 degrees Fahrenheit above ambient. The corresponding instantaneous peak temperature rise is not expected to exceed about 6 degrees Fahrenheit. Use of the extended stack design would approximately halve these values. With both exhaust stacks, non-zero temperatures occur only for a narrow range of wind directions (0 to 60 degrees) and full-scale wind speeds in excess of 15 miles per hour. Since the prevailing wind direction in the area is from the southwest (235 deg.), the CRF inlet should be completely isolated from the hot exhaust for most of the time.

Measurements were made inside of the porous-walled CRF building to determine the temperature there. The maximum time-averaged temperature rise with the standard stack was again 1.2 degrees Fahrenheit. It occurs with a wind direction of 330 degrees and a full-scale wind speed of about 30 miles per hour. Extending the stack reduced the maximum to 0.3 deg. Fahrenheit. Here again the hot exhaust should not create problems since the induced temperature rise is small and the corresponding wind is not from the prevailing direction.

Data were measured at three locations on the roof of the CRF. The highest time-averaged temperature rise observed anywhere in the flowfield occurred at two of these locations. With the standard stack the maximum time-averaged value reached 8 degrees Fahrenheit for a wind direction of 30 degrees and a full-scale wind speed of about 20 miles per hour. The corresponding instantaneous peak temperature rise for this situation is estimated to be no larger than 160 degrees Fahrenheit. The maximum 8 degree time-average and 160 degree instantaneous peak values do not appear large enough to cause concern over ignition of the roofing material on the CRF. Moreover these values occur only for non-prevailing northerly wind directions and at full-scale wind speeds in excess of 15 miles per hour. For other wind conditions the temperature rise on the roof is negligible. Use of the extended stack reduces the maximum time-averaged temperature rise on the roof by more than 40 percent.

Measurements were made to determine temperatures at the location of 10 intakes for ventilation systems on nearby buildings. The largest effect occurred on intakes north of the CRF, near buildings 23 and 62. With the standard stack, the maximum time-averaged temperature rise was near 3 degrees Fahrenheit for a wind direction of 150 degrees and a full-scale wind speed of about 24 miles per hour. The corresponding instantaneous peak temperature rise is estimated to be 15 degrees Fahrenheit or less. Other ventilation intakes located south and west of the CRF displayed maximum time-averaged temperature rises less than half of the above and these maxima occurred for non-prevailing wind directions. In general these results suggest that there are no serious temperature problems at the building ventilation intakes. The

40

buildings serviced by the intakes north of the CRF (presumably building 23 and 62) may become slightly uncomfortable on a hot day with southerly winds and full-scale wind speeds in excess of 10 miles per hour. The extended stack was not very effective in reducing the temperature at the ventilation intakes north of the CRF.

The final set of measurements in the immediate vicinity of the CRF were made at two ground level locations near the rotor whirl tower situated just north of the CRF exhaust stack. The flow visualization studies with smoke suggested that pedestrians might encounter high temperatures in this area if the wind is approaching from the south. The quantitative measurements showed a maximum time-averaged temperature rise of 5½ degrees Fahrenheit for a wind direction of 200 degrees and a full-scale wind speed of 24 miles per hour. Instantaneous temperature peaks of 25 to 30 degrees Fahrenheit above ambient are expected under these conditions. These temperatures could be very uncomfortable to pedestrians on a hot day. The extended stack reduced the observed maximum temperature rise only a moderate amount (about 20 percent). Since the wind directions which induce these ground level temperatures are near the prevailing wind direction, it is recommended that the area near the whirl tower be closed to pedestrian traffic when the CRF is operated.

To assess the effect of the CRF exhaust plume on trees and other vegetation in the park area east of the CRF, measurements were made to determine temperatures on a circular arc segment 1600 feet downwind of the exhaust stack in full scale. In this way data were obtained in the park area for winds from the west and additional data were obtained on a 1600 foot radius circle for other wind directions. The maximum time-averaged temperature rise observed in any of these tests was 0.3 degrees Fahrenheit. This low value should have no effect on trees or other vegetation. The corresponding instantaneous temperature rise may reach 1 or 2 degrees Fahrenheit in the park area and may be just noticeable to pedestrians.

Table 1

SUMMARY OF CRF MODEL FLOW QUANTITIES AND CONVERSION FACTORS

	EXHAUST CONDITION 1	EXHAUST CONDITION 2
FULL-SCALE COMPRESSOR WEIGHT FLOW, W_f (lb/sec)	90	150
FULL-SCALE EXHAUST TEMPERATURE RISE, ΔT_{s_f}, (°F)	950	570
FULL-SCALE EXHAUST GAS TO AMBIENT AIR DENSITY RATIO, $(\rho_s/\rho_a)_f$	0.3624	0.4865
MODEL EXHAUST GAS TO AMBIENT AIR DENSITY RATIO, $(\rho_s/\rho_a)_m$	0.0779	0.1402
MODEL INTAKE VOLUME FLOW, ϕ_{i_m}, (cm³/sec)	414	689
MODEL EXHAUST VOLUME FLOWS: HELIUM, ϕ_{H_e}, (cm³/sec)	300	300
HYDROGEN, ϕ_{H_2}, (cm³/sec)	2161	2152
NITROGEN, ϕ_{N_2}, (cm³/sec)	0	185
TOTAL EXHAUST, ϕ_{s_m}, (cm³/sec)	2461	2637
MODEL TO FULL-SCALE WIND VELOCITY RATIO, $\left(\dfrac{U_{a_m}}{U_{a_f}}\right)$	0.072	0.072

RELATION BETWEEN FULL-SCALE TEMPERATURE RISE, (ΔT_f), AND MODEL HELIUM CONCENTRATION, C_m

$$\Delta T_f = \frac{1.307 \times 10^3 \, C_m}{1 - 2.43 \times 10^{-3} \, C_m} \qquad \left(\begin{array}{c}\text{SAME FOR BOTH}\\ \text{EXHAUST CONDITIONS}\end{array}\right)$$

GENERAL: GEOMETRIC SCALE RATIO 1:600

FULL-SCALE AMBIENT AIR TEMPERATURE, $T_{a_f} = 80$ °F = 540 °R; AMBIENT AIR DENSITY, $\rho_{a_m} = \rho_{a_f} = 0.0023$ slugs/ft³

GAS DENSITY RATIOS: $\rho_{H_2}/\rho_a = 0.0695$, $\rho_{H_e}/\rho_a = 0.1381$; $\rho_{N_2}/\rho_a = 0.9675$

Table 2
SCHEDULE OF QUANTITATIVE TESTS ON CRF MODEL

	MODEL REFERENCE VELOCITY, $U_{m_{ref}}$ (ft/sec)				
UPSTREAM GROUND	ALL WOODEN BLOCKS (48 ft)			32 ft WOODEN BLOCKS + 12 ft GRAVEL	
WIND DIRECTION (degrees)	CONDITION 1 EXHAUST W_f = 90 lb/sec, ΔT_{t_f} = 950 °F	CONDITION 2 EXHAUST W_f = 150 lb/sec, ΔT_{t_f} = 570 °F	CONDITION 101 EXHAUST (CONDITION 1 WITH STACK EXTENSION)	CONDITION 1 EXHAUST W_f = 90 lb/sec, ΔT_{s_f} = 950 °F	CONDITION 101 EXHAUST (CONDITION 1 WITH EXTENSION)
0	3, 5, 7	5, 7	3, 5, 7		
30	2, 3, 5, 7	5, 7	2, 3, 5, 7		
60	3, 5, 7	5, 7	3, 5, 7		
90	3, 5, 7	5			
120	5, 7	5			
150	3, 5, 7	5, 7	5, 7		
180	3, 5, 7	5, 7	3, 5, 7		
210	3, 5, 7	5	5	3, 5, 7	3, 5, 7
240	5, 7	5, 7	5		
270	3, 5, 7	5, 7	3, 5, 7	3, 5, 7	3, 5, 7
300	3, 5, 7	5	3, 5, 7		
330	3, 5, 7	5, 7	3, 5, 7		

Table 3

SUMMARY OF CRF INLET TEMPERATURE RISE, $\Delta T_{f_{inlet}}$

FOR CONDITION 1 EXHAUST GAS; W_f = 90 lb/sec, ΔT_{s_f} = 950 °F

INLET TEMPERATURE RISE, $\Delta T_{f_{inlet}}$ (FULL-SCALE °F)

REFERENCE VELOCITY	$U_{m_{ref}}$ = 2 ft/sec		$U_{m_{ref}}$ = 3 ft/sec		$U_{m_{ref}}$ = 5 ft/sec		$U_{m_{ref}}$ = 7 ft/sec	
WIND DIRECTION (degrees)	STANDARD STACK	EXTENDED STACK	STANDARD STACK	EXTENDED STACK	STANDARD STACK*	EXTENDED STACK	STANDARD STACK	EXTENDED STACK
0	—	—	0.1	0	0.1	0	0.1	0
30	0.2	0	0.5	0.2	1.1	0.5	1.0	0.5
60	—	—	0	0	0.2	0	0.2	0.1
90	—	—	0	—	0	—	0	—
120	—	—	—	—	0	—	0	—
150	—	—	0	0	0	0	0	0
180	—	—	0	0	0	0	0	0
210	—	—	0	—	0	0	0	—
240	—	—	—	—	0	0	0	—
270	—	—	0	0	0, (0.3)	0	0, (0.4)	0, (0.1)
300	—	—	0, (0.2)	0	0.1, (0.6)	0, (0.1)	0.1, (0.9)	0, (0.2)
330	—	—	0.1, (0.3)	0, (0.1)	0.2, (0.7)	0, (0.2)	0.2, (1.2)	0.1, (0.3)

NOTE. NUMBERS IN PARENTHESES SHOW NON-ZERO ΔT_f VALUES MEASURED AT SAMPLING POINT NO. 2 INSIDE CRF BUILDING.

Table 4

SUMMARY OF MAXIMUM NEAR-FIELD TEMPERATURE RISE, $\Delta T_{f_{max}}$, AND ITS LOCATION. CONDITION 1 EXHAUST GAS; $W_f = 90$ lb/sec, $\Delta T_{s_f} = 950°F$

MAXIMUM TEMPERATURE RISE, $\Delta T_{f_{max}}$ (FULL-SCALE °F), & CORRESPONDING SAMPLING POINT NUMBER (IN PARENTHESES). SEE FIGURE 8 FOR SAMPLING POINT LOCATIONS

REFERENCE VELOCITY	$U_{m_{ref}} = 2$ ft/sec		$U_{m_{ref}} = 3$ ft/sec		$U_{m_{ref}} = 5$ ft/sec		$U_{m_{ref}} = 7$ ft/sec	
WIND DIRECTION (degrees)	STANDARD STACK	EXTENDED STACK	STANDARD STACK	EXTENDED STACK	STANDARD STACK	EXTENDED STACK	STANDARD STACK	EXTENDED STACK
0	–	–	0.8 (4)	0.4, (3)	1.0, (4)	0.8 (4)	1.0, (4)	0.8, (4)
30	2.9, (3)	0.4, (3)	7.1, (3)	1.3, (3)	7.5, (3)	4.1, (3)	5.6, (3)	4.1, (3)
60	–	–	2.4, (3) [1.1, (13)]	0.7, (13) [0.2, (3)]	2.0, (3) [0.9, (13)]	0.9, (13) [0.6, (3)]	1.3, (3) [1.2, (10)]	0.9, (10) [0.8, (3)]
90	–	–	0.6, (9	–	1.2, (9)	–	1.4, (9)	–
120	–	–	–	–	0.9, (9)	–	1.1, (9)	–
150	–	–	2.7, (14b) [1.3, (8)]	0.7, (8) [0.5, (14b)]	3.5, (14b) [2.5, (6)]	2.1, (14b) [2.1, (6)]	3.7, (14b) [2.1, (6)]	2.7 (14b) [2.2, (6)]
180	–	–	2.8, (15b) [1.9, (14b)]	1.1, (14b) [0.7, (15b)]	4.7, (15b) [4.2, (14b)]	2.9, (14b) [2.8, (15b)]	4.3, (14b) [3.9, (15b)]	3.7, (15b) [3.0, (14b)]
210	–	–	2.0, (15b)	–	4.8, (15b)	3.3, (15b)	4.3, (15b)	–
240	–	–	–	–	0.1, (15b)	0	0.2, (15b)	–
270	–	–	0.3, (5)	0.1 (5)	0.7, (5)	0.2, (5)	0.7 (5)	0.3, (5)
300	–	–	3.8, (5)	0.9 (5)	6.3, (5)	2.4, (5)	5.8 (5)	3.2, (5)
330	–	–	1.8, (5) [1.7, (4)]	0.5, (4) [0.3, (5)]	3.2, (5)	1.0, (5)	3.5, (5)	1.2, (5)

Table 5
COMPARISDN OF ΔT_f DATA FOR STACK EXHAUST CONDITIONS 1 AND 2
MODEL REFERENCE VELOCITY $U_{m_{ref}}$ = 5 ft/sec

TEMPERATURE RISE, ΔT_f (FULL-SCALE °F)

WIND DIRECTION	0°		30°		60°		150°		180°		210°		270°		300°		330°	
SAMPLING POINT NO.	CONDITION 1	2	CONDITION 1	2	CONDITION 1	2	CONDITION 1	2	CONDITION 1	2	CONDITION 1	2	CONDITION 1	2	CONDITION 1	2	CONDITION 1	2
NEAR-FIELD (SEE FIGURE 8)																		
1	0.1	0.1	1.1	0.9	0.2	0.1	0	0	0	0	0	0	0	0	0.1	0.1	0.2	0.2
2	0	0	0	0	0	0	0	0	0	0	0	0	0.3	0.1	0.6	0.4	0.7	0.6
3	0.8	0.7	7.5	7.1	2.0	1.7	0	0	0	0	0	0	0	0	0	0	0	0
4	1.0	1.1	0.1	0.1	0	0	0	0	0	0	0	0	0	0	0.2	0.1	1.7	1.3
5	0.1	0.1	0	0	0	0	0	0	0	0	0	0	0.7	0.6	6.3	5.6	3.2	2.9
6	0	0	0	0	0	0	2.5	2.3	0.8	0.7	0	0	0	0	0	0	0	0
7	0	0	0	0	0	0	2.3	2.1	0.1	0.1	0	0	0	0	0	0	0	0
8	0	0	0	0	0	0	2.0	1.8	0.1	0.1	0	0	0	0	0	0	0	0
9	0	0	0	0	0.9	0.8	0.3	0.2	0	0	0	0	0	0	0	0	0	0
10	0	0	0.9	0.7	1.3	1.1	0	0	0	0	0	0	0	0	0	0	0	0
11	0	0	0.9	0.8	0.5	0.4	0	0	0	0	0	0	0	0	0	0	0	0
12	0	0	0.7	0.6	0.4	0.3	0	0	0	0	0	0	0	0	0	0	0	0
13	0	0	0.1	0	0.9	0.9	0	0	0	0	0	0	0	0	0	0	0	0
14(a)	0	0	0.2	0.2	0.4	0.4	-	-	-	-	-	-	-	-	0	0	0	0
15(a)	0.2	0.2	0.5	0.5	0	0	-	-	-	-	-	-	-	-	-	-	-	-
14(b)	-	-	-	-	-	-	3.5	3.2	4.2	3.5	0.2	0.2	0	0	-	-	-	-
15(b)	-	-	-	-	-	-	0.1	0.1	4.7	5.1	4.8	4.9	0	0	-	-	-	-
FAR FIELD (SEE FIGURE 9)																		
₵ - 30°	0	0	0	0	0	0	0	0	0	0	0	0	0	0	0	0	0	0
₵ - 15°	0.1	0.1	0.1	0.1	0.1	0.1	0	0	0	0	0.1	0.1	0.1	0.1	0.1	0.1	0.1	0.1
DOWNWIND ₵	0.2	0.2	0.2	0.3	0.3	0.3	0.3	0.3	0.3	0.3	0.3	0.3	0.3	0.2	0.3	0.3	0.3	0.2
₵ + 15°	0	0	0.1	0	0	0.1	0.1	0.1	0.1	0.1	0.1	0.1	0	0	0.1	0.1	0	0
₵ + 30°	0	0	0	0	0	0	0	0	0	0	0	0	0	0	0	0	0	0

Table 6

COMPARISON OF ΔT_f DATA OBTAINED WITH TWO DIFFERENT UPSTREAM GROUND CONFIGURATIONS. CONDITION 1 EXHAUST GAS;

$$W_f = 90 \text{ lb/sec}, \quad \Delta T_{s_f} = 950\ ^\circ F$$

TEMPERATURE RISE. ΔT_f (FULL-SCALE $^\circ$F)

MODEL REFERENCE VELOCITY $U_{m_{ref}}$ (ft/sec)	WIND DIRECTION = 210 degrees						WIND DIRECTION = 270 degrees					
	SAMPLE POINT NO 14(b)		SAMPLE POINT NO 15 (b)		FAR-FIELD MAXIMUM		SAMPLE POINT NO. 2		SAMPLE POINT NO. 5		FAR-FIELD MAXIMUM	
	ALL BLOCK GROUND	BLOCK PLUS GRAVEL	ALL BLOCK GROUND	BLOCK PLUS GRAVEL	ALL BLOCK GROUND	BLOCK PLUS GRAVEL	ALL BLOCK GROUND	BLOCK PLUS GRAVEL	ALL BLOCK GROUND	BLOCK PLUS GRAVEL	ALL BLOCK GROUND	BLOCK PLUS GRAVEL
STANDARD STACK												
3	0.1	0.1	2.0	2.0	0.3	0.3	0	0	0.3	0.4	0.2	0.2
5	0.2	0.2	4.8	4.7	0.3	0.3	0.3	0.3	0.7	0.6	0.3	0.3
7	0.2	0.2	4.3	4.6	0.2	0.3	0.4	0.4	0.7	0.6	0.2	0.3
EXTENDED STACK												
3	—	0.1	—	1.6	—	0.3	0	0	0.1	0.1	0.2	0.2
5	0.1	0.1	3.2	3.9	0.3	0.3	0	0.1	0.2	0.2	0.2	0.3
7	—	0	—	3.4	—	0.3	0.1	0.1	0.3	0.3	0.1	0.2

NOTE   ALL OTHER SAMPLING POINT LOCATIONS IN THE NEAR FIELD GAVE $\Delta T_f = 0$ FOR WIND DIRECTIONS OF 210 AND 270 degrees

TEST SECTION
NOMINAL SIZE = 6 FT HIGH X 8 FT WIDE
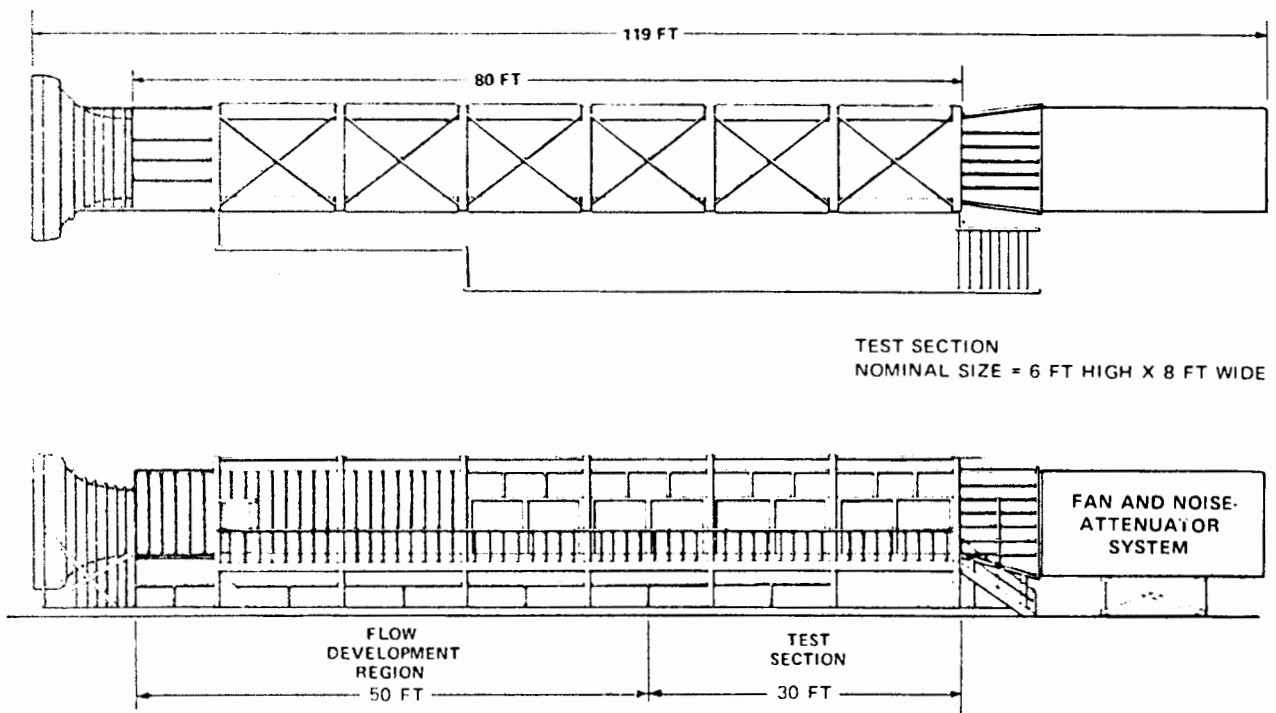
Figure 1   THE CALSPAN ATMOSPHERIC SIMULATION FACILITY (ASF)
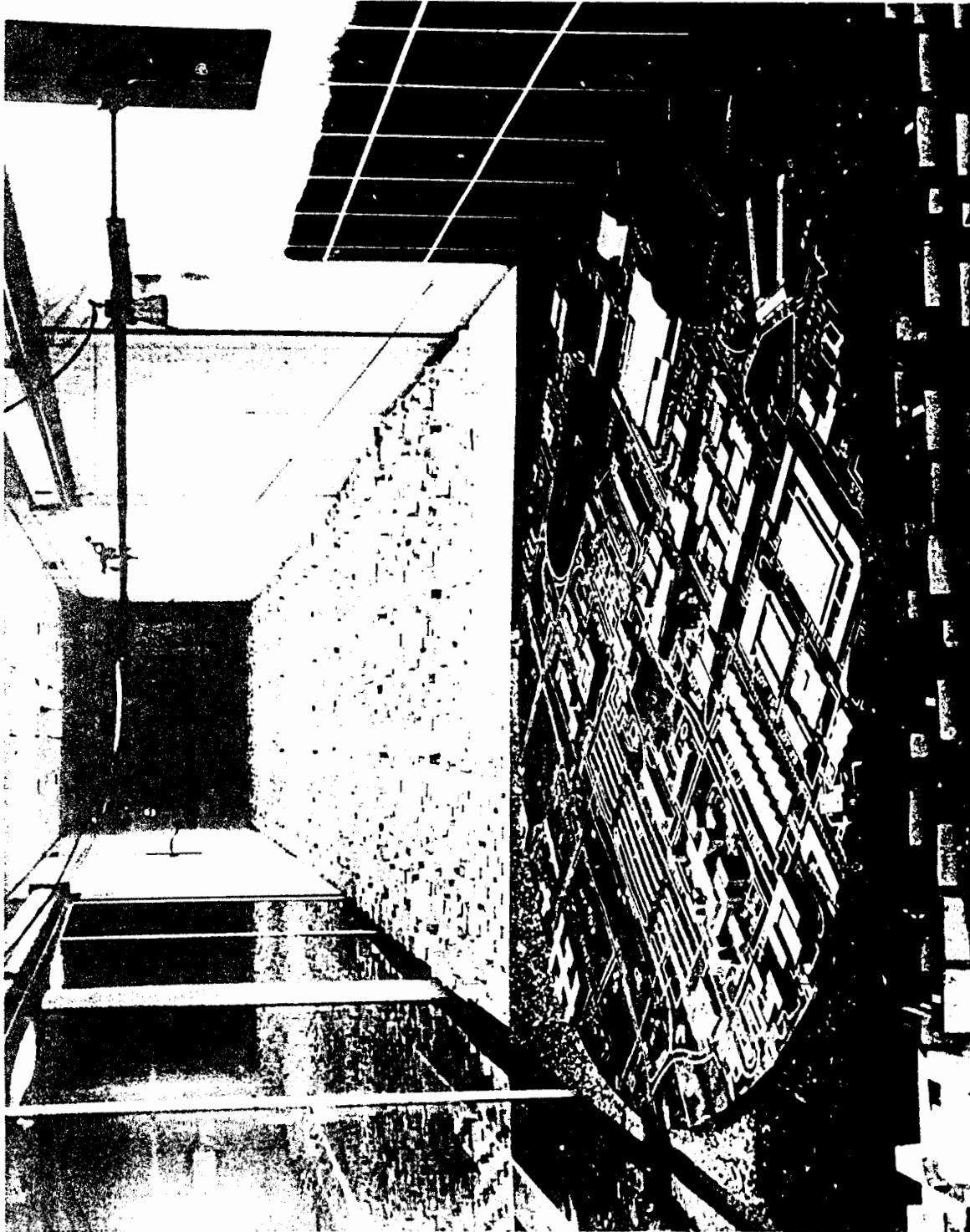
Figure 2   OVERALL VIEW OF CRF MODEL INSTALLED IN ATMOSPHERIC SIMULATION FACILITY (LOOKING UPSTREAM)
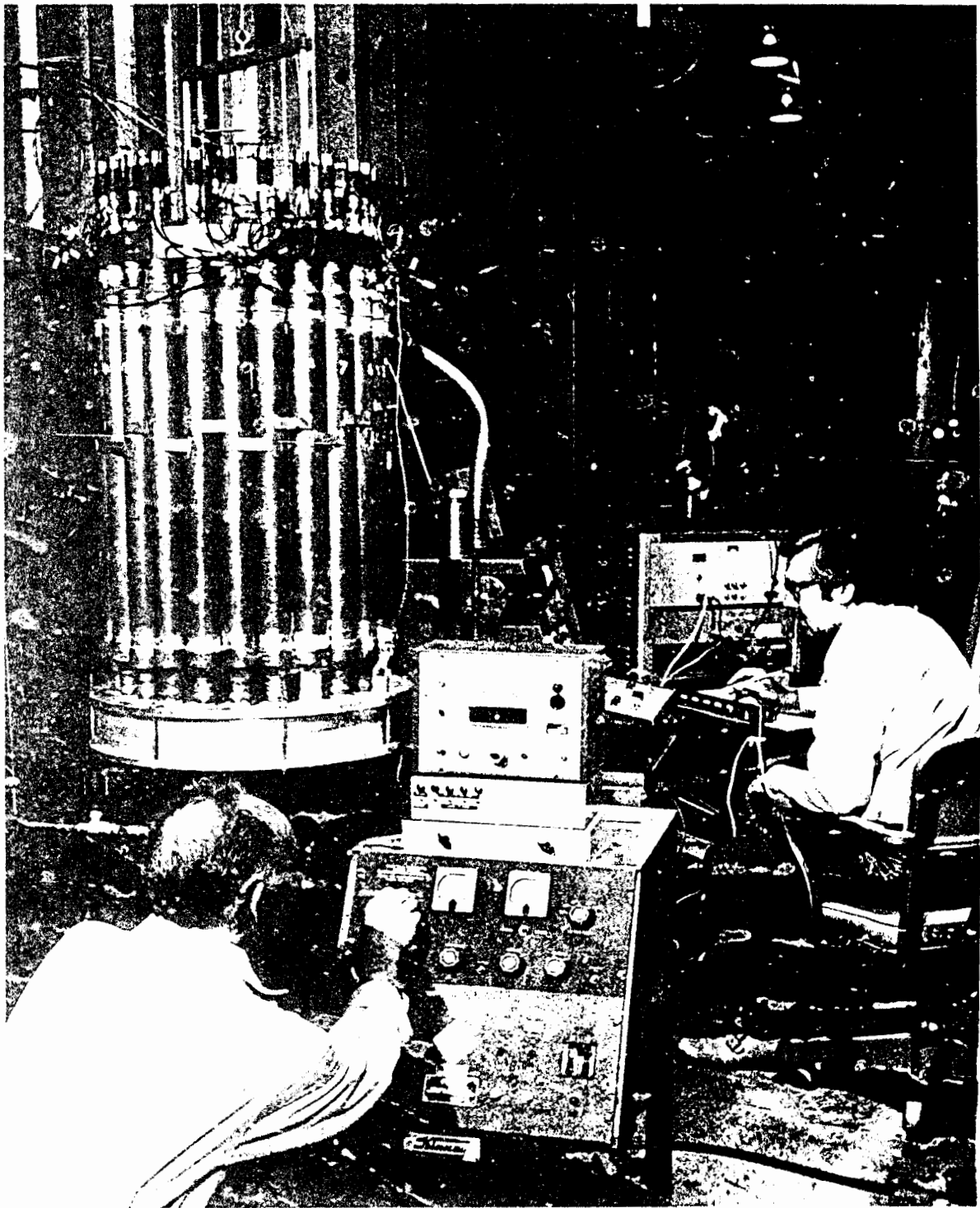
Figure 3   CONCENTRATION SAMPLING SYSTEM
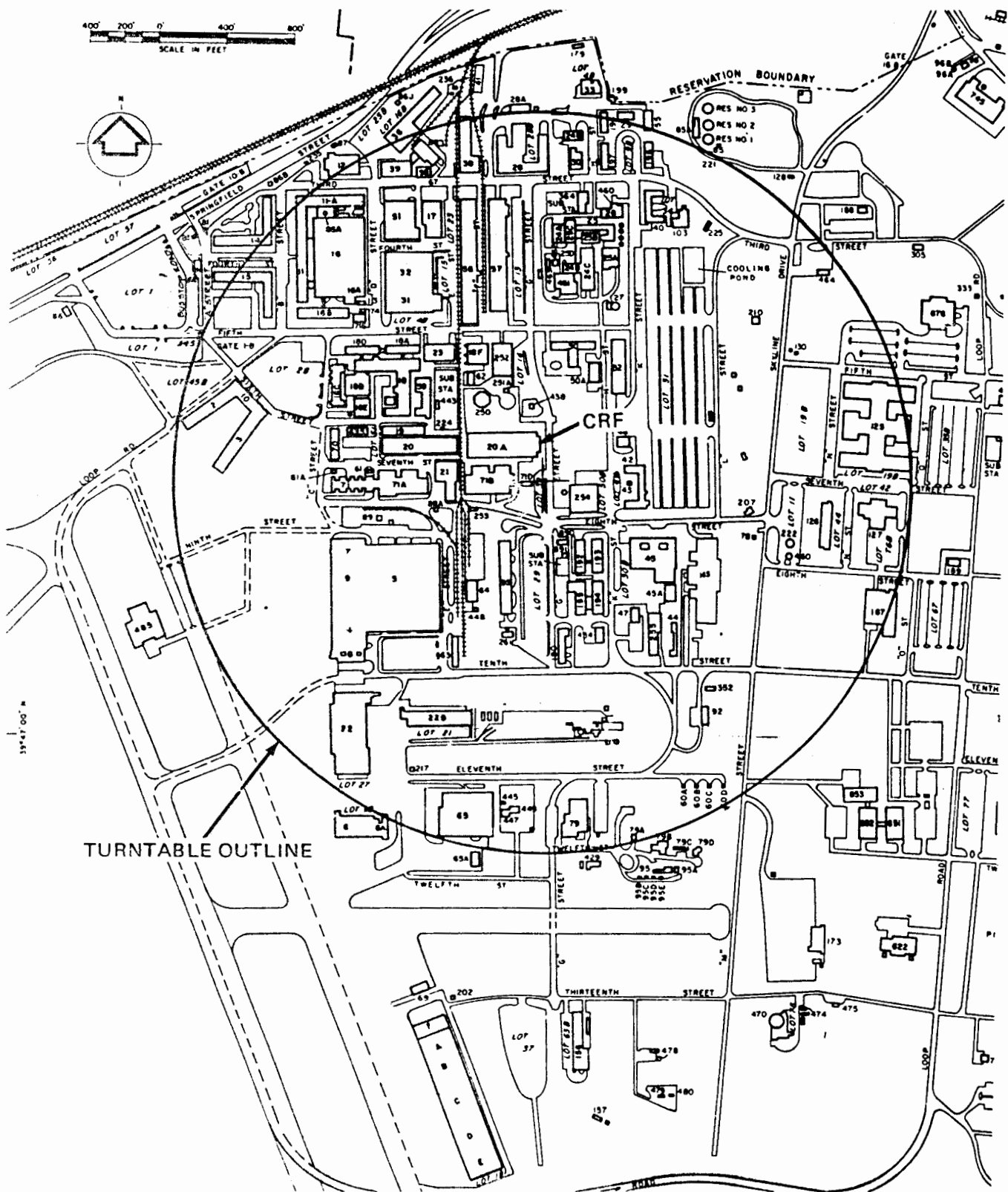
Figure 4   PLAN VIEW OF CRF AND SURROUNDING VICINITY OF AREA B
MODELED ON ASF TURNTABLE
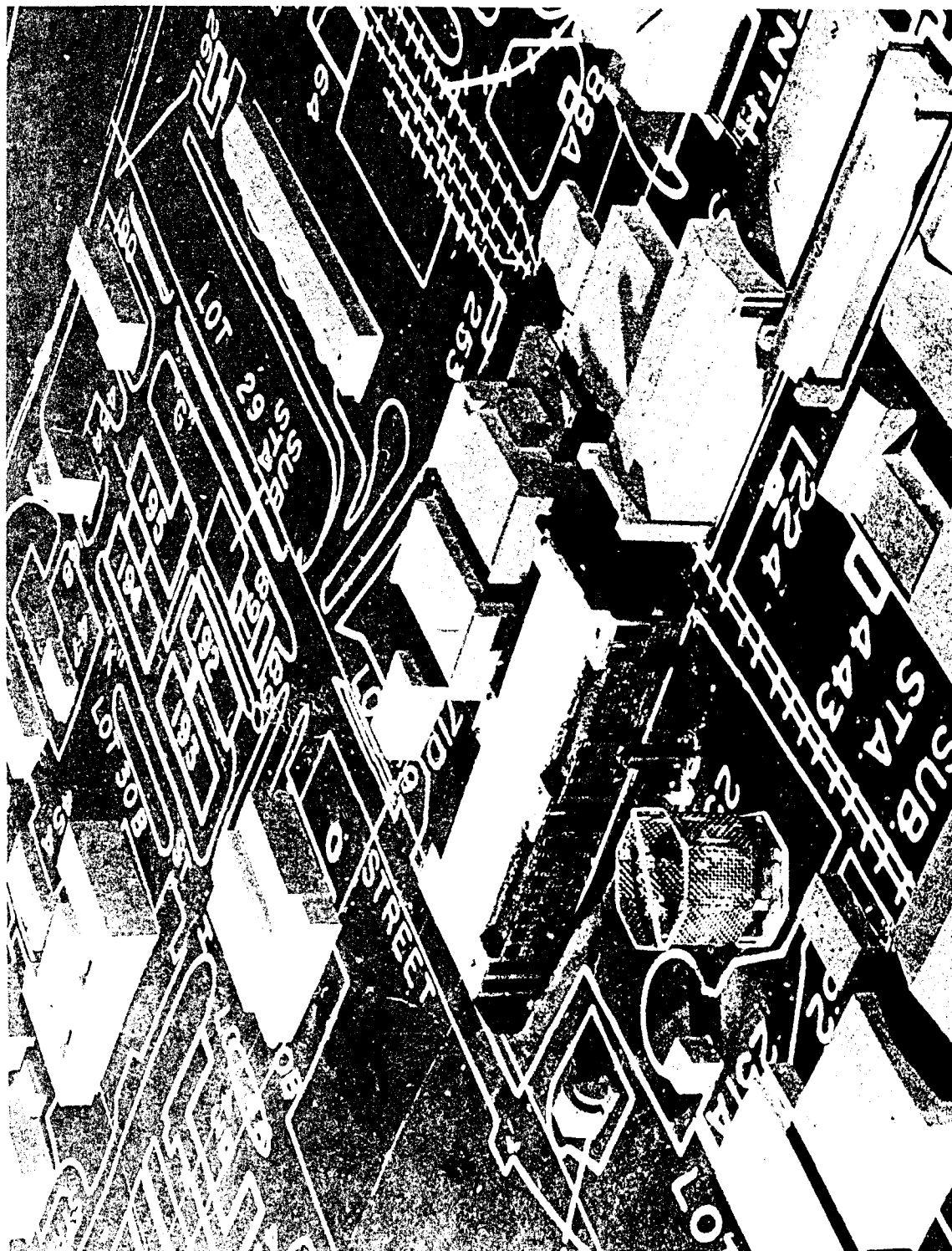
Figure 5   VIEW OF CRF MODEL WITH STANDARD EXHAUST STACK
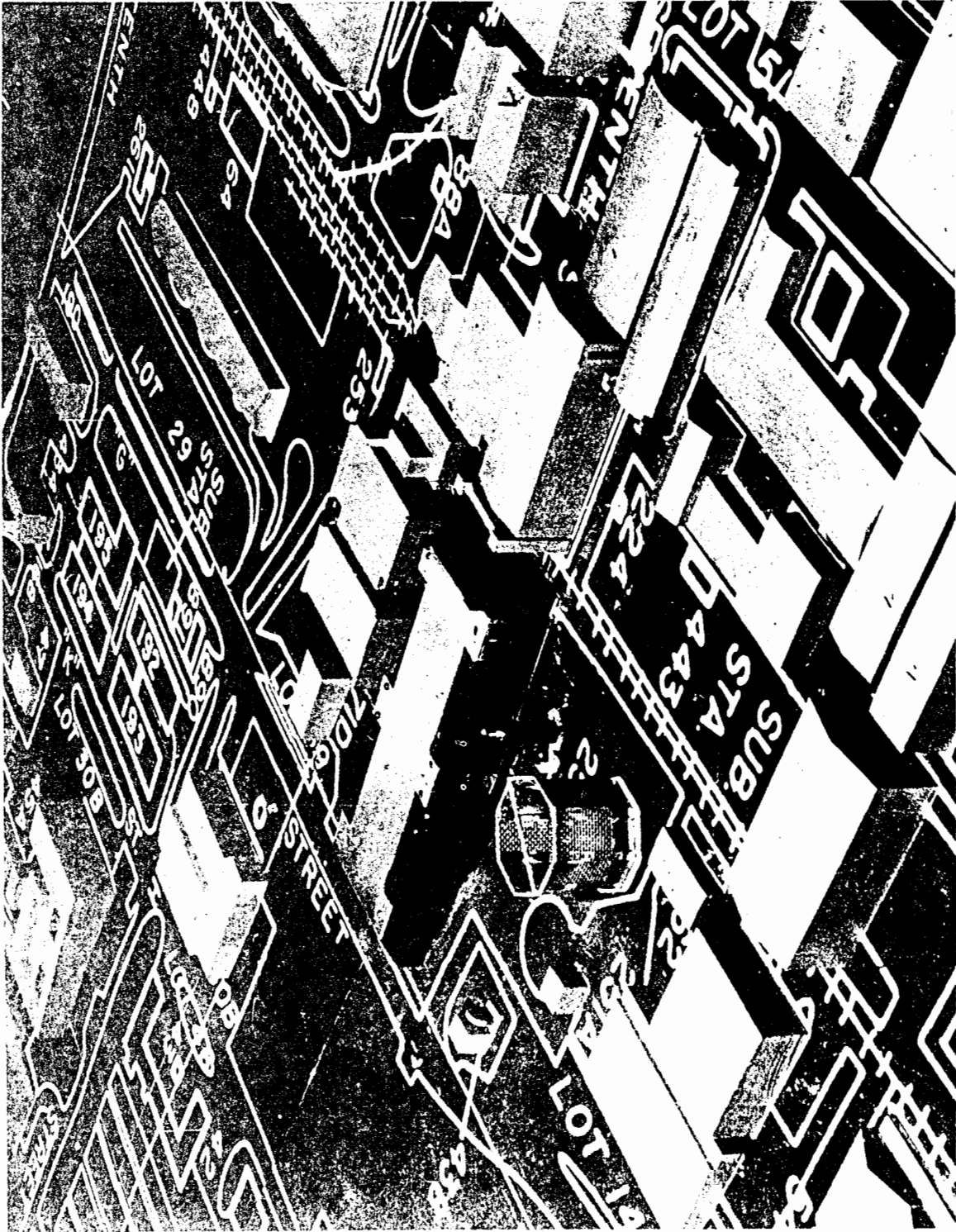
Figure 6 VIEW OF CRF MODEL WITH EXTENDED EXHAUST STACK
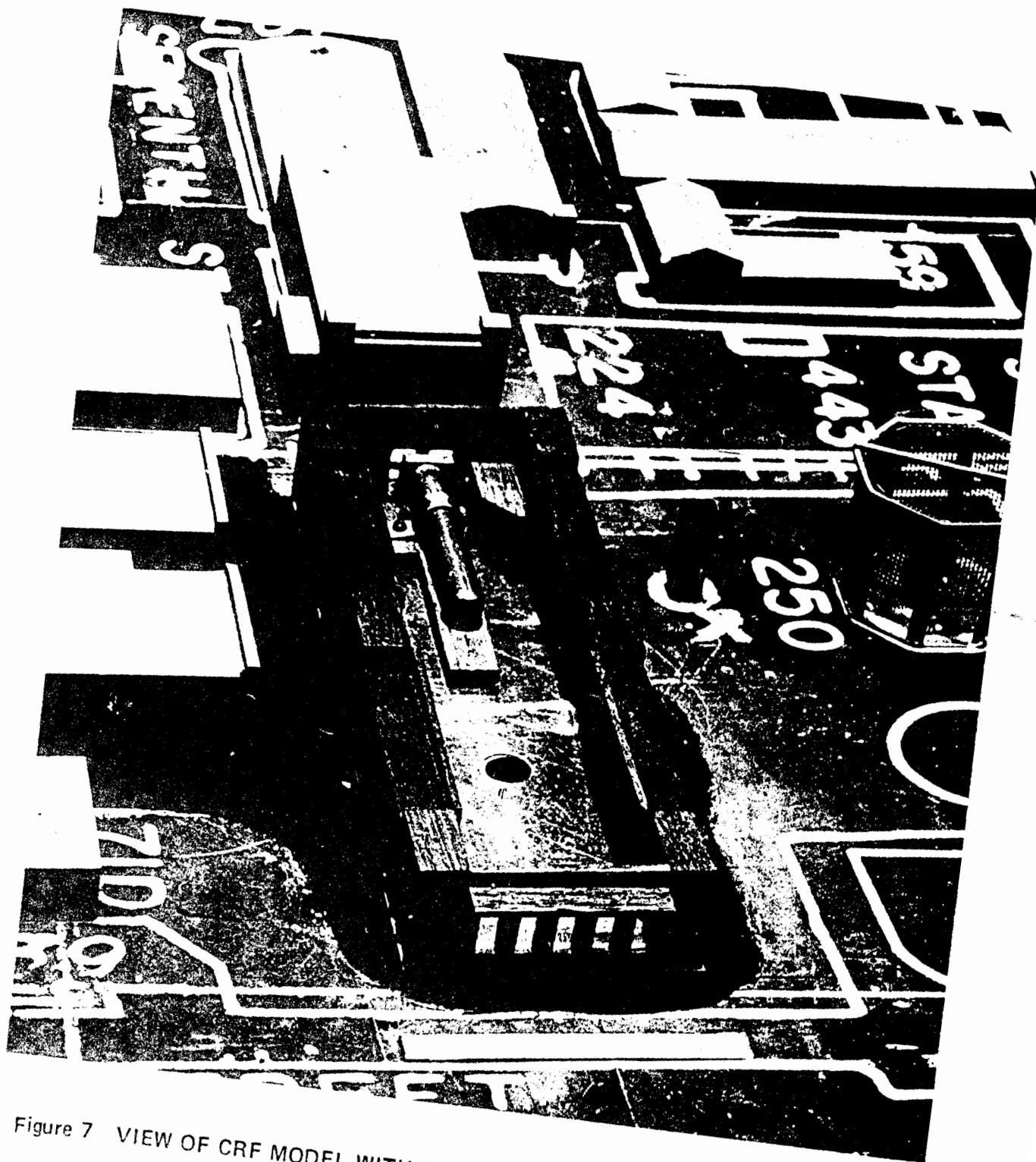
Figure 7   VIEW OF CRF MODEL WITH ROOF REMOVED TO SHOW INLET DUCTING

Figure 8   NEAR-FIELD SAMPLING POINT LOCATIONS FOR DETERMINING TEMPERATURE RISE ABOVE AMBIENT

NOTE: SAMPLING POINT LOCATIONS VARY WITH WIND DIRECTION. THEY ARE POSITIONED RELATIVE TO THE WIND VECTOR AS SHOWN.

NORTH

500'   250'   0'   500'

FULL-SCALE FEET

-30°

-15°

+15°

+30°

SAMPLING POINTS

1600 ft

EXHAUST STACK

TURNTABLE CENTER

WIND DIRECTION, θ (deg)

WIND
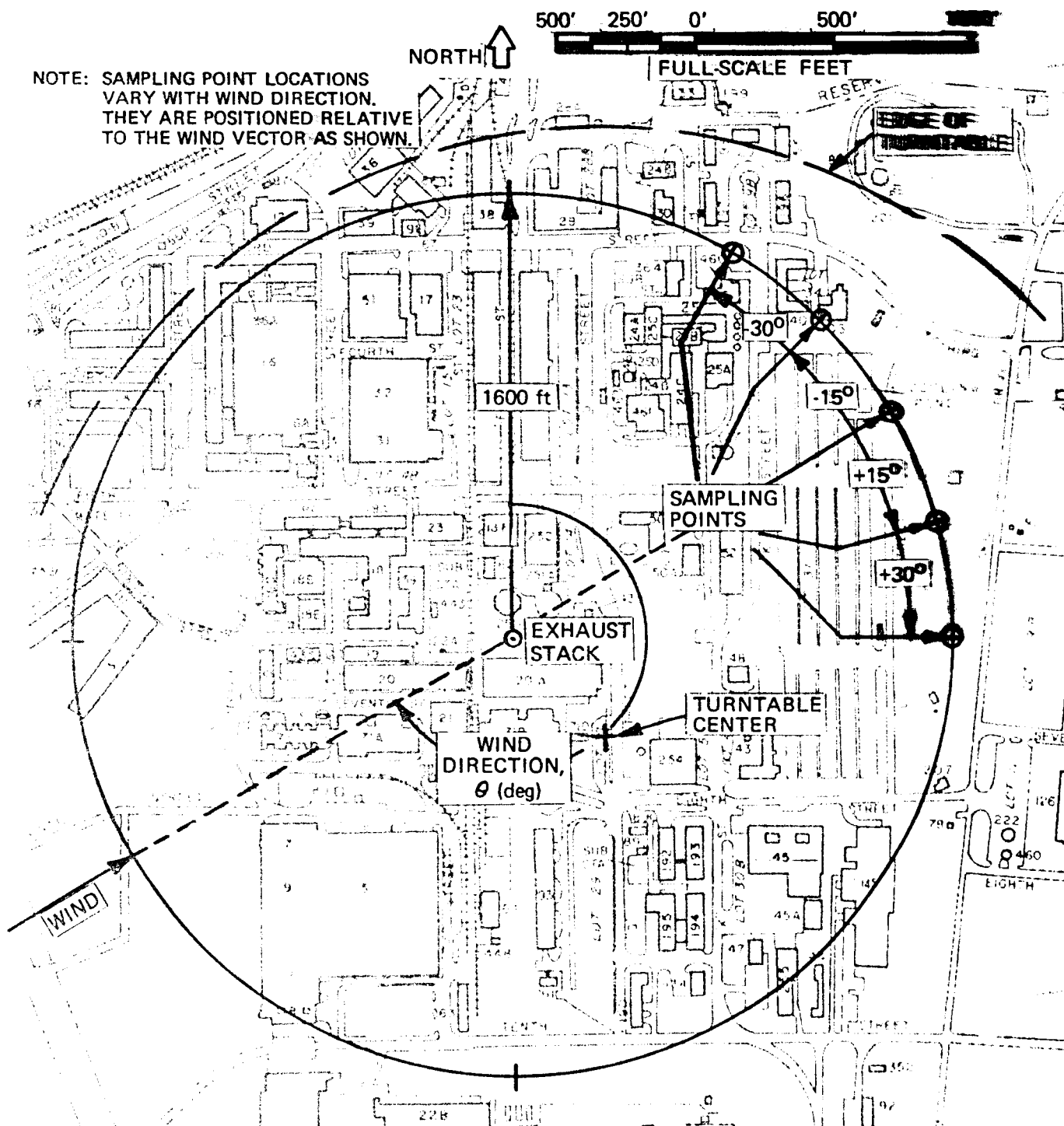
Figure 9   TYPICAL FAR-FIELD SAMPLING POINT LOCATIONS FOR DETERMINING TEMPERATURE RISE ABOVE AMBIENT

56
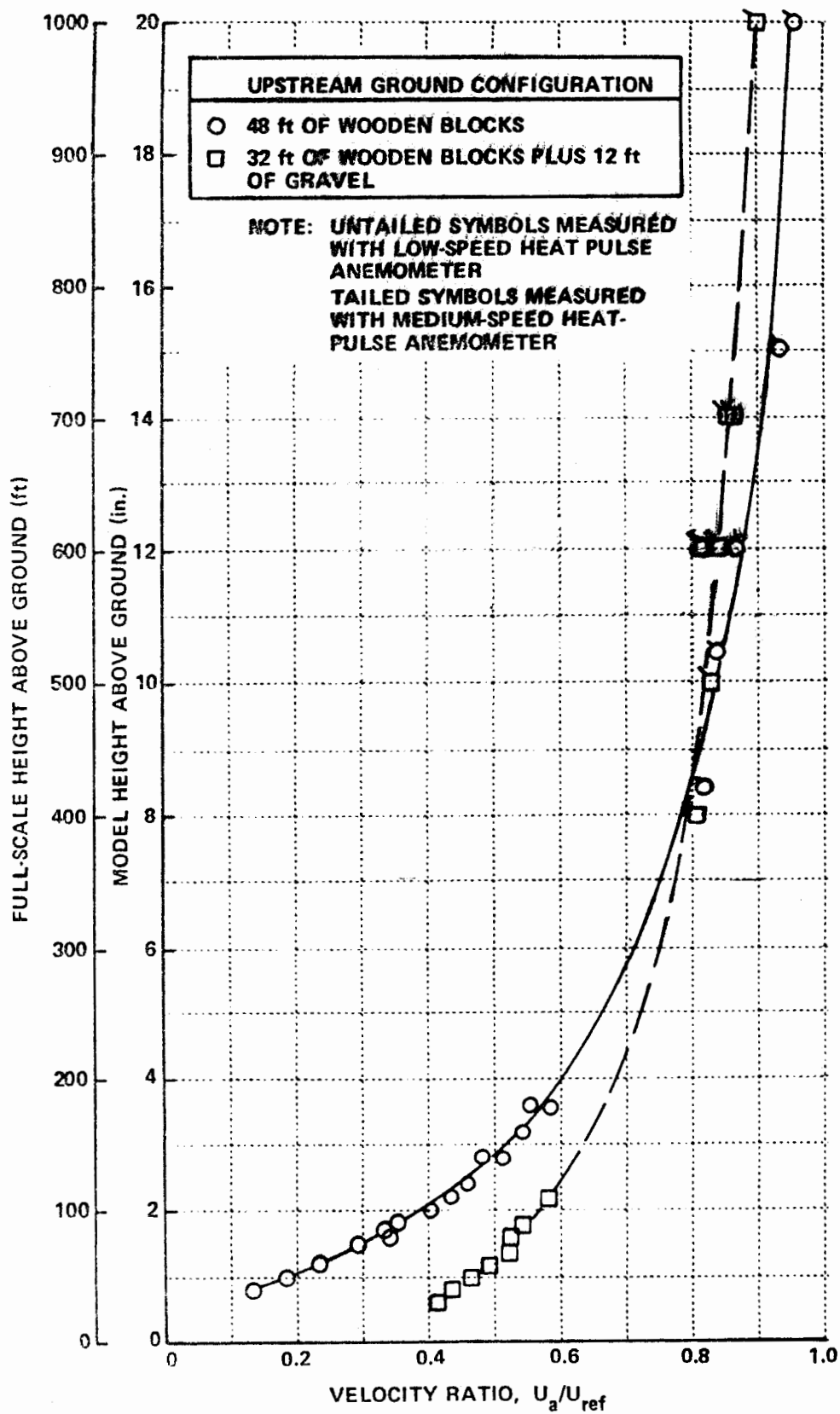
Figure 10   MEAN VELOCITY PROFILES MEASURED TWO FEET UPSTREAM OF TURNTABLE

57
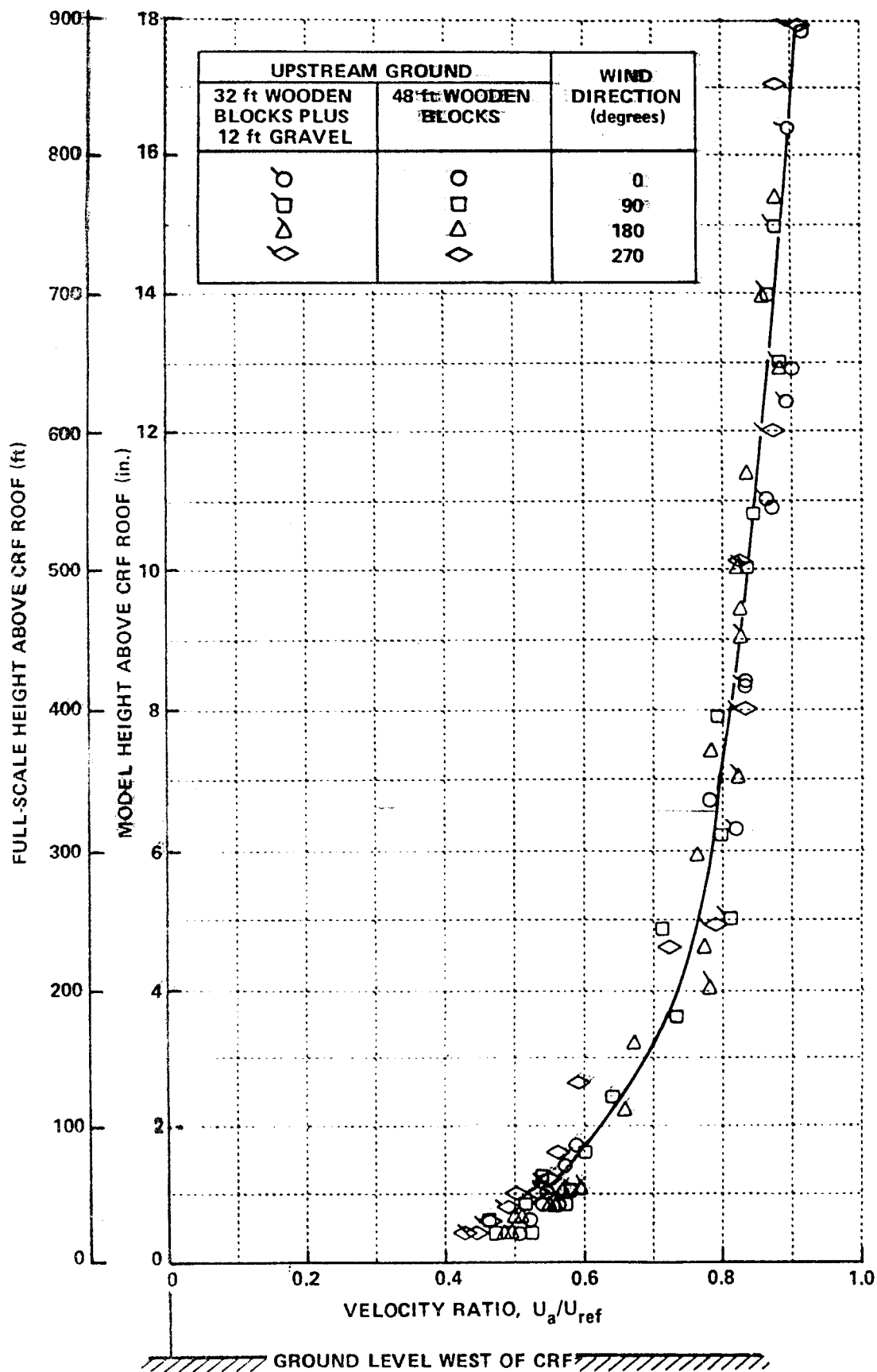
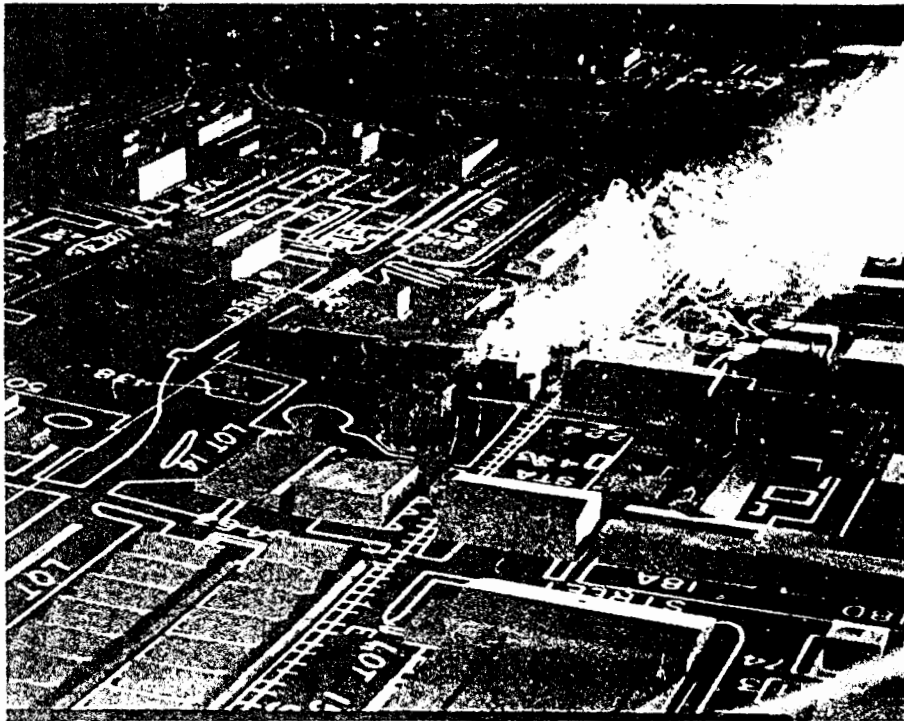Figure 11 MEAN VELOCITY PROFILES MEASURED ABOVE CRF BUILDING

58
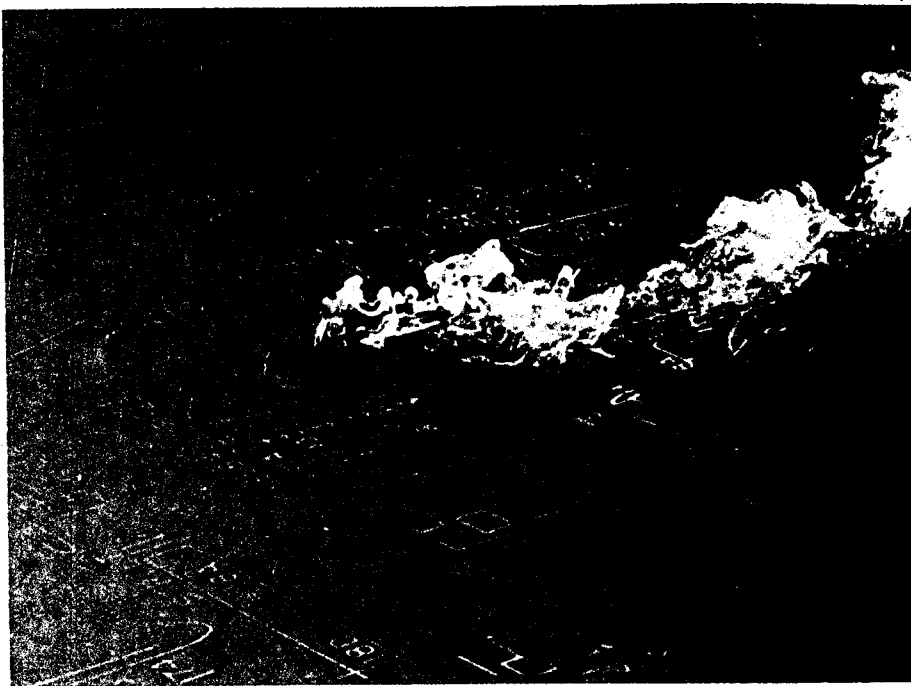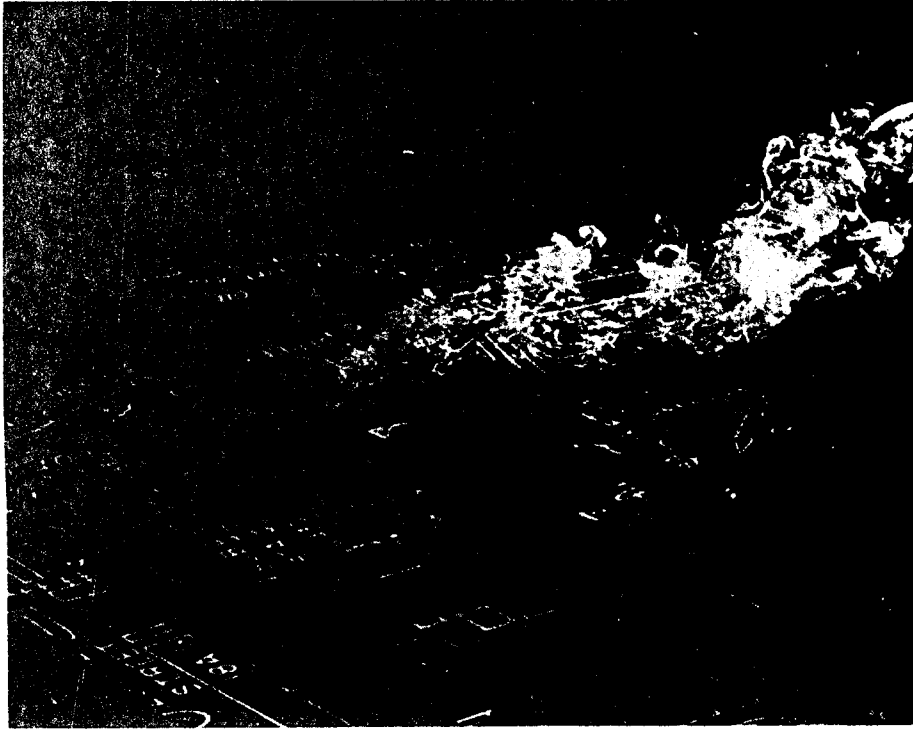
(a) MODEL REFERENCE WIND VELOCITY, $U_{m_{ref}} = 3$ fps

Figure 12 CRF MODEL SMOKE STUDIES
STANDARD STACK, 0 deg WIND
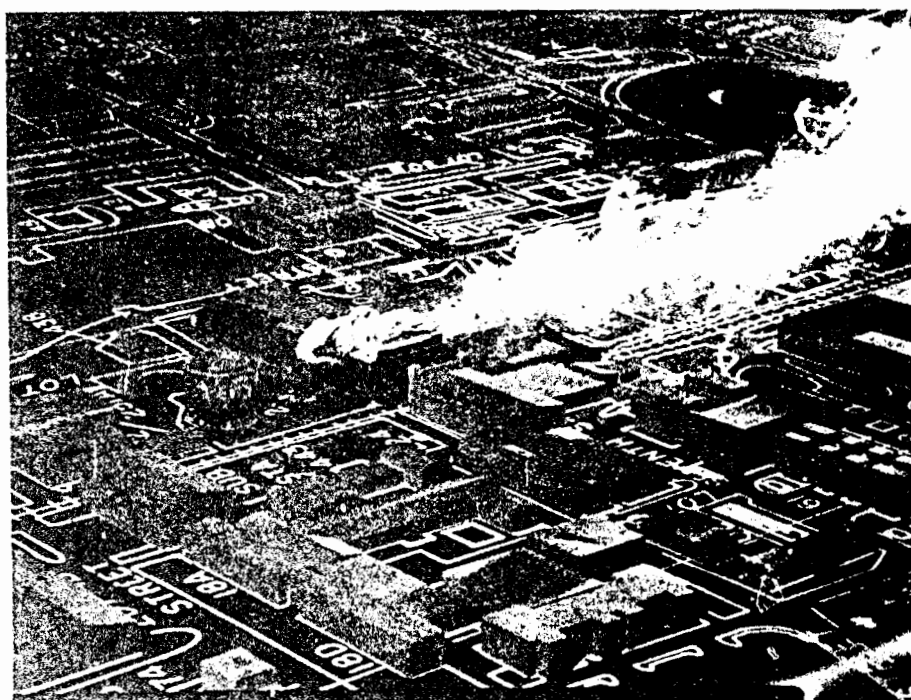
(b) MODEL REFERENCE WIND VELOCITY, $U_{m_{ref}}$ = 5 fps

Figure 12 (Cont.) CRF MODEL SMOKE STUDIES
STANDARD STACK, 0 deg WIND
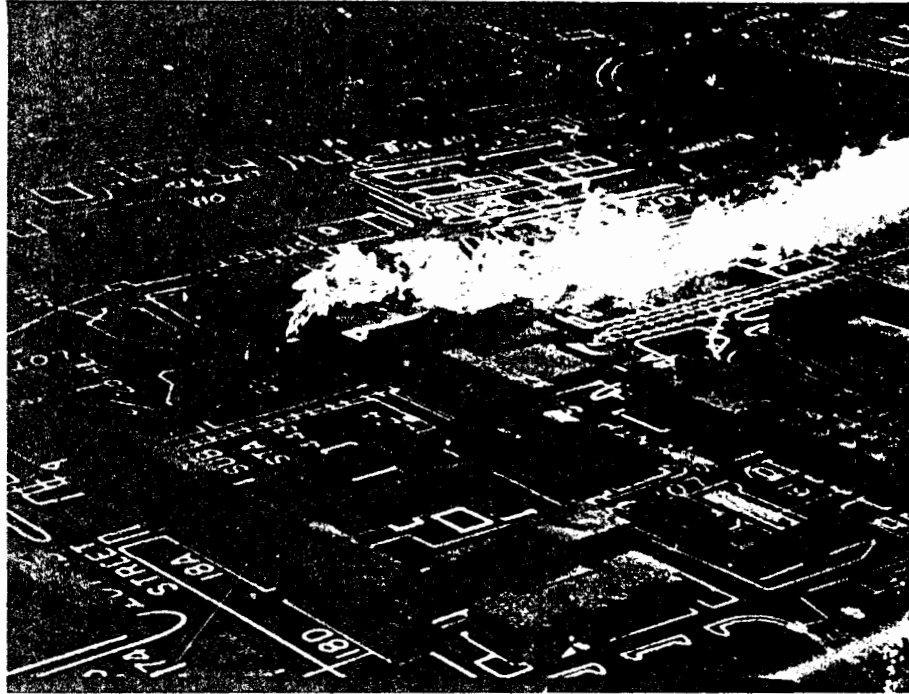
(c) MODEL REFERENCE WIND VELOCITY, $U_{m_{ref}}$ = 7 fps

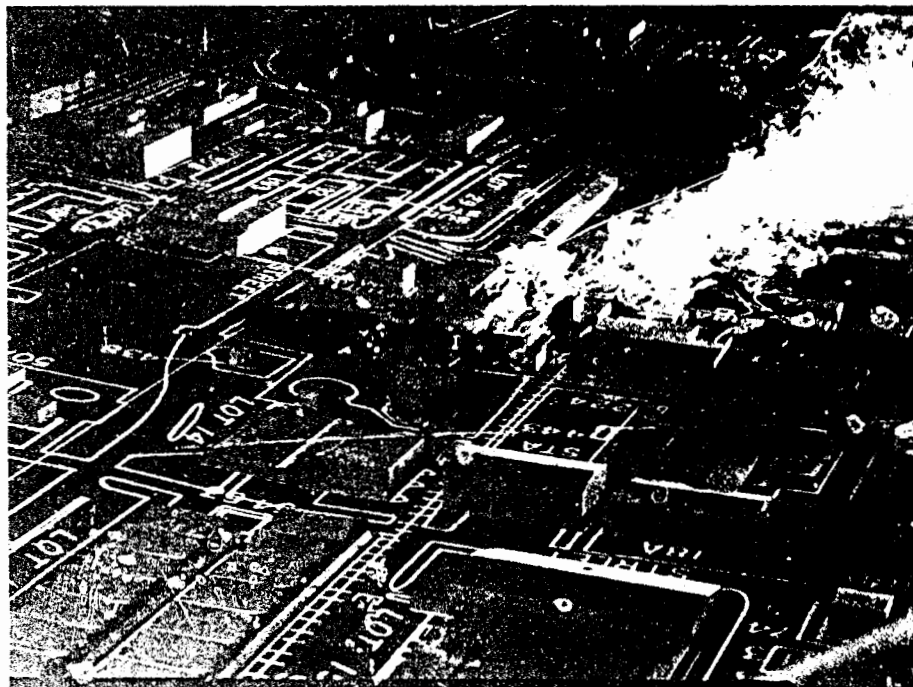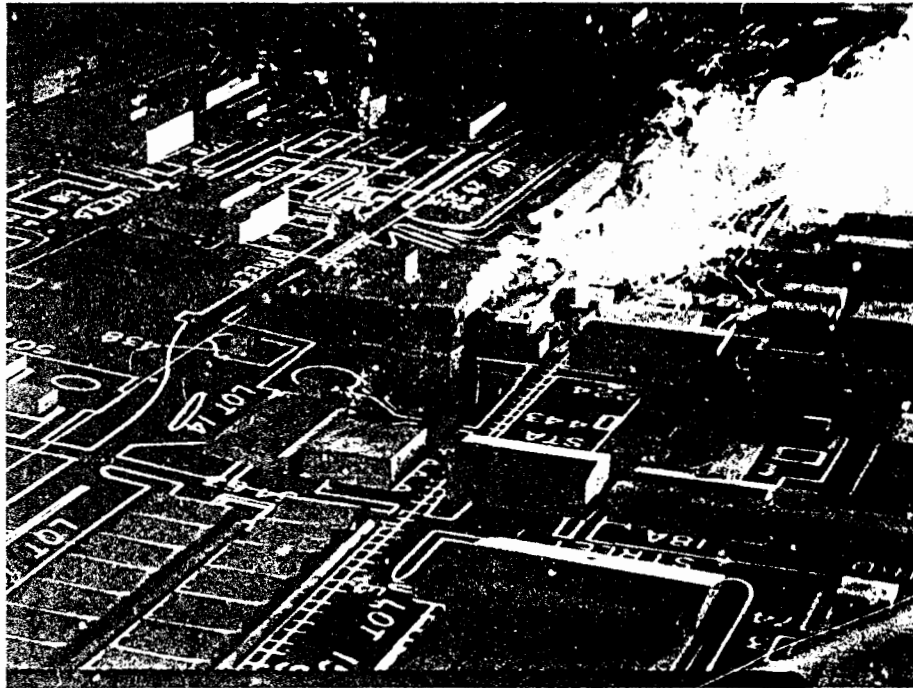Figure 12 (Cont.) CRF MODEL SMOKE STUDIES
STANDARD STACK, 0 deg WIND
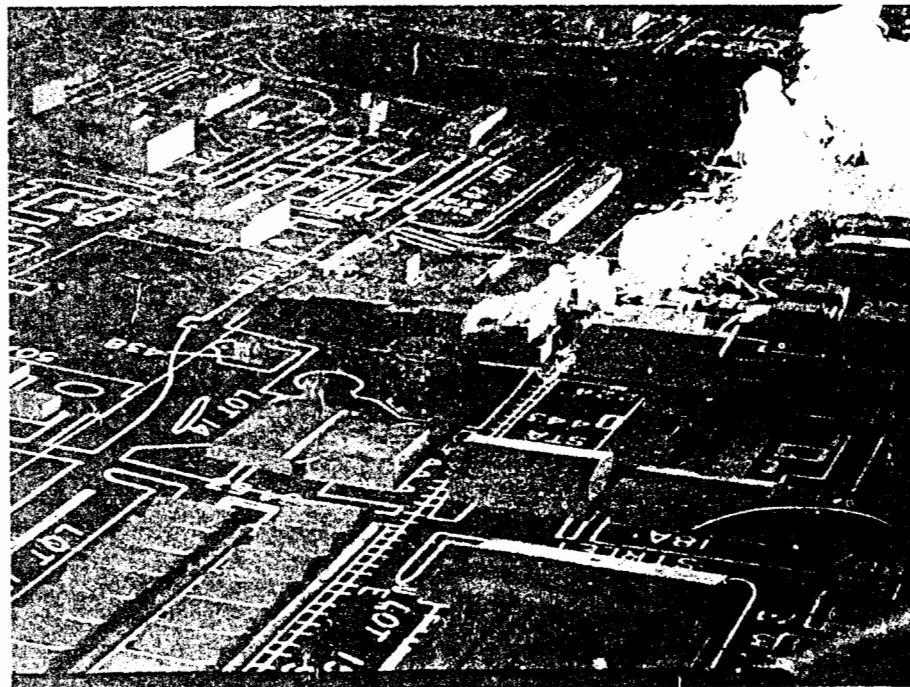
(a) MODEL REFERENCE WIND VELOCITY, $U_{m_{ref}}$ = 3 fps

Figure 13   CRF MODEL SMOKE STUDIES
STANDARD STACK, 30 deg WIND
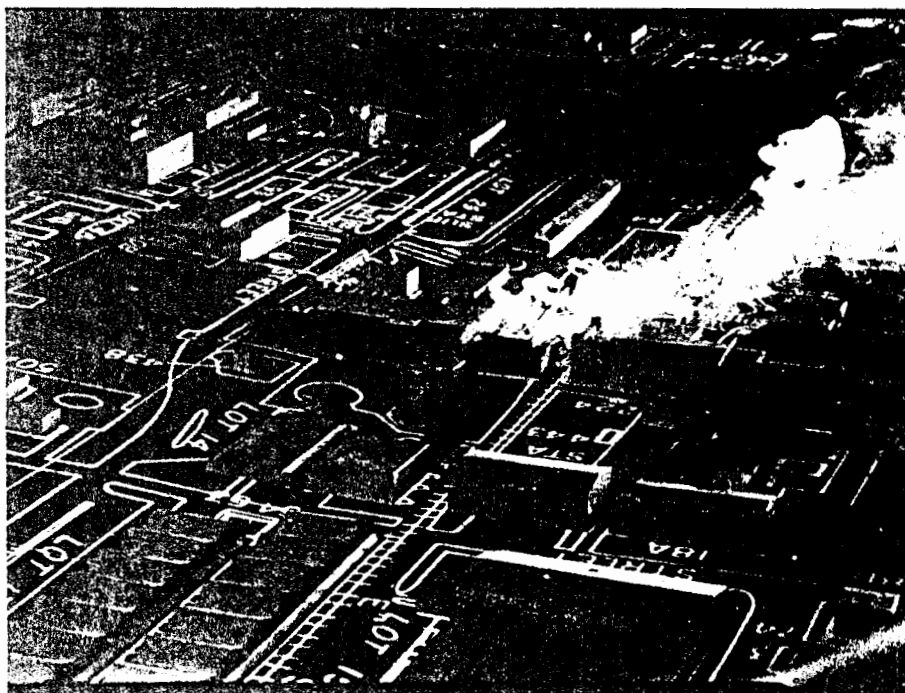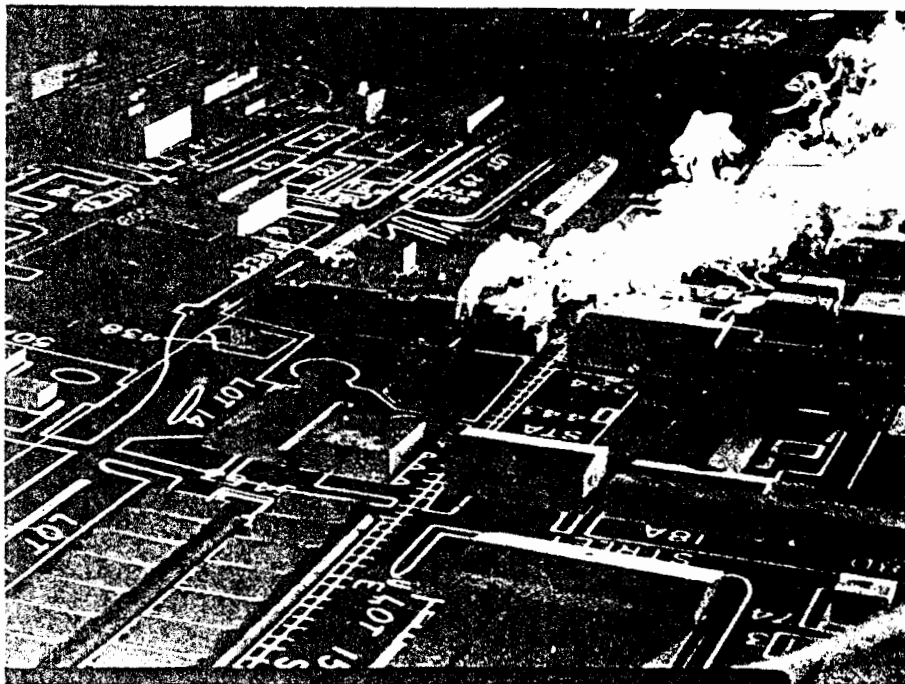
(b) MODEL REFERENCE WIND VELOCITY, $U_{m_{ref}}$ = 5 fps

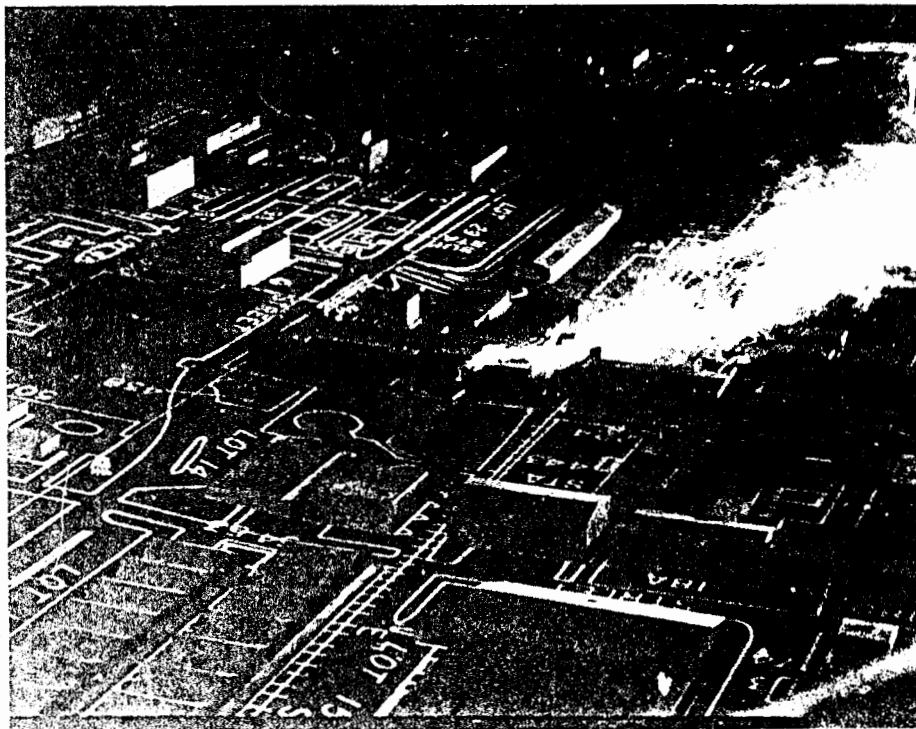Figure 13 (Cont.)   CRF MODEL SMOKE STUDIES
STANDARD STACK, 30 deg WIND
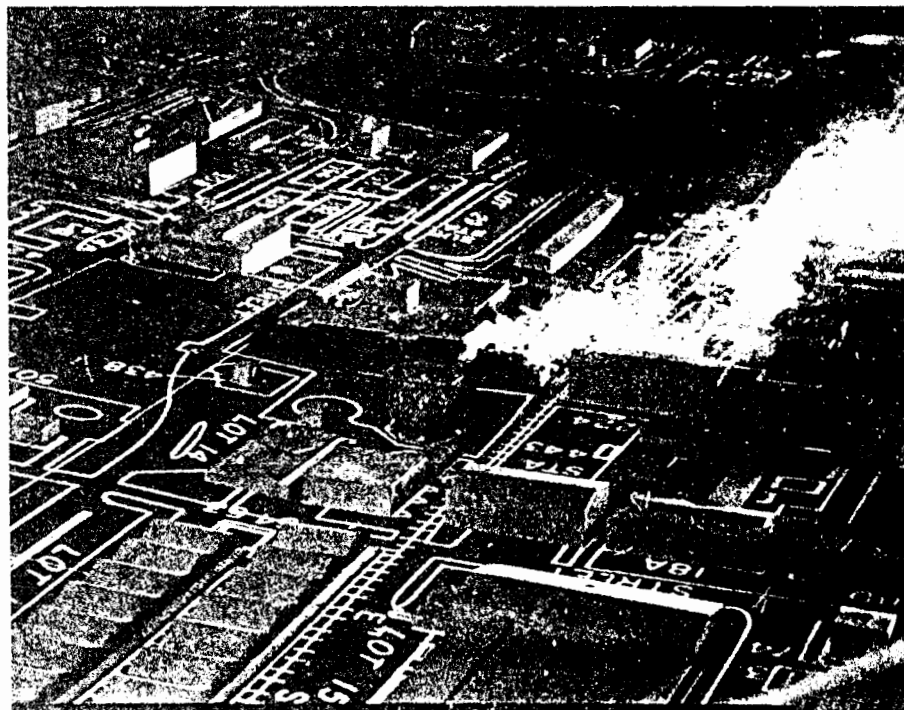
(c) MODEL REFERENCE WIND VELOCITY, $U_{m_{ref}}$ = 7 fps

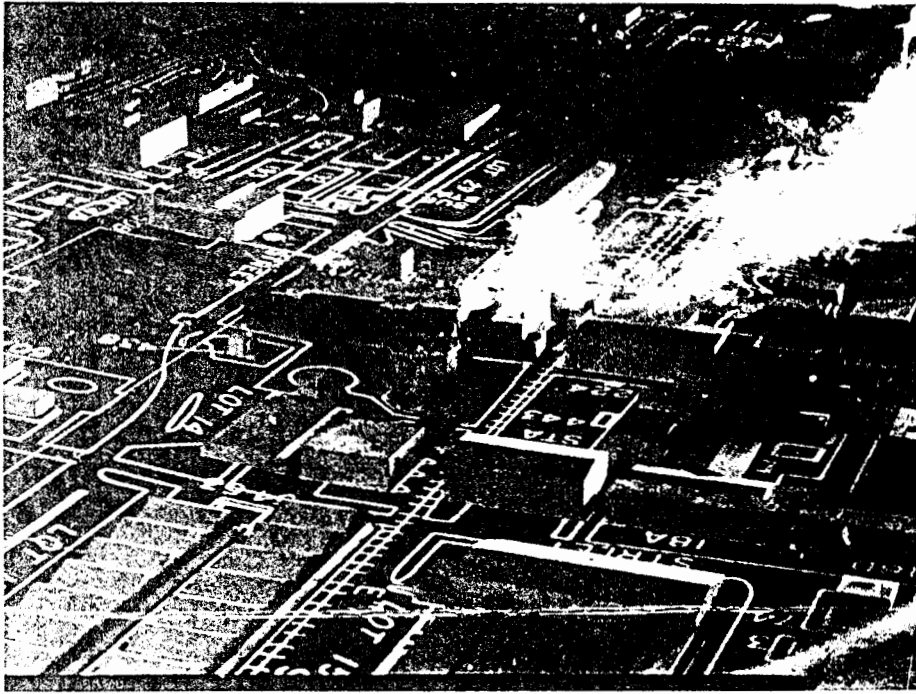Figure 13 (Cont.)   CRF MODEL SMOKE STUDIES
STANDARD STACK, 30 deg WIND

(a) MODEL REFERENCE WIND VELOCITY, $U_{m_{ref}}$ = 3 fps

Figure 14   CRF MODEL SMOKE STUDIES
EXTENDED STACK, 30 deg WIND

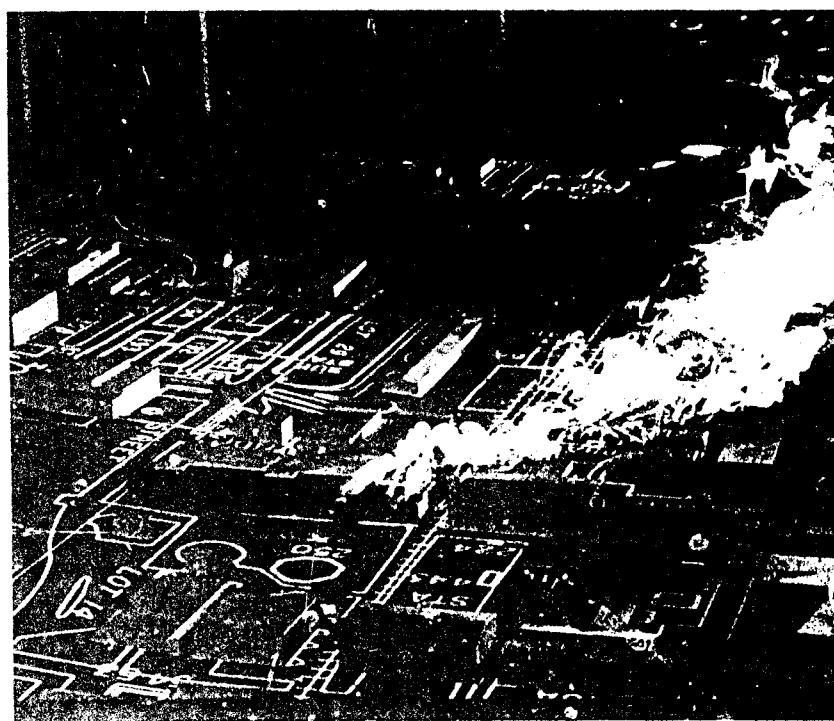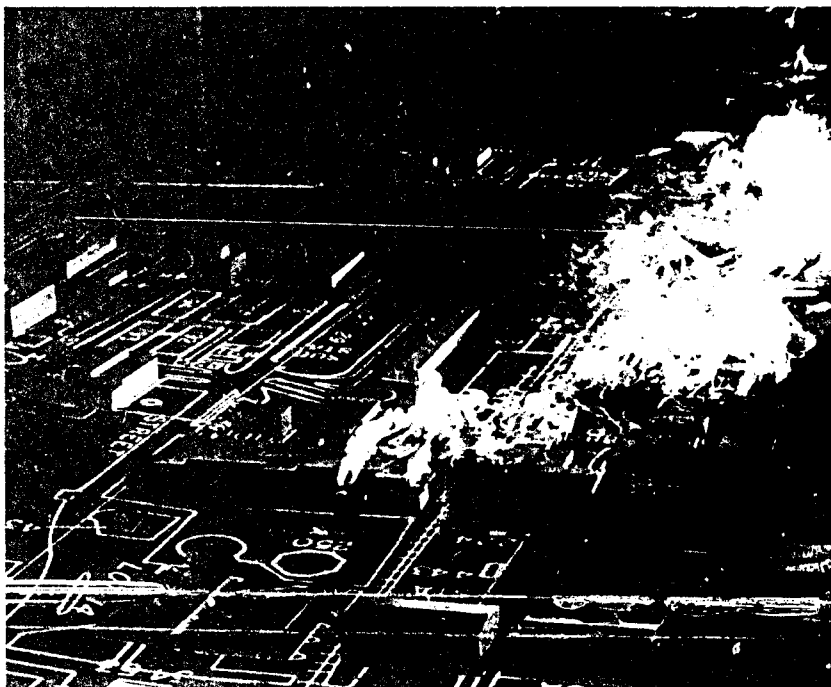(b) MODEL REFERENCE WIND VELOCITY, $U_{m_{ref}}$ = 5 fps

Figure 14 (Cont.)   CRF MODEL SMOKE STUDIES
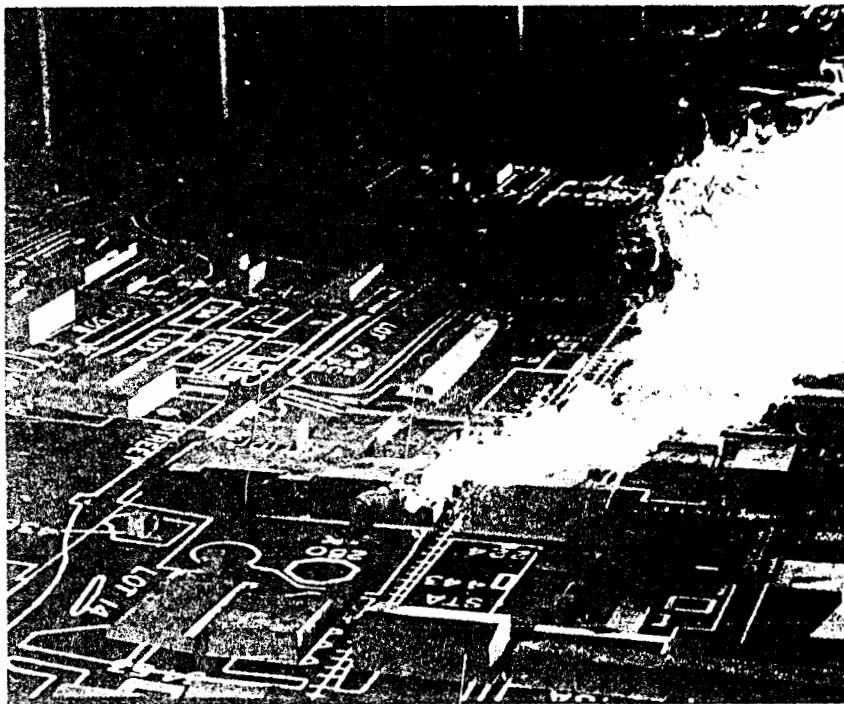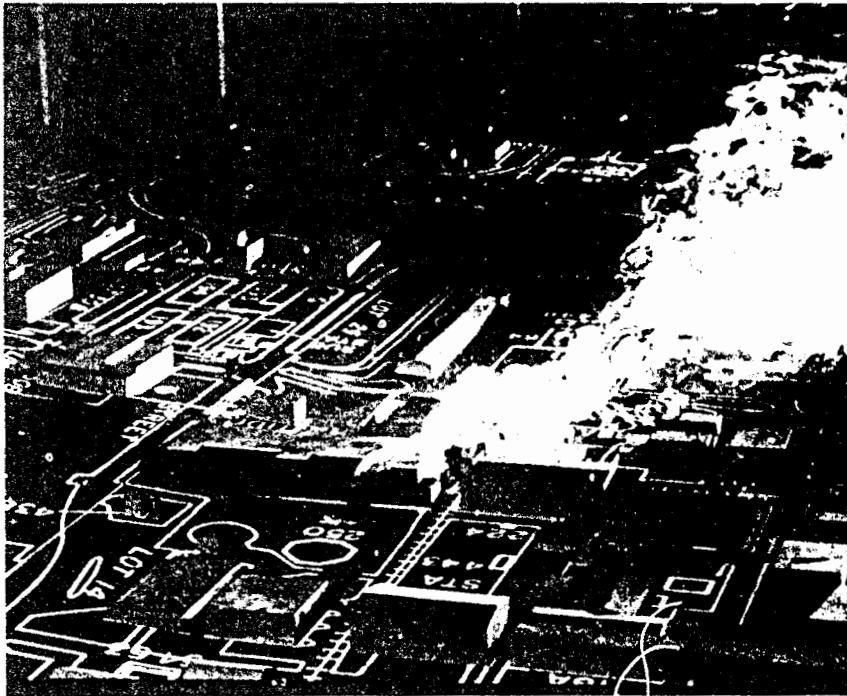EXTENDED STACK, 30 deg WIND

(c) MODEL REFERENCE WIND VELOCITY, $U_{m_{ref}}$ = 7 fps

Figure 14 (Cont.)   CRF MODEL SMOKE STUDIES
EXTENDED STACK, 30 deg WIND

(a) MODEL REFERENCE WIND VELOCITY, $U_{m_{ref}}$ = 3 fps

Figure 15   CRF MODEL SMOKE STUDIES
             STANDARD STACK, 30 deg WIND, WHIRL TOWER REMOVED

(b) MODEL REFERENCE WIND VELOCITY, $U_{m_{ref}}$ = 5 fps

Figure 15 (Cont.)   CRF MODEL SMOKE STUDIES
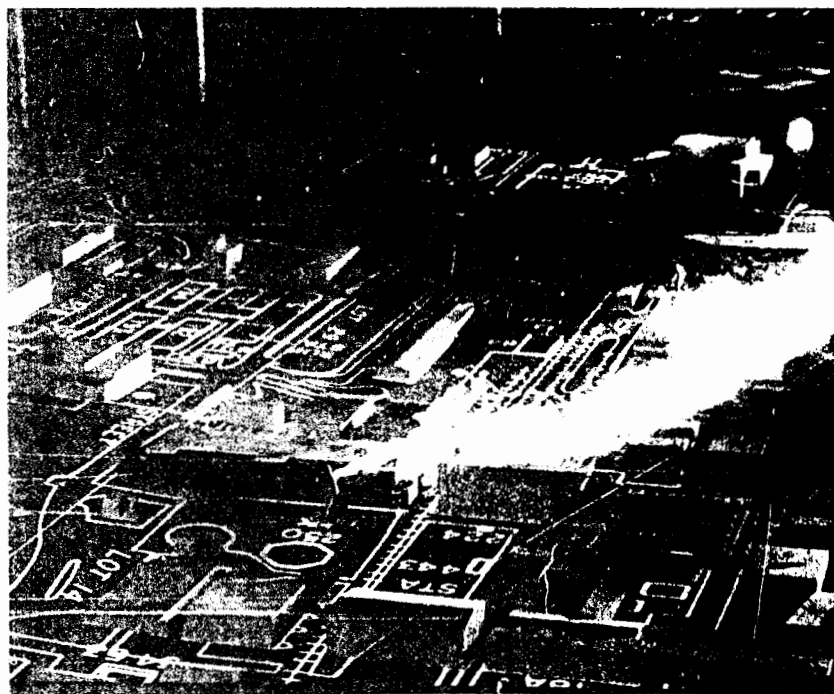   STANDARD STACK, 30 deg WIND, WHIRL TOWER REMOVED

(c) MODEL REFERENCE WIND VELOCITY, $U_{m_{ref}}$ = 7 fps

Figure 15 (Cont.)   CRF MODEL SMOKE STUDIES
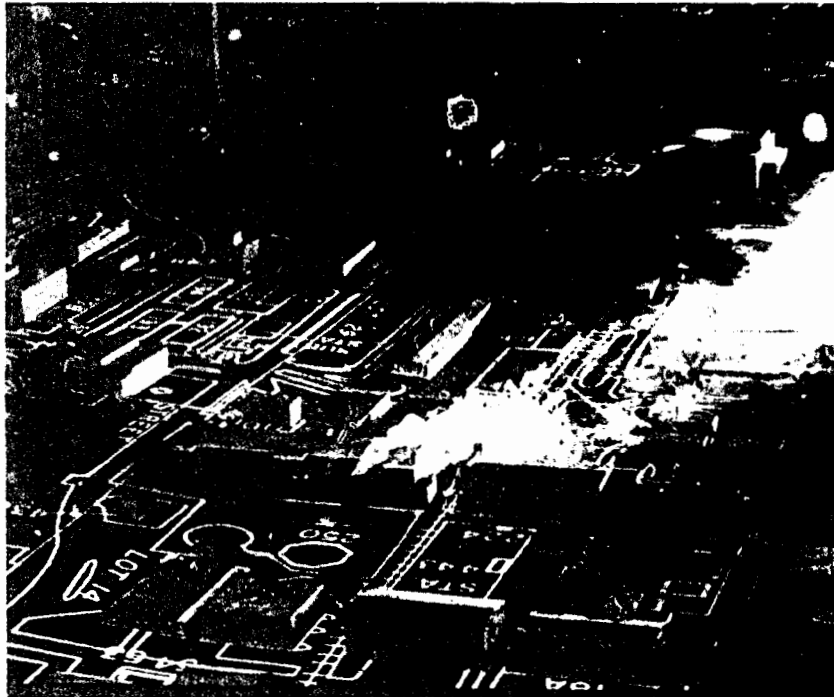STANDARD STACK, 30 deg WIND, WHIRL TOWER REMOVED

(a) MODEL REFERENCE WIND VELOCITY, $U_{m_{ref}}$ = 5 fps

Figure 16   CRF MODEL SMOKE STUDIES
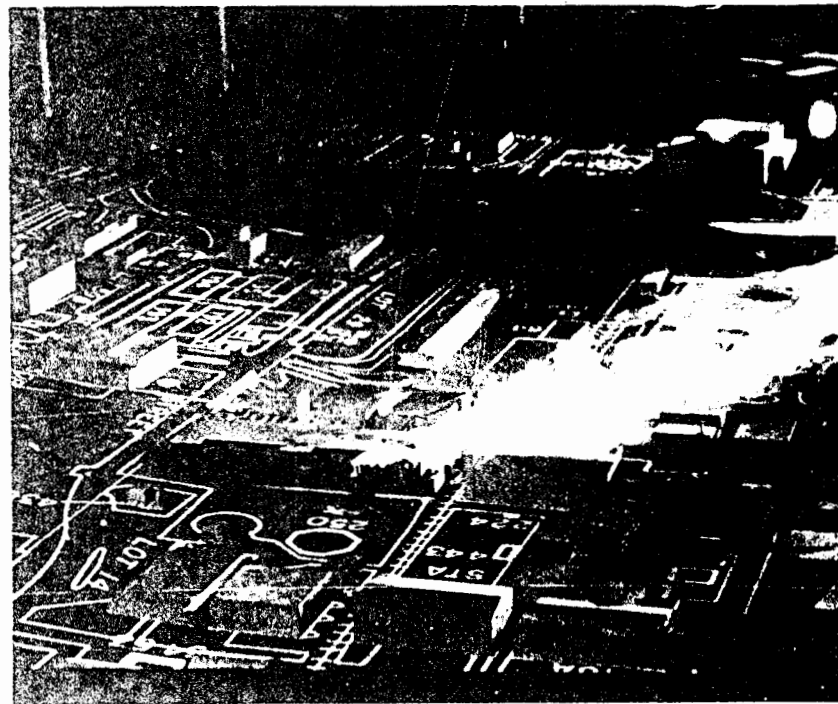EXTENDED STACK, 30 deg WIND, WHIRL TOWER REMOVED

71

(b) MODEL REFERENCE WIND VELOCITY, $U_{m_{ref}}$ = 7 fps

Figure 16 (Cont.)   CRF MODEL SMOKE STUDIES
EXTENDED STACK, 30 deg WIND, WHIRL TOWER REMOVED

73

(a) MODEL REFERENCE WIND VELOCITY, $U_{m_{ref}}$ = 3 fps

Figure 17   CRF MODEL SMOKE STUDIES
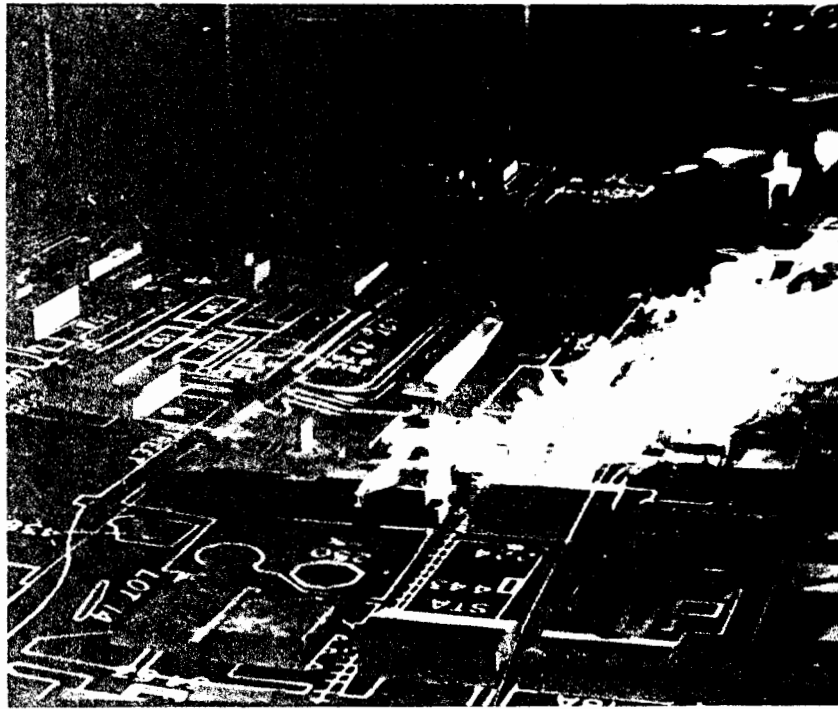STANDARD STACK, 180 deg WIND

(b) MODEL REFERENCE WIND VELOCITY, $U_{m_{ref}}$ = 5 fps

Figure 17 (Cont.)   CRF MODEL SMOKE STUDIES
                       STANDARD STACK, 180 deg WIND

(c) MODEL REFERENCE WIND VELOCITY, $U_{m_{ref}}$ = 7 fps

Figure 17 (Cont.)   CRF MODEL SMOKE STUDIES
STANDARD STACK, 180 deg WIND

75
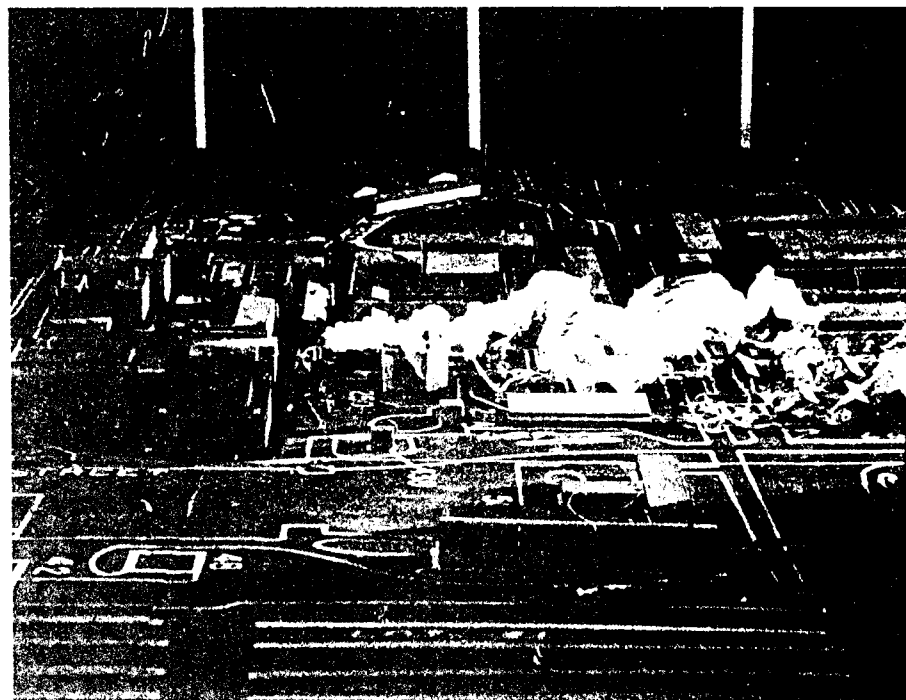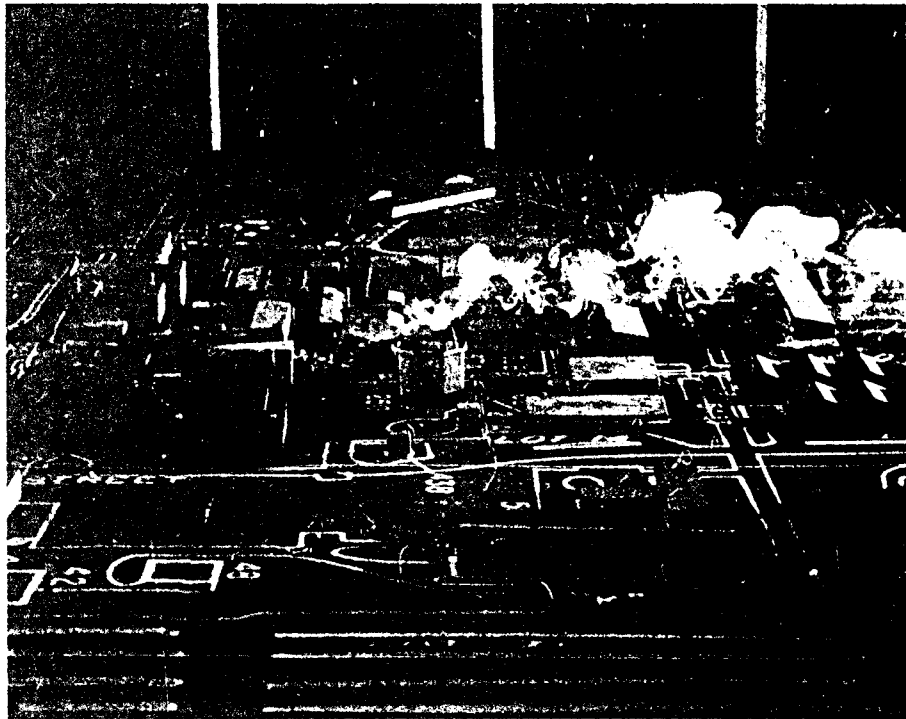
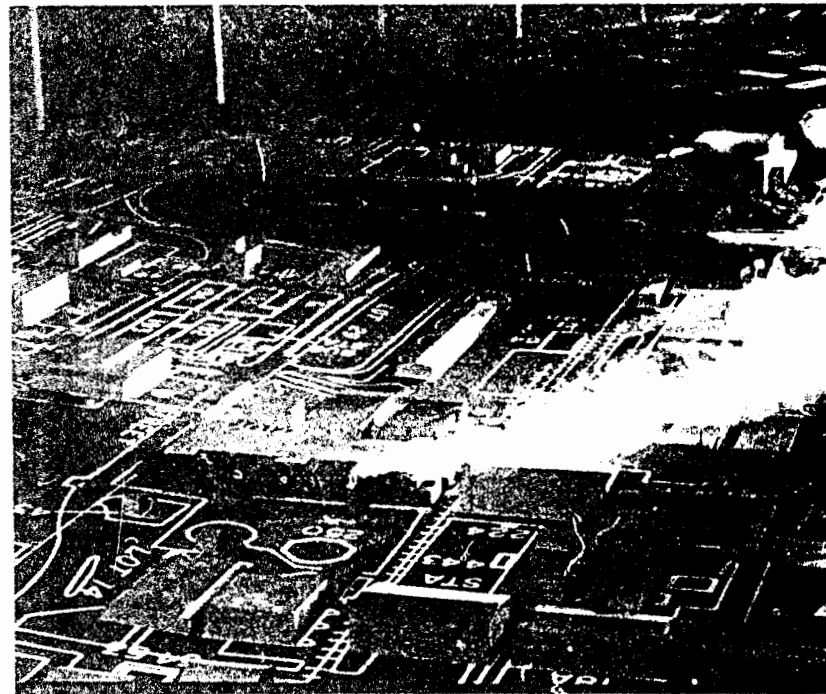(a) MODEL REFERENCE WIND VELOCITY, $U_{m_{ref}}$ = 3 fps

Figure 18   CRF MODEL SMOKE STUDIES
EXTENDED STACK, 180 deg WIND
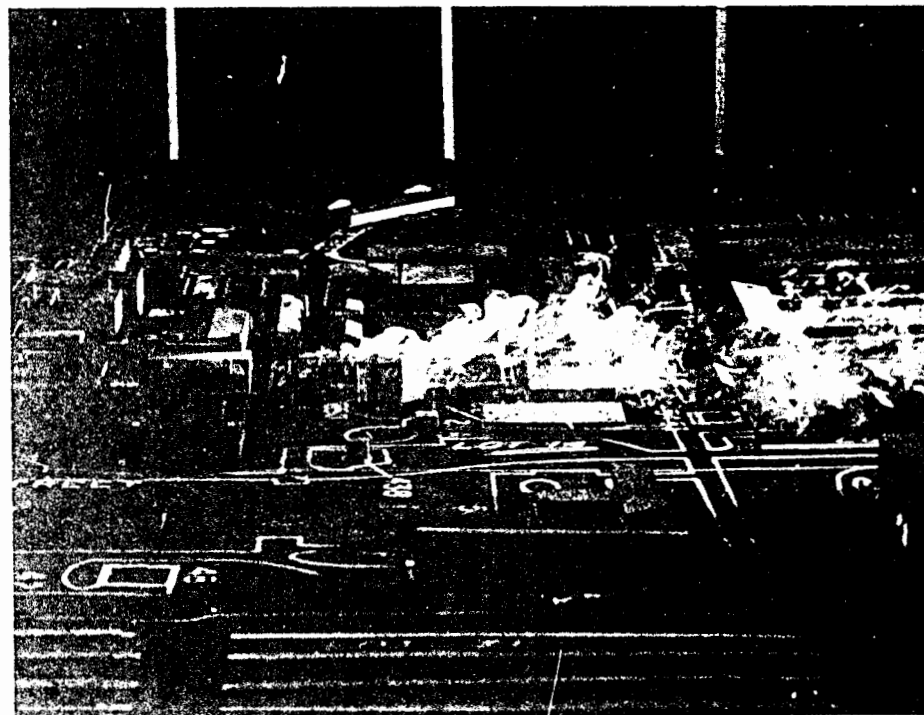
(b) MODEL REFERENCE WIND VELOCITY, $U_{m_{ref}}$ = 5 fps

Figure 18 (Cont.)   CRF MODEL SMOKE STUDIES
EXTENDED STACK, 180 deg WIND
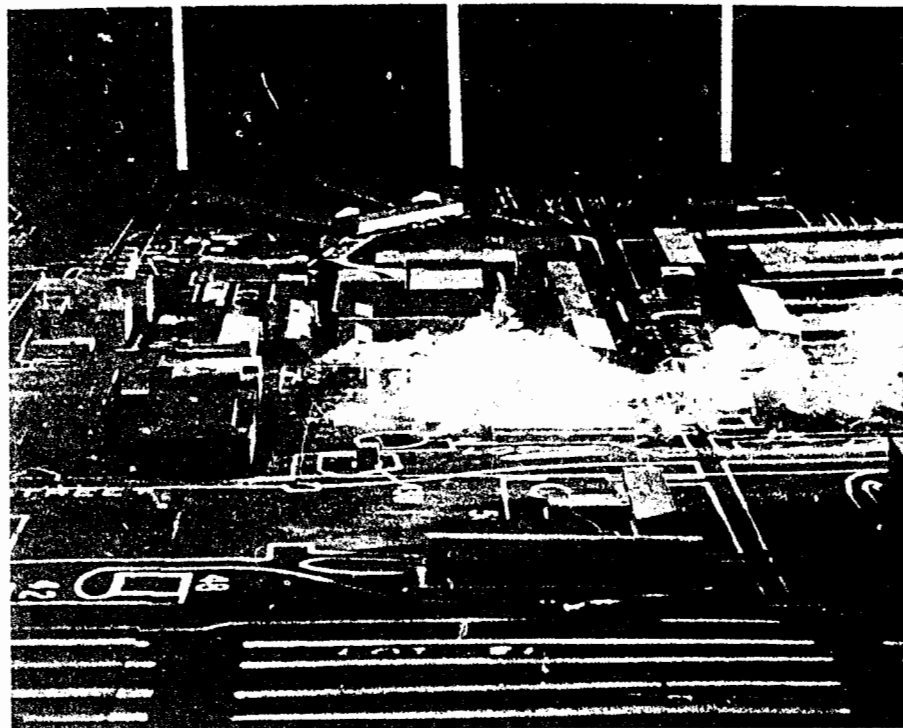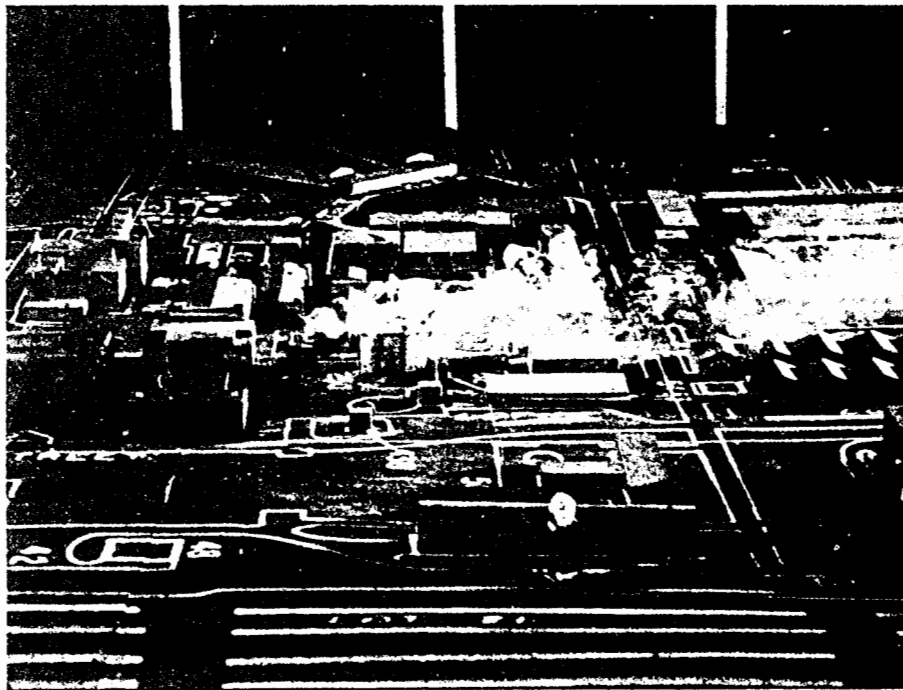
(c) MODEL REFERENCE WIND VELOCITY, $U_{m_{ref}}$ = 7 fps

Figure 18 (Cont.) CRF MODEL SMOKE STUDIES
EXTENDED STACK, 180 deg WIND
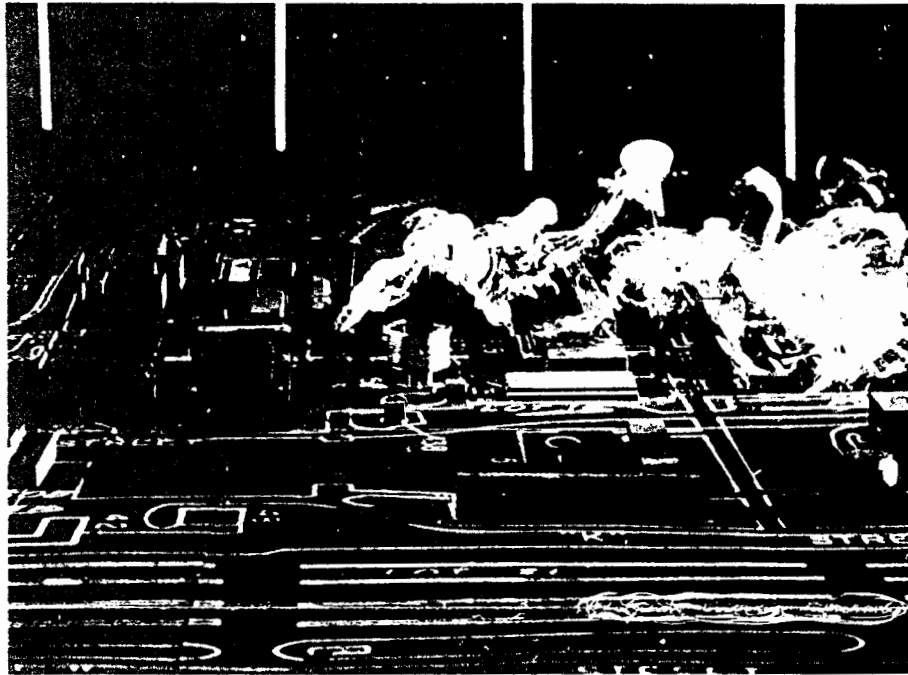
(a) MODEL REFERENCE WIND VELOCITY, $U_{m_{ref}} = 2$ fps

Figure 19   CRF MODEL SMOKE STUDIES
STANDARD STACK, 200 deg WIND

(b) MODEL REFERENCE WIND VELOCITY, $U_{m_{ref}}$ = 3 fps

Figure 19 (Cont.)   CRF MODEL SMOKE STUDIES
STANDARD STACK, 200 deg WIND
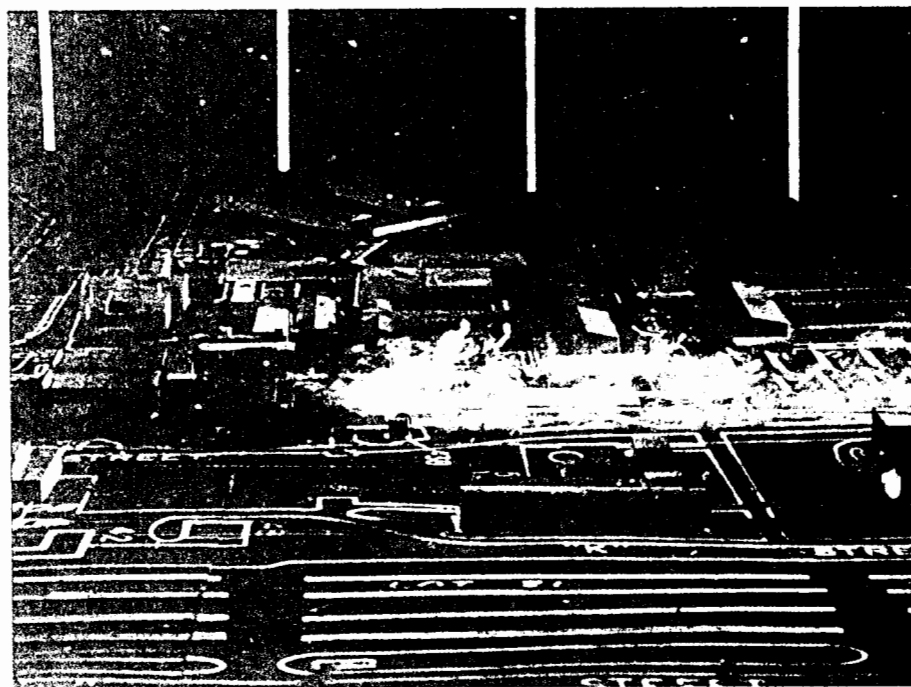
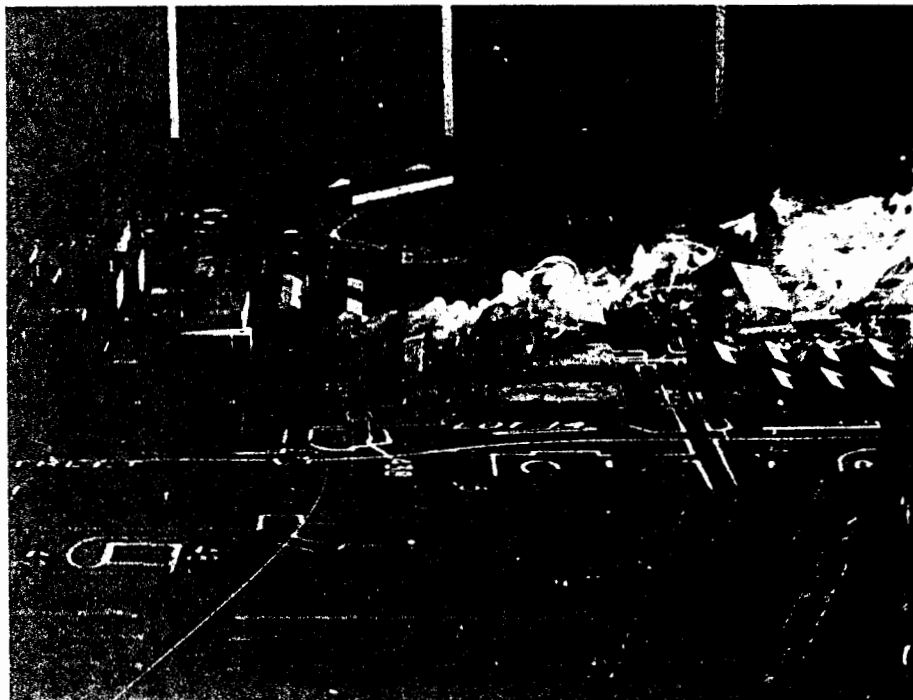(c) MODEL REFERENCE WIND VELOCITY, $U_{m_{ref}}$ = 5 fps

Figure 19 (Cont.)   CRF MODEL SMOKE STUDIES
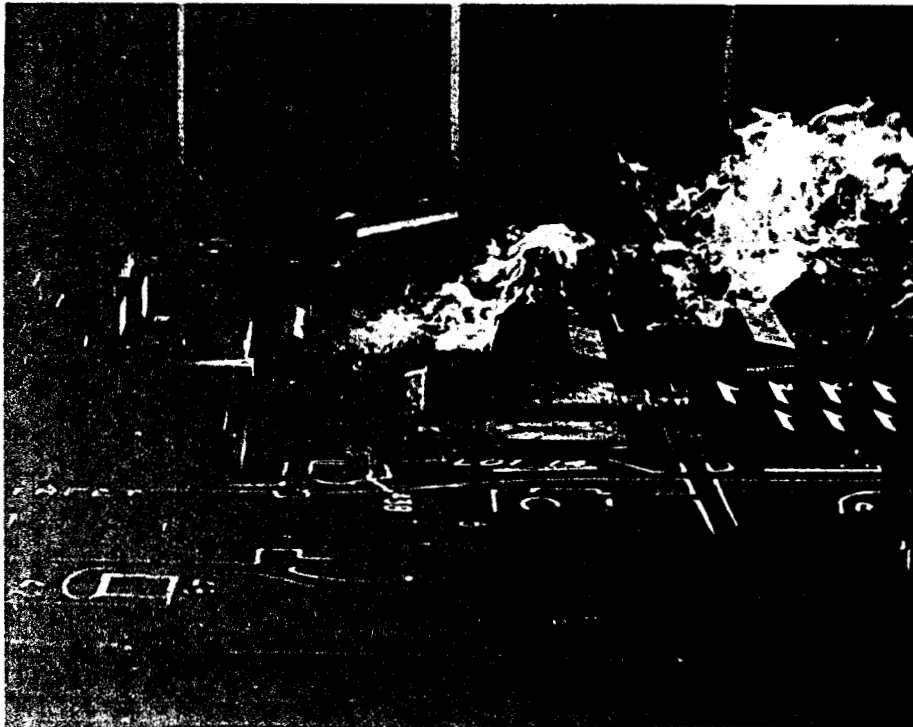STANDARD STACK, 200 deg WIND
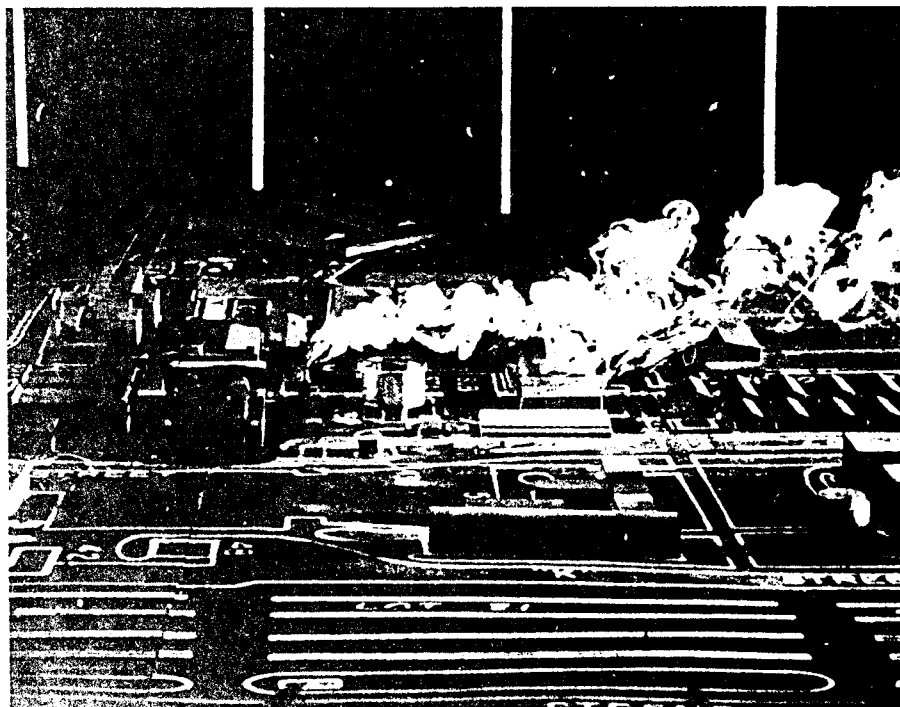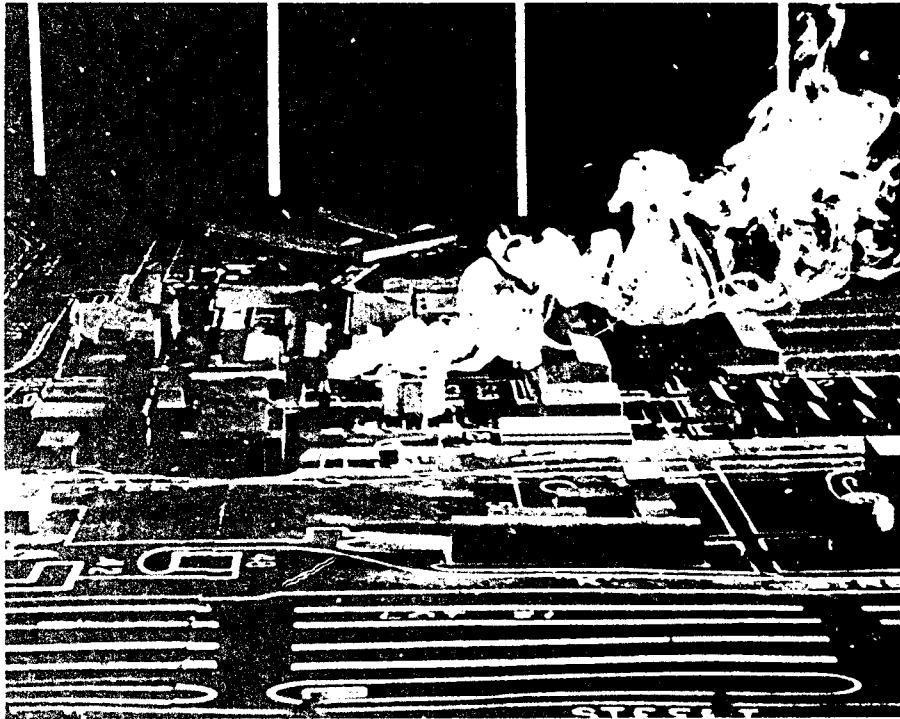
(a) MODEL REFERENCE WIND VELOCITY, $U_{m_{ref}}$ = 2 fps

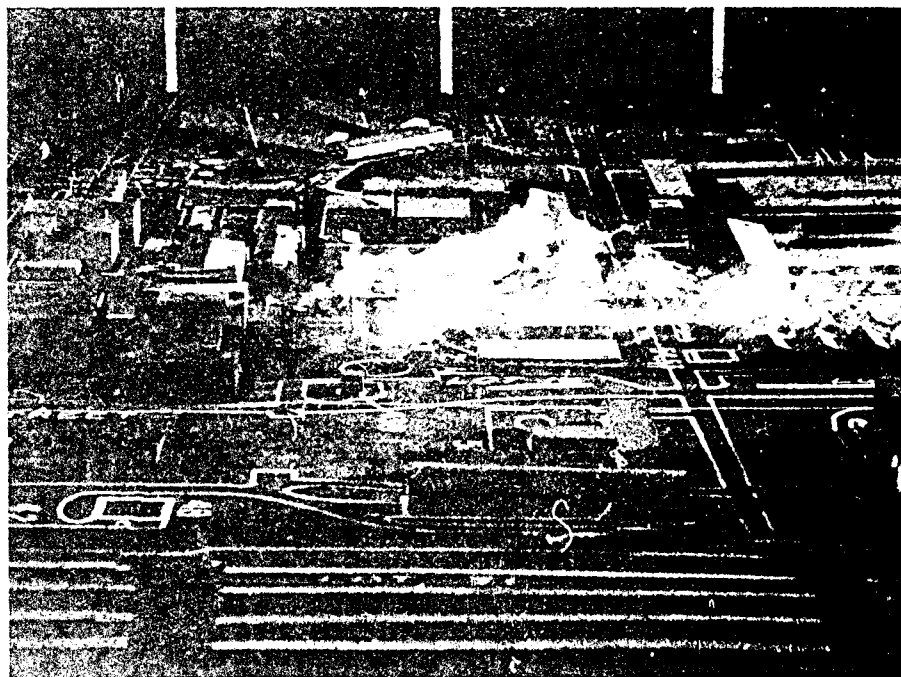Figure 20   CRF MODEL SMOKE STUDIES
EXTENDED STACK, 200 deg WIND
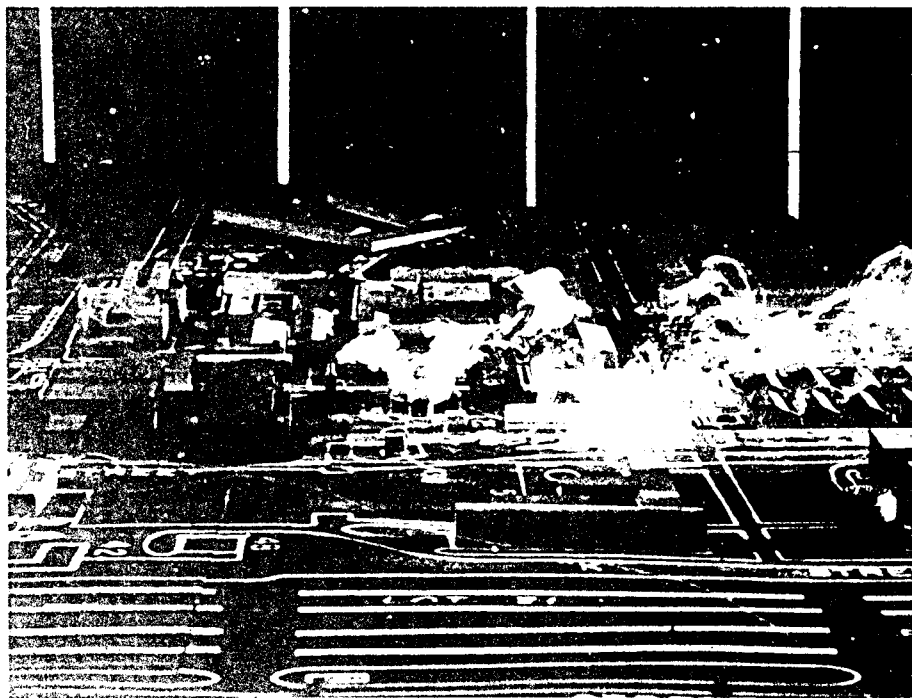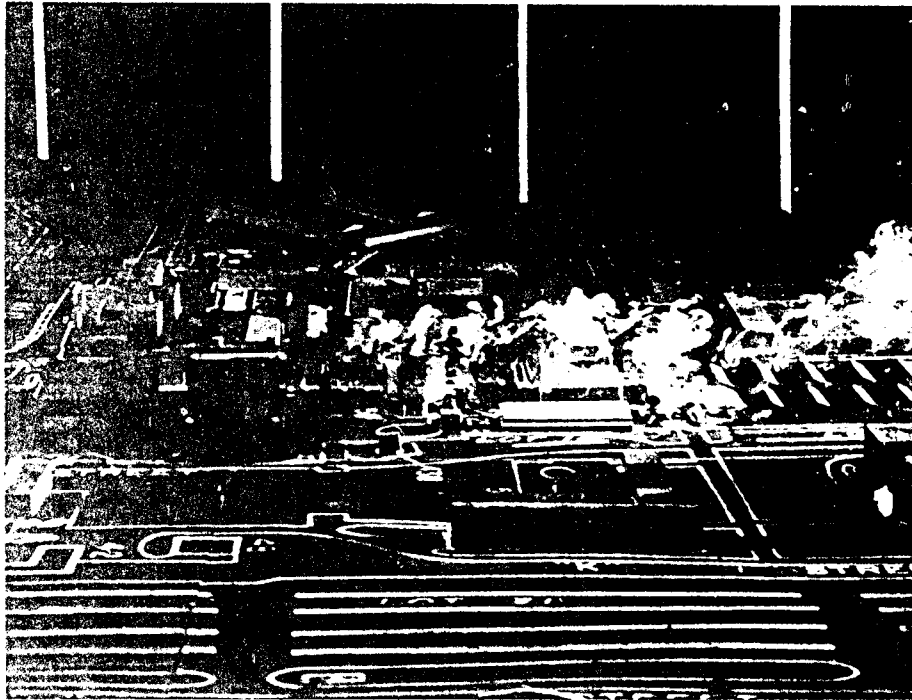
(b) MODEL REFERENCE WIND VELOCITY, $U_{m_{ref}}$ = 3 fps

Figure 20 (Cont.)   CRF MODEL SMOKE STUDIES
EXTENDED STACK, 200 deg WIND
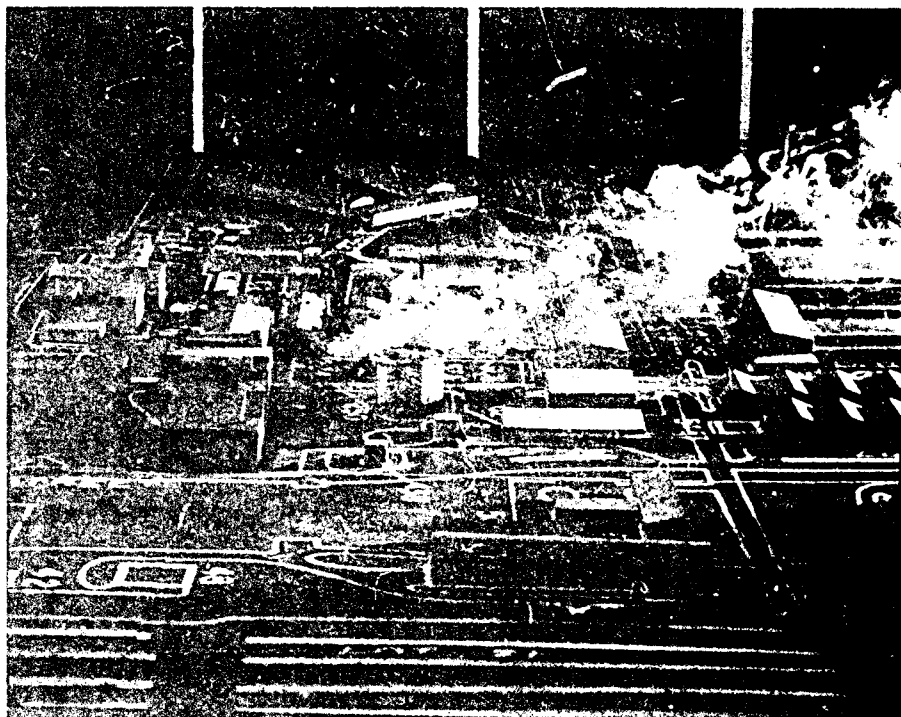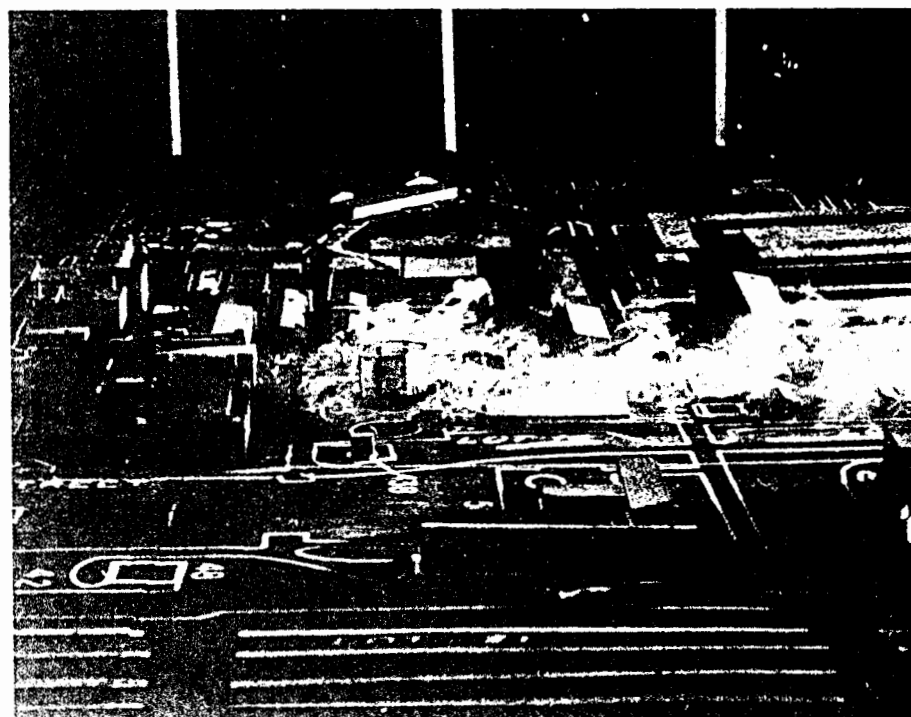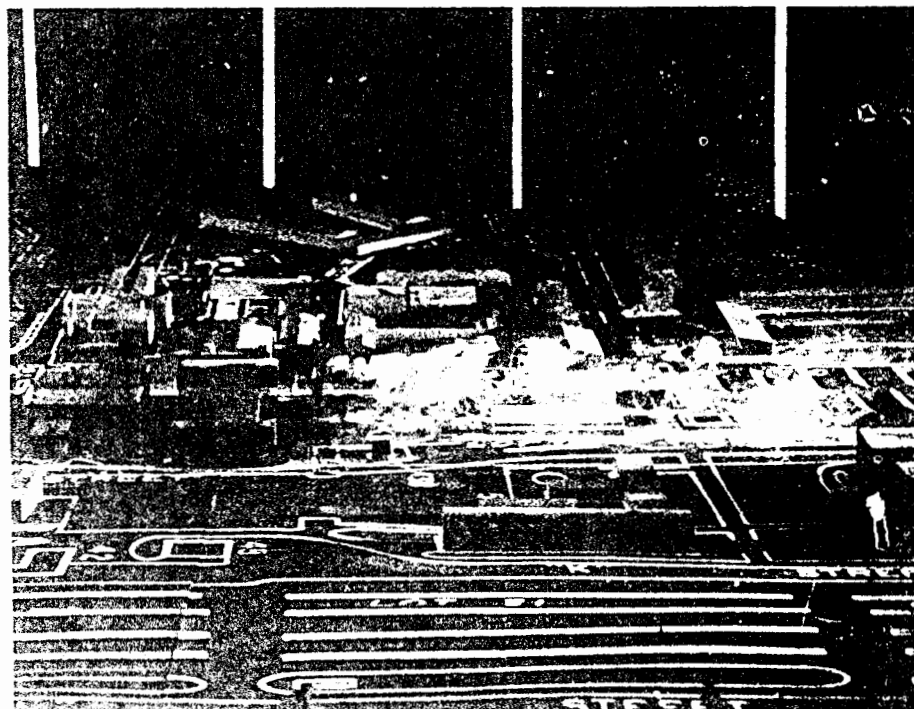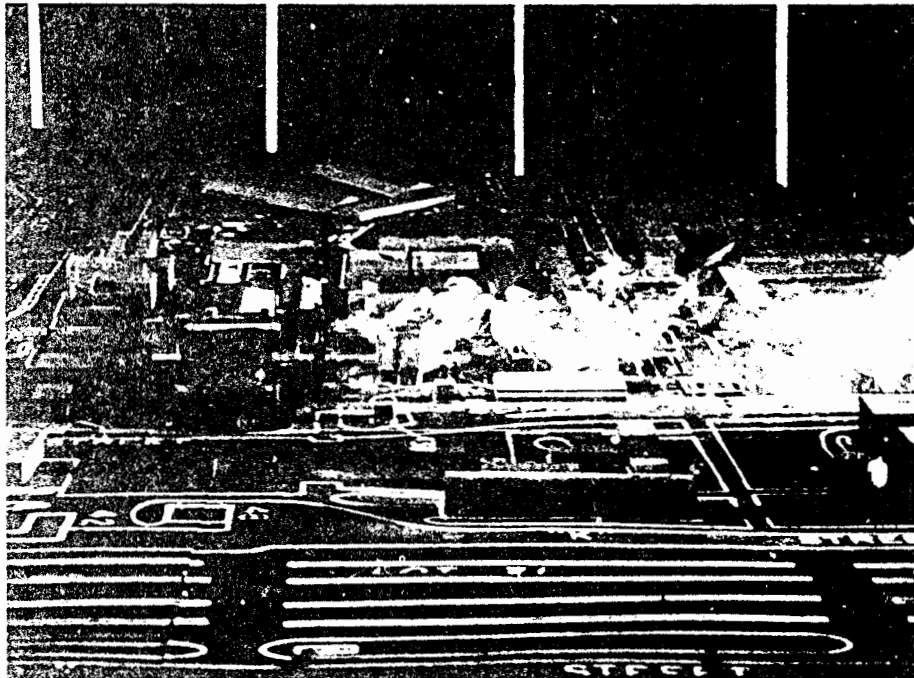
(c) MODEL REFERENCE WIND VELOCITY, $U_{m_{ref}}$ = 5 fps

Figure 20 (Cont.)   CRF MODEL SMOKE STUDIES
EXTENDED STACK, 200 deg WIND
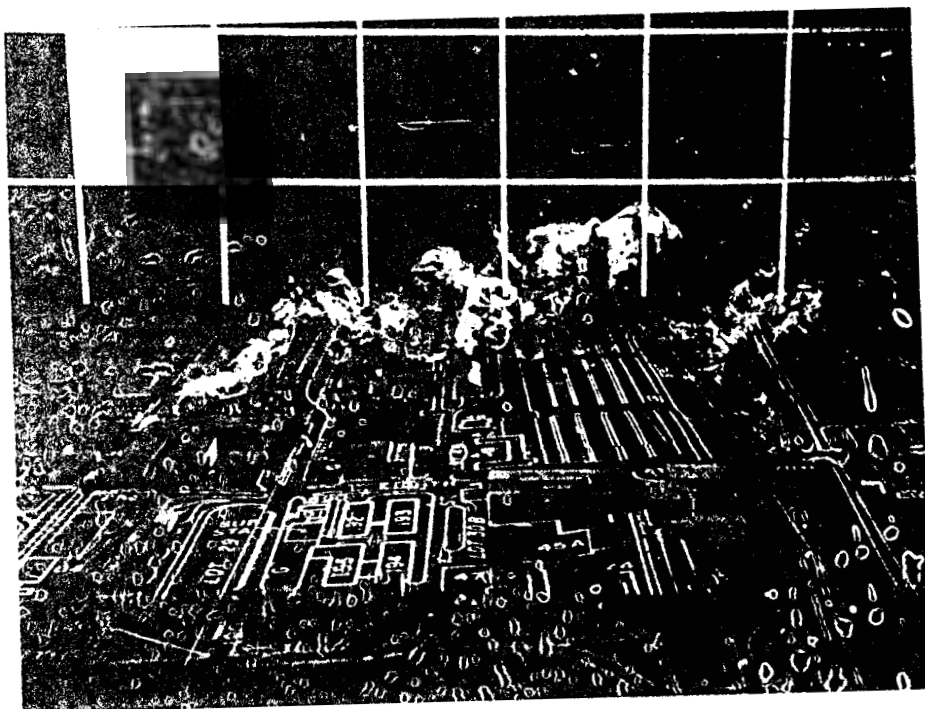
EXTENDED STACK
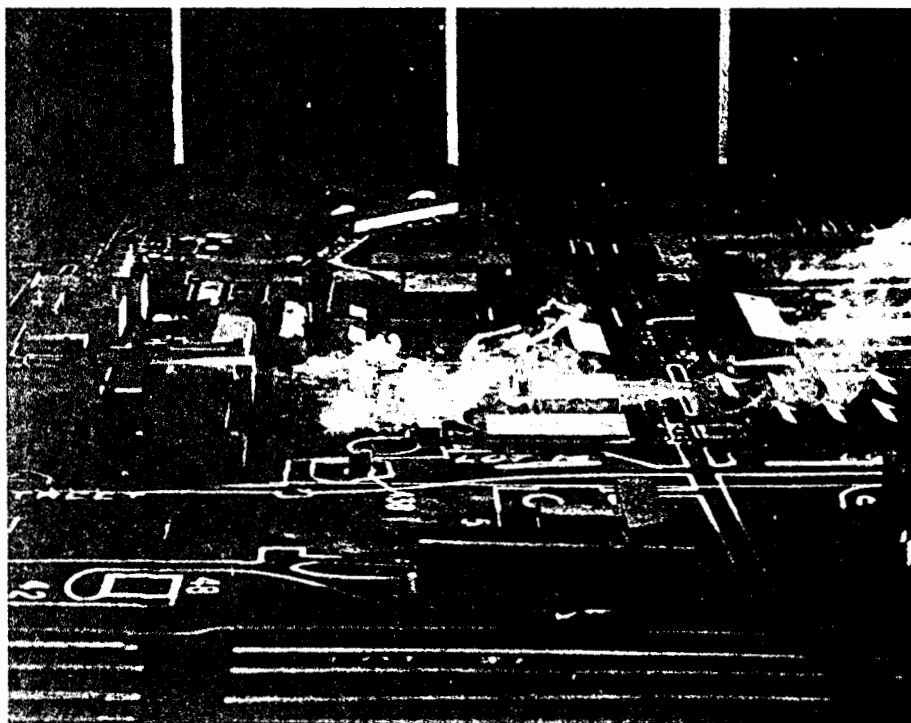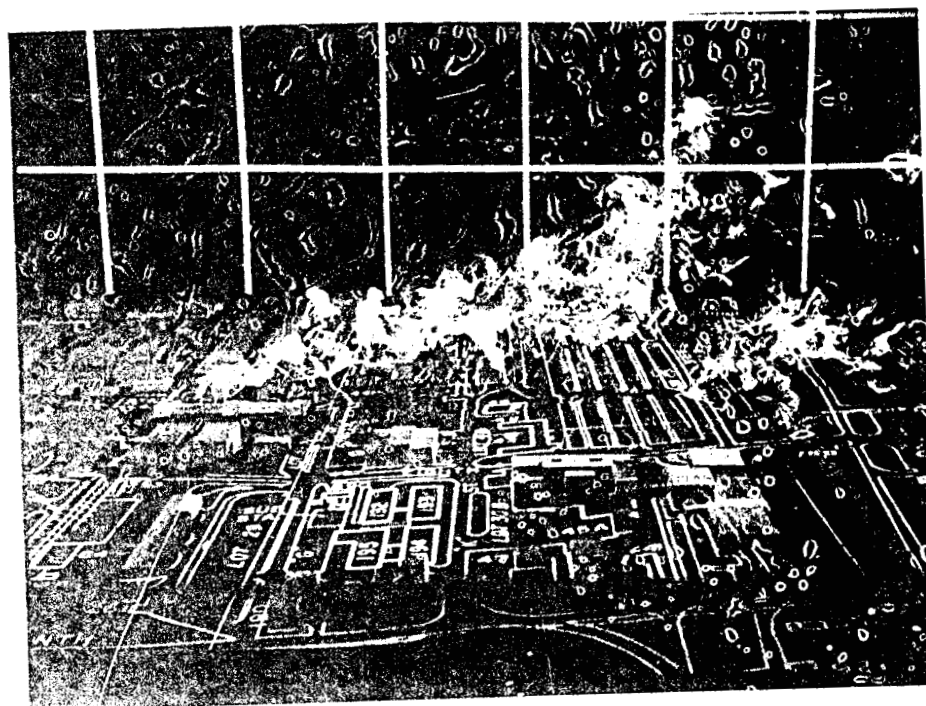

STANDARD STACK

(a) MODEL REFERENCE WIND VELOCITY, $U_{m_{ref}}$ = 2 fps

Figure 21   CRF MODEL SMOKE STUDIES
STANDARD STACK AND EXTENDED STACK, 270 deg WIND
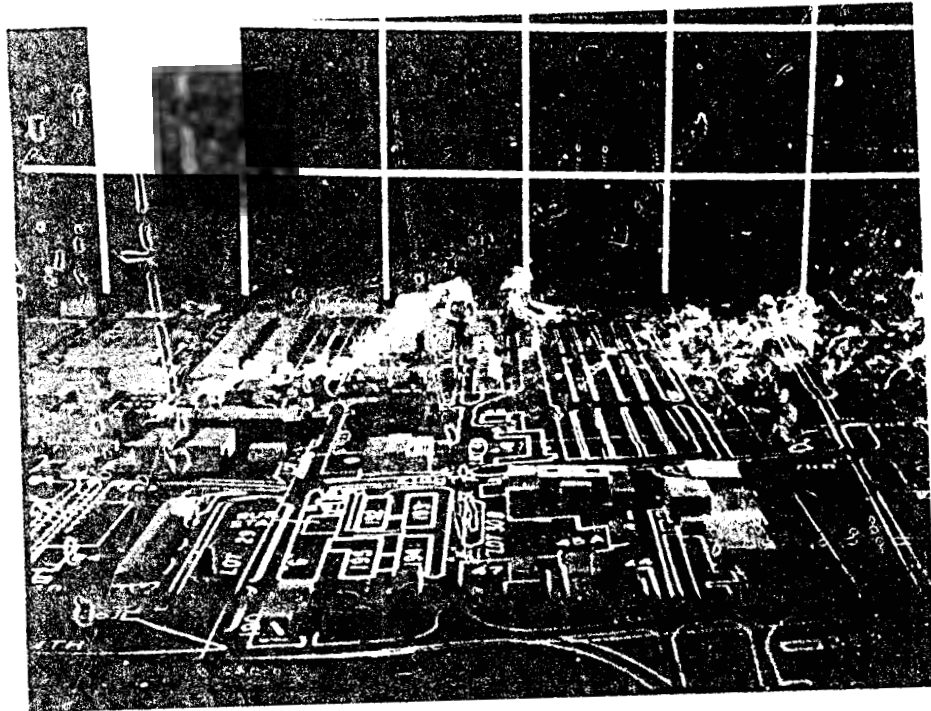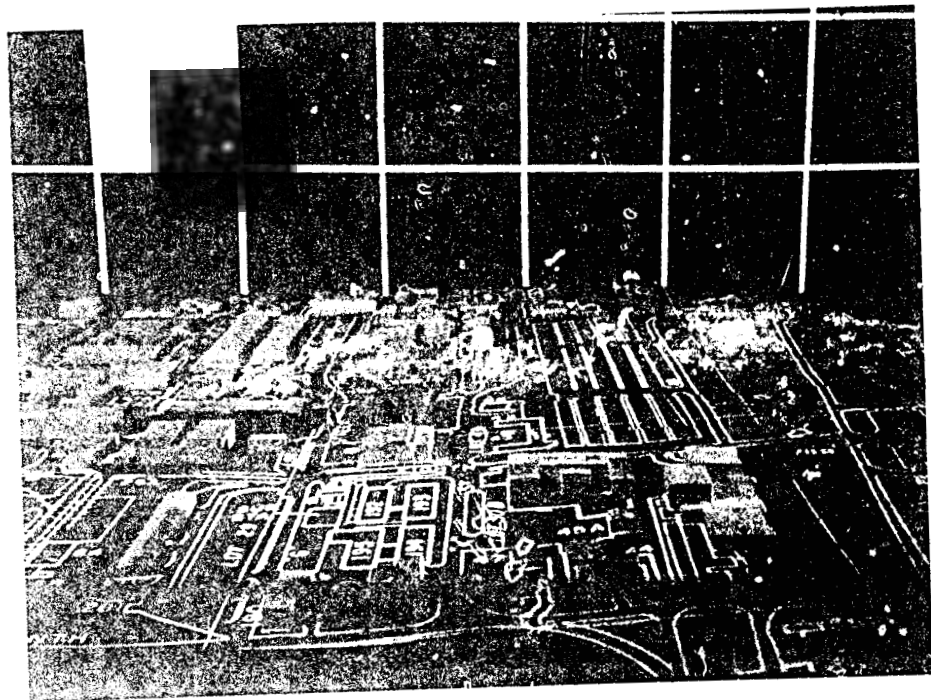
EXTENDED STACK

STANDARD STACK

(b) MODEL REFERENCE WIND VELOCITY, $U_{m_{ref}}$ 3 fps

Figure 21 (Cont.) CRF MODEL SMOKE STUDIES
STANDARD STACK AND EXTENDED STACK, 270 deg WIND
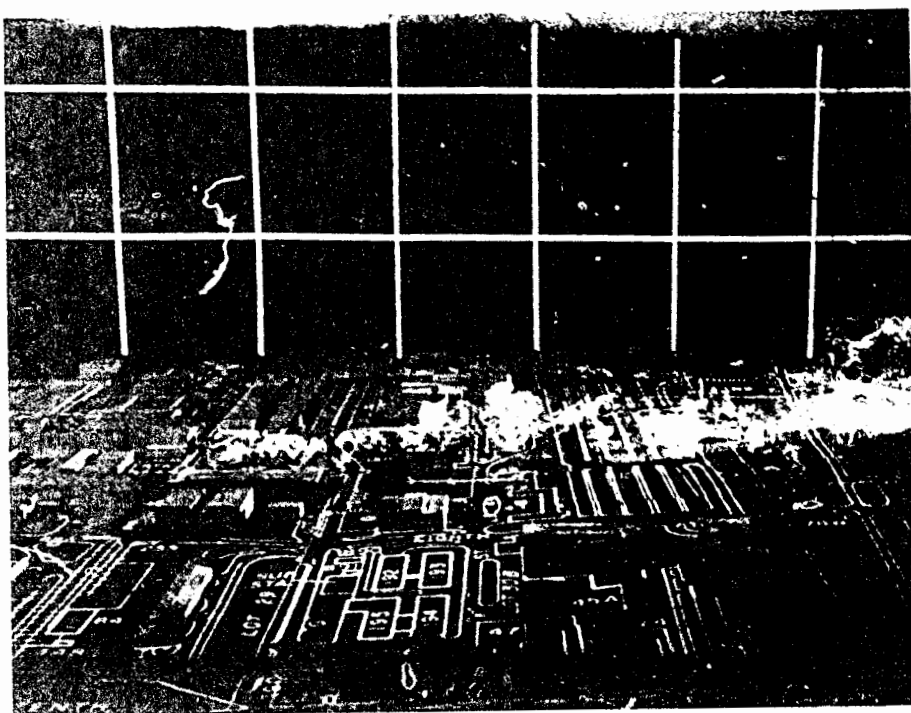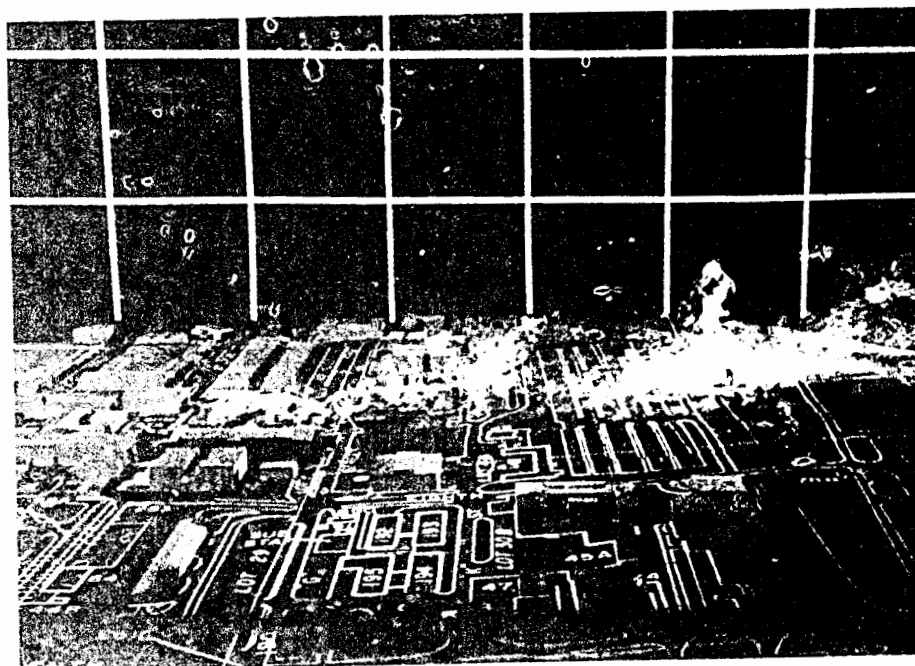
EXTENDED STACK

STANDARD STACK

(c) MODEL REFERENCE WIND VELOCITY, $U_{m_{ref}}$ = 5 fps

Figure 21 (Cont.) CRF MODEL SMOKE STUDIES
STANDARD STACK AND EXTENDED STACK, 270 deg WIND
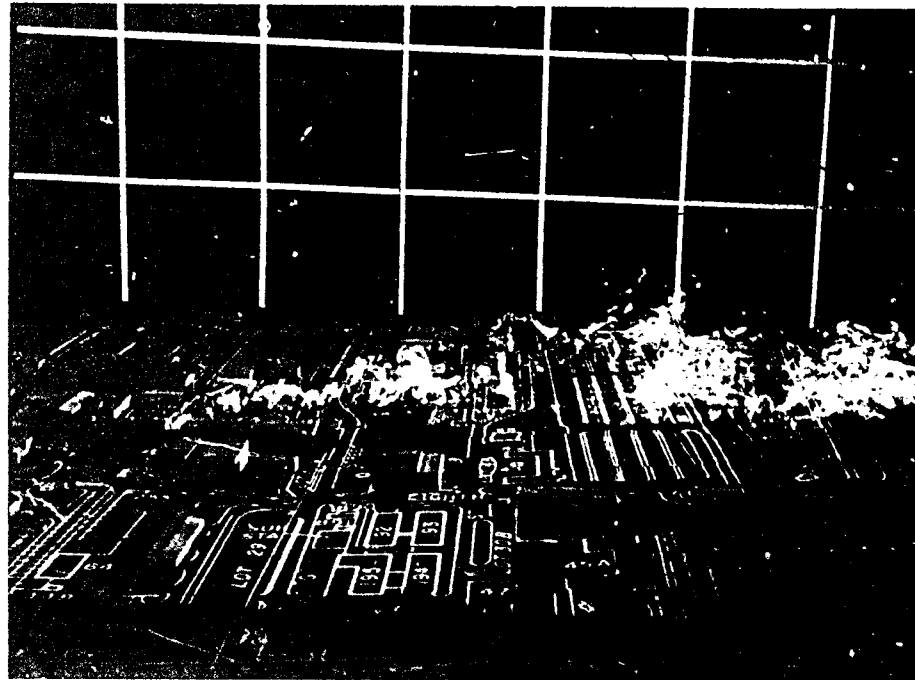
EXTENDED STACK

STANDARD STACK

(d) MODEL REFERENCE WIND VELOCITY, $U_{m_{ref}}$ = 7 fps

Figure 21 (Cont.)   CRF MODEL SMOKE STUDIES
STANDARD STACK AND EXTENDED STACK, 270 deg WIND
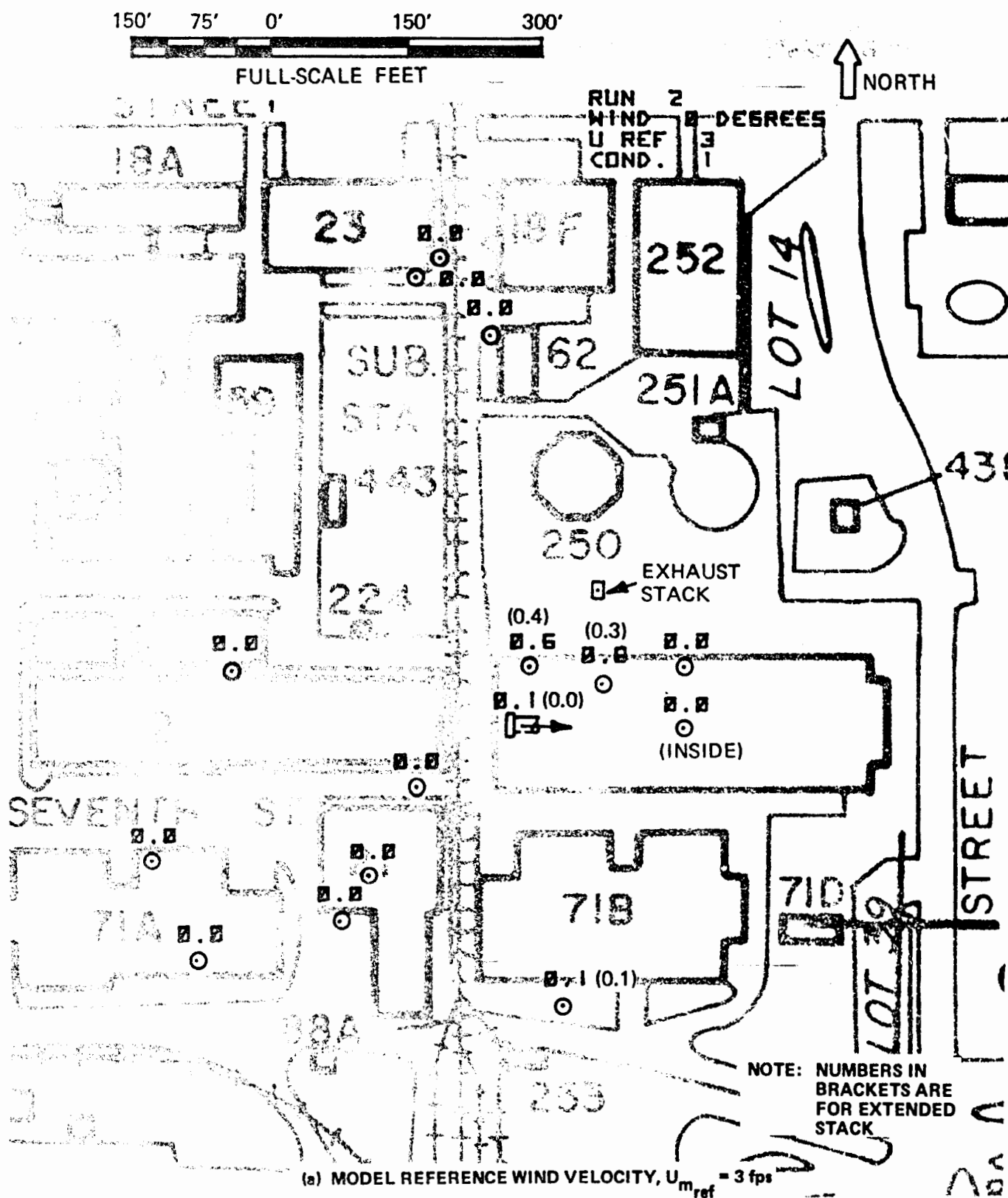
(a) MODEL REFERENCE WIND VELOCITY, $U_{m_{ref}}$ = 3 fps

Figure 22   NEAR-FIELD TEMPERATURE RISE ABOVE AMBIENT, ΔT_f, FULL-SCALE °F
STANDARD STACK, 0 deg WIND

89

Figure 22   NEAR-FIELD TEMPERATURE RISE ABOVE AMBIENT, ΔT_f, FULL-SCALE °F STANDARD STACK, 0 deg WIND

Figure 22 NEAR-FIELD TEMPERATURE RISE ABOVE AMBIENT, ΔT_f, FULL-SCALE °F STANDARD STACK, 0 deg WIND

91

(a) MODEL REFERENCE WIND VELOCITY, $U_{m_{ref}}$ = 2 fps

Figure 23   NEAR-FIELD TEMPERATURE RISE ABOVE AMBIENT, ΔT_f, FULL-SCALE °F
STANDARD STACK, 30 deg WIND

(b) MODEL REFERENCE WIND VELOCITY, $U_{m_{ref}}$ = 3 fps

Figure 23   NEAR-FIELD TEMPERATURE RISE ABOVE AMBIENT, ΔT_f, FULL-SCALE °F
STANDARD STACK, 30 deg WIND

93

150'   75'   0'   150'   300'

FULL-SCALE FEET

RUN   13
WIND 30 DEGREES
U REF 5
COND. 1

NORTH

0.0
⊙
⊙ 0.0
0.0
⊙

EXHAUST
◻◄ STACK

(4.1)   (0.0)
7.5   0.1   0.0
⊙   ⊙
0.0   (0.5) ⊙   0.0
◻►   ⊙
                     (INSIDE)

0.0
⊙

0.9 (0.4)
⊙

0.1 (0.0)
⊙

0.9 (0.7)
⊙
0.7 (0.5)
⊙

0.2 (0.1)
⊙

0.5 (0.5)
⊙

SF

NOTE: NUMBERS IN
        BRACKETS ARE
        FOR EXTENDED
        STACK

(c) MODEL REFERENCE WIND VELOCITY, $U_{m_{ref}}$ = 5 fps

Figure 23   NEAR-FIELD TEMPERATURE RISE ABOVE AMBIENT, ΔT_f, FULL-SCALE °F
            STANDARD STACK, 30 deg WIND

94

FULL-SCALE FEET

150' 75' 0' 150' 300'

NORTH

RUN 14
WIND 30 DEGREES
U REF 7
COND. 1

0.0
⊙

⊙ 0.0

0.0
⊙

EXHAUST
STACK

(4.1)
5.5 (0.0) 0.0
⊙   0.1 ⊙
     ⊙

0.1(0.0)
⊙

1.0(0.5)
⊏▶   0.0
            ⊙
            (INSIDE)

0.0(0.5)
⊙

0.0
⊙

STREE

0.5(0.6)
⊙

0.5(0.4)
⊙

0.1(0.1)
⊙

0.5(0.5)
⊙

NOTE: NUMBERS IN
        BRACKETS ARE
        FOR EXTENDED
        STACK

(d) MODEL REFERENCE WIND VELOCITY, $U_{m_{ref}}$ = 7 fps

Figure 23   NEAR-FIELD TEMPERATURE RISE ABOVE AMBIENT, ΔT_f, FULL-SCALE °F STANDARD STACK, 30 deg WIND

95

FULL-SCALE FEET

RUN 22
WIND 60 DEGREES
U REF 3
COND. 1

NORTH

0.0
⊙
⊙ 0.0
0.0
⊙

EXHAUST
STACK

(0.2)
2.4
⊙

0.4 (0.1)
⊙

0.0
⊙

0.0
⊙

0.0
⊙

0.0
⊙
(INSIDE)

0.6 (0.2)
⊙

1.1 (0.7)
⊙

0.2 (0.1)
⊙

0.2 (0.1)
⊙

0.5 (0.3)
⊙

0.0
⊙

NOTE: NUMBERS IN
BRACKETS ARE
FOR EXTENDED
STACK

(a) MODEL REFERENCE WIND VELOCITY, $U_{m_{ref}}$ = 3 fps

Figure 24   NEAR-FIELD TEMPERATURE RISE ABOVE AMBIENT, ΔT_f, FULL-SCALE °F
STANDARD STACK, 60 deg WIND

96

(c) MODEL REFERENCE WIND VELOCITY, $U_{m_{ref}}$ = 7 fps

Figure 24   NEAR-FIELD TEMPERATURE RISE ABOVE AMBIENT, ΔT_f, FULL-SCALE °F
STANDARD STACK, 60 deg WIND

150' 75' 0'   150'   300'

FULL-SCALE FEET

RUN 31
WIND 90 DEGREES
U REF 3
COND. 11

NORTH

(a) MODEL REFERENCE WIND VELOCITY, $U_{m_{ref}}$ = 3 fps

Figure 25   NEAR-FIELD TEMPERATURE RISE ABOVE AMBIENT, ΔT_f, FULL-SCALE °F
STANDARD STACK, 90 deg WIND

150'   150'   300'

RUN   32
WIND   90 DEGREES
U REF : 5

NORTH

EXHAUST
STACK

1.2

0.0   -0.0   -0.0

0.0

-0.0
(INSIDE)

0.0

0.0

0.0

0.0

-0.0

-0.0

SEV

STRF

(b) MODEL REFERENCE WIND VELOCITY, $U_{m_{ref}}$ = 5 fps

Figure 25   NEAR-FIELD TEMPERATURE RISE ABOVE AMBIENT, ΔT_f, FULL-SCALE ^{o}F
STANDARD STACK, 90 deg WIND

100

150'   75'   150'   300'

NORTH

RUN   33
WIND   90 DEGREES
U REF   7
COND.   1

EXHAUST
STACK

1.4

0.0   -0.0   -0.0

-0.0

-0.6
(INSIDE)

0.0

SEV

0.0

-0.0

-0.0

-0.0

-0.0

STRE

(c) MODEL REFERENCE WIND VELOCITY, $U_{m_{ref}}$ ≈ 7 fps

Figure 25   NEAR-FIELD TEMPERATURE RISE ABOVE AMBIENT, ΔT_f, FULL-SCALE °F
STANDARD STACK, 90 deg WIND

101

150'   75'

FULL-SCALE FEET

RUN   36
WIND 120 DEGREES
U REF 5
COND.   1

NORTH

0.0
⊙
⊙ 0.1
      0.1
      ⊙

0.0   -0.0
0   0

EXHAUST
□← STACK

0.9
⊙

-0.0 -0.0   -0.0
⊙   ⊙   ⊙

0.0   -0.0
□⟹   ⊙
              (INSIDE)

-0.0
⊙

-0.0
⊙

-0.0
⊙   -0.0
       ⊙

⊙

⊙

(a) MODEL REFERENCE WIND VELOCITY, $U_{m_{ref}}$ = 5 fps

Figure 26   NEAR-FIELD TEMPERATURE RISE ABOVE AMBIENT, ΔT_f, FULL-SCALE °F
STANDARD STACK, 120 deg WIND

102

150' 75'   150'   300'

FULL-SCALE FEET

RUN 37
WIND 120 DEGREES
U REF 7
COND. 1

NORTH

0.0
⊙
⊙ 0.1
0.0
⊙

0.0
0

EXHAUST
STACK

1.1
⊙

-0.0   -0.0   -0.0
⊙   ⊙   ⊙

-0.0   -0.0
⊙

(INSIDE)

-0.0
⊙

SE

-0.0
⊙

-0.0
⊙

-0.0
⊙

⊙

⊙

(b) MODEL REFERENCE WIND VELOCITY, $U_{m_{ref}}$ = 7 fps

Figure 26   NEAR-FIELD TEMPERATURE RISE ABOVE AMBIENT, ΔT_f, FULL-SCALE °F
STANDARD STACK, 120 deg WIND

103

(a) MODEL REFERENCE WIND VELOCITY, $U_{m_{ref}}$ = 3 fps

Figure 27   NEAR-FIELD TEMPERATURE RISE ABOVE AMBIENT, ΔT_f, FULL-SCALE °F
STANDARD STACK, 150 deg WIND

104

(b) MODEL REFERENCE WIND VELOCITY, $U_{m_{ref}}$ = 5 fps

Figure 27   NEAR-FIELD TEMPERATURE RISE ABOVE AMBIENT, ΔT_f, FULL-SCALE °F
STANDARD STACK, 150 deg WIND

105

150'   75'   0'   150'   300'

FULL-SCALE FEET

NORTH

RUN   42
WIND   150 DEGREES
U REF   7
COND.   1

1.6 (1.6)

1.7 (1.9)

2.1 (2.2)

3.7 (2.7)   0.1 (0.0)

EXHAUST
STACK

0.3 (0.1)

0.0   0.0   0.0
         0.0

-0.0   0.0
                  (INSIDE)

-0.0

0.0

-0.0

-0.0

NOTE: NUMBERS IN
        BRACKETS ARE
        FOR EXTENDED
        STACK

(c) MODEL REFERENCE WIND VELOCITY, $U_{m_{ref}}$ = 7 fps

Figure 27   NEAR-FIELD TEMPERATURE RISE ABOVE AMBIENT, ΔT_f, FULL-SCALE °F
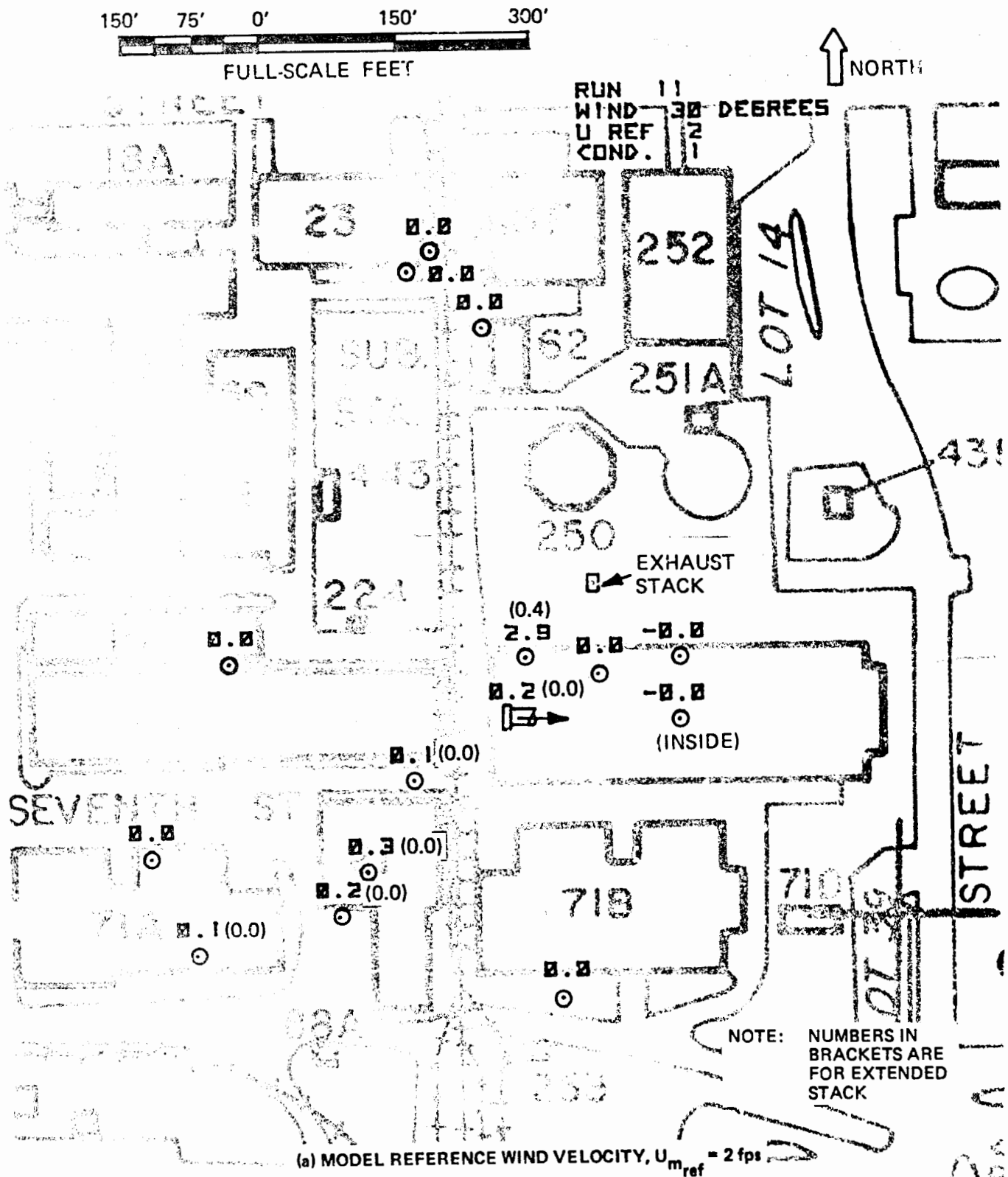STANDARD STACK, 150 deg WIND

106

150'   75'   0'   150'   300'

FULL-SCALE FEET

NORTH

RUN 50
WIND 180 DEGREES
U REF 3
COND. 1

252

0.1 (0.0)
0.1 (0.0)
0.4 (0.3)

1.9 (1.1)   2.8 (0.7)

EXHAUST
STACK

0.0   0.0   0.0

0.0   -0.0
(INSIDE)

0.0

0.0   -0.0
-0.0

SF

STRF

NOTE: NUMBERS IN
BRACKETS ARE
FOR EXTENDED
STACK

(a) MODEL REFERENCE WIND VELOCITY, $U_{m_{ref}}$ = 3 fps
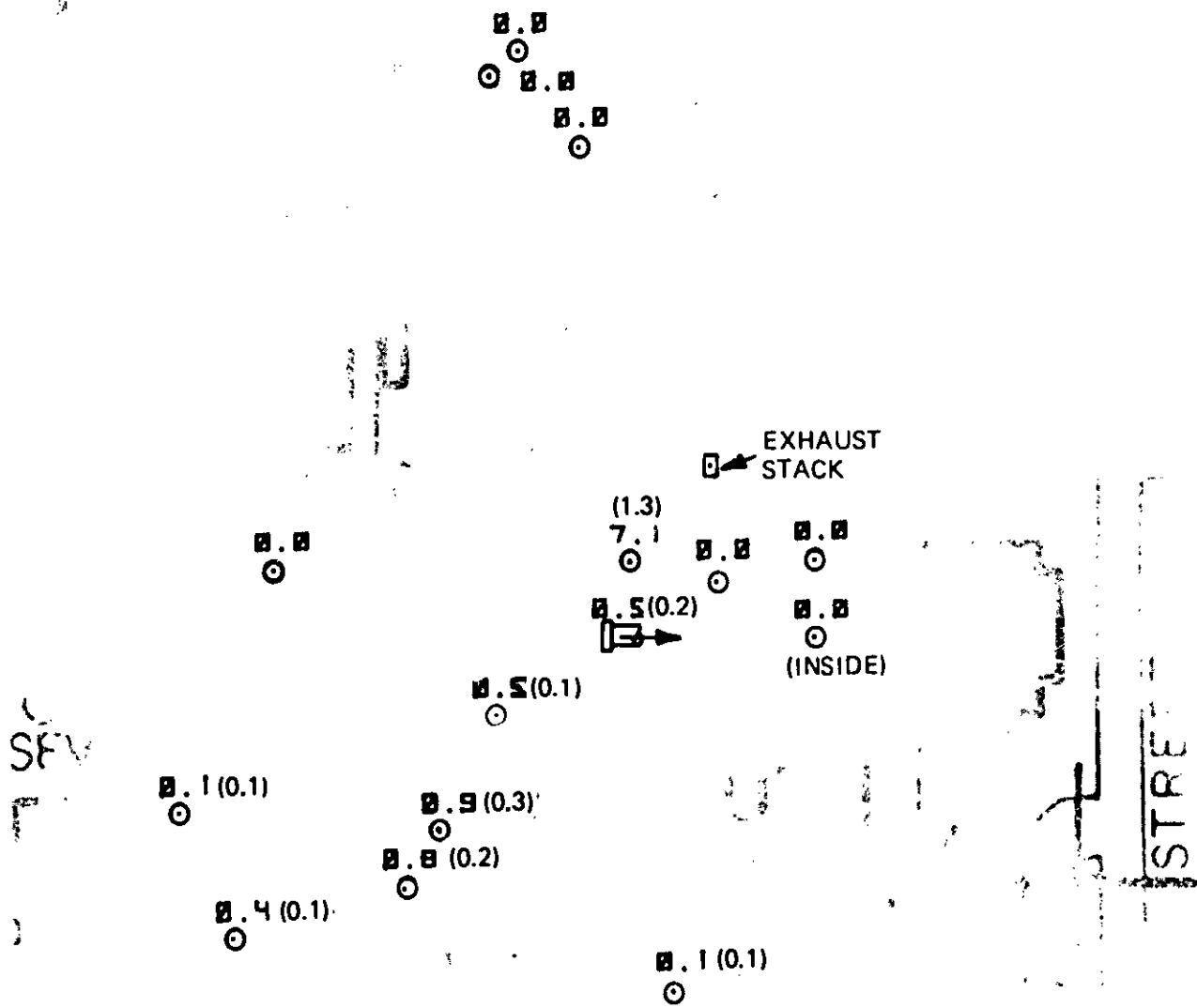
Figure 28   NEAR-FIELD TEMPERATURE RISE ABOVE AMBIENT, ΔT_f, FULL-SCALE °F
STANDARD STACK, 180 deg WIND

107

150'   75'   0'   150'   300'

FULL-SCALE FEET

RUN 51
WIND 180 DEGREES
U REF 5
COND. 1

↑ NORTH

0.1 (0.2)
⊙
⊙ 0.1 (0.1)
0.8 (0.9)
⊙

4.2 (2.9)   4.7 (2.8)
0   0

EXHAUST
0 ← STACK

0.0   0.0   0.0   0.0
⊙   ⊙   ⊙   ⊙

0.0   0.0
⊡→   ⊙
                    (INSIDE)

0.0
⊙

0.0   -0.0
⊙   ⊙

-0.0
⊙

⊙

⊙
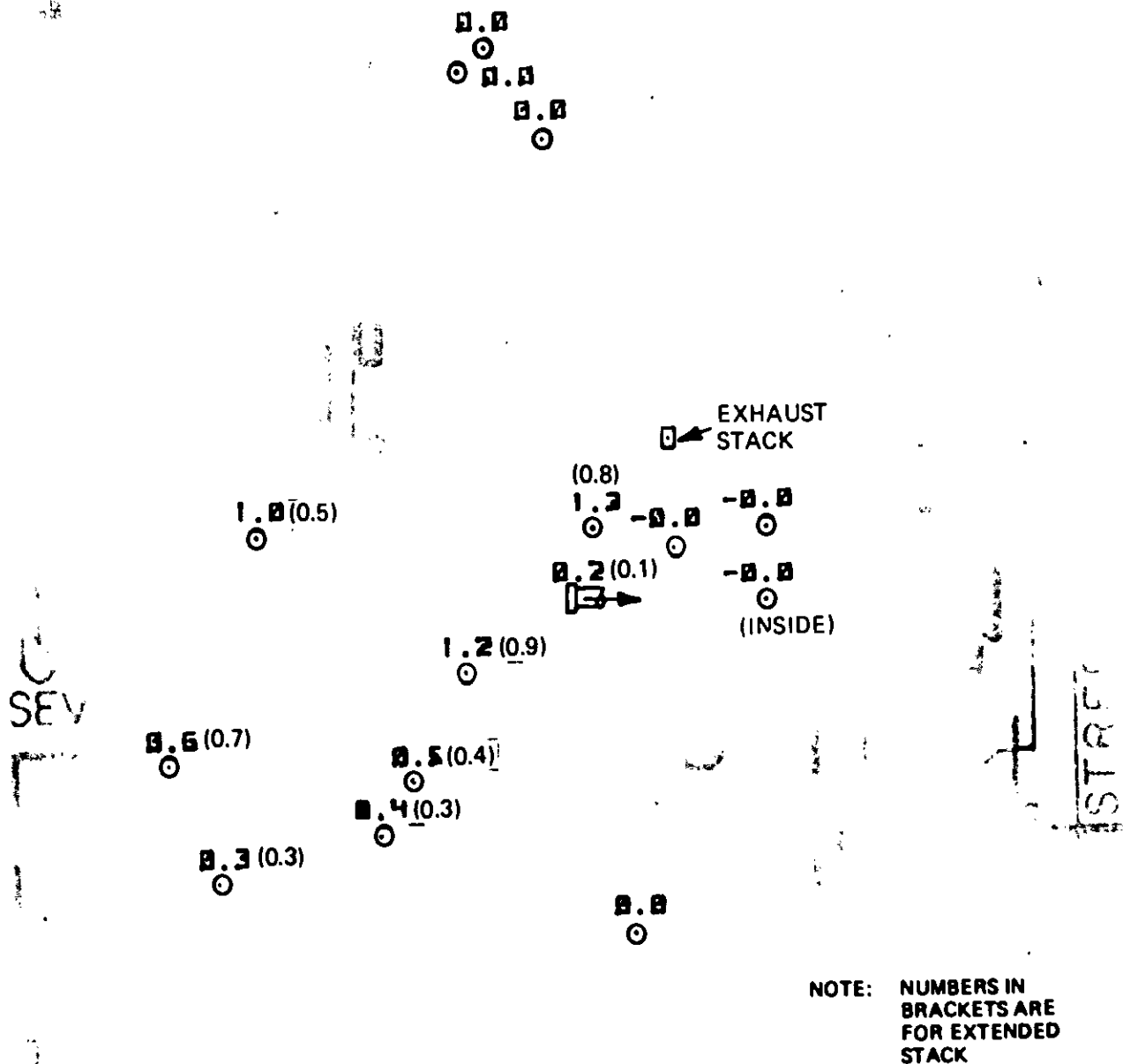
NOTE: NUMBERS IN
        BRACKETS ARE
        FOR EXTENDED
        STACK

(b) MODEL REFERENCE WIND VELOCITY, $U_{m_{ref}}$ = 5 fps

Figure 28   NEAR-FIELD TEMPERATURE RISE ABOVE AMBIENT, ΔT_f, FULL-SCALE °F
STANDARD STACK, 180 deg WIND

108

Figure 28 NEAR-FIELD TEMPERATURE RISE ABOVE AMBIENT, ΔT_f, FULL-SCALE °F STANDARD STACK, 180 deg WIND

(a) MODEL REFERENCE WIND VELOCITY, $U_{m_{ref}}$ = 3 fps

Figure 29   NEAR-FIELD TEMPERATURE RISE ABOVE AMBIENT, ΔT_f, FULL-SCALE °F
STANDARD STACK, 210 deg WIND

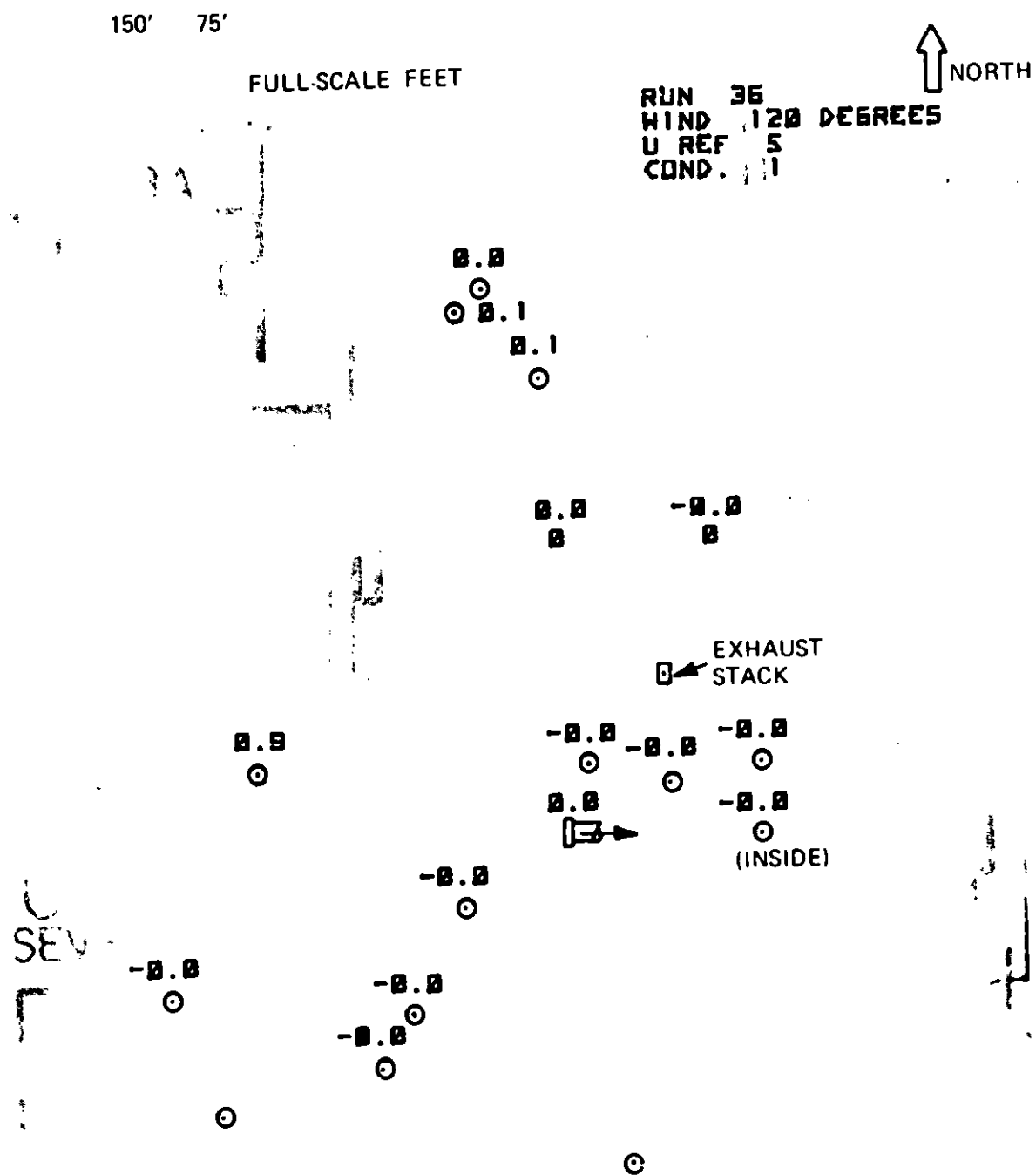150'   75'   0'   150'   300'

FULL-SCALE FEET

⇧ NORTH

RUN 60
WIND 210 DEGREES
U REF 5
COND.   1

-0.0
⊙
⊙-0.0
0.0
⊙

0.2 (0.1)   4.0 (3.3)
0   0

EXHAUST
▣◀ STACK

0.0   0.0   0.0
⊙   -0.0   ⊙
⊙

0.0   -0.0
▯▣▶   ⊙
(INSIDE)

-0.0
⊙

-0.0
⊙

-0.0
⊙

-0.0
⊙

-0.0
⊙

⊙

⊙

NOTE: NUMBERS IN
BRACKETS ARE
FOR EXTENDED
STACK

(b) MODEL REFERENCE WIND VELOCITY, $U_{m_{ref}}$ = 5 fps

Figure 29   NEAR-FIELD TEMPERATURE RISE ABOVE AMBIENT, ΔT_f, FULL-SCALE °F
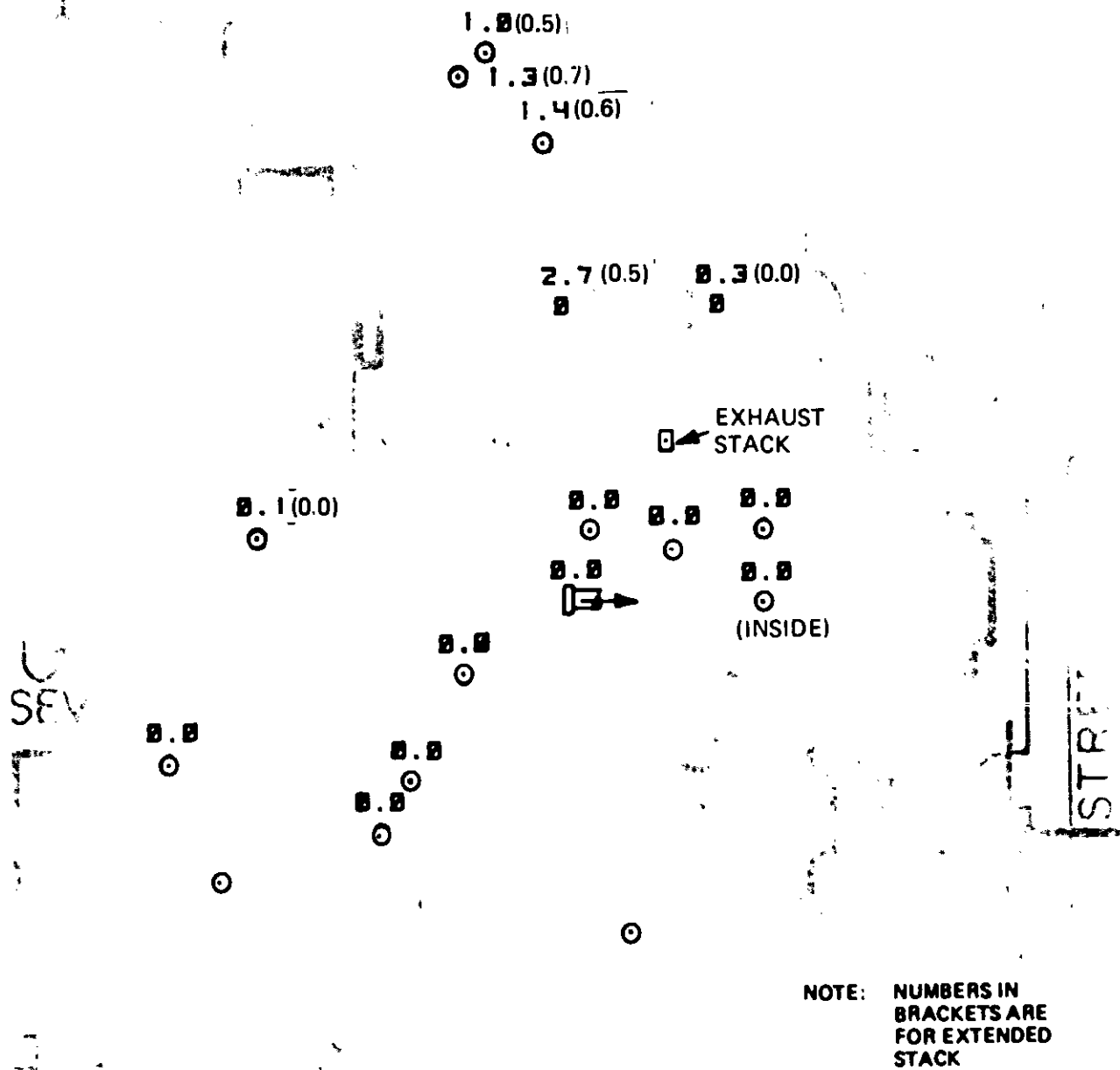STANDARD STACK, 210 deg WIND

iii

FULL-SCALE FEET

RUN 61
WIND 210 DEGREES
U REF 7
COND. 1

NORTH

-0.0

0-0.0

0.0

0.2   4.3

EXHAUST
STACK

-0.0   0.0   -0.0   -0.0

-0.0   0.0
                   (INSIDE)

-0.0

-0.0

-0.0

-0.0

SE

STP

(c) MODEL REFERENCE WIND VELOCITY, $U_{m_{ref}}$ = 7 fps

Figure 29   NEAR-FIELD TEMPERATURE RISE ABOVE AMBIENT, ΔT_f, FULL-SCALE °F
STANDARD STACK, 210 deg WIND

112

150'   75'   150'   300'

FULL-SCALE FEET

RUN   66
WIND 240 DEGREES   NORTH

SE\

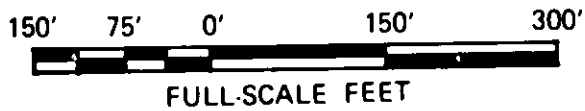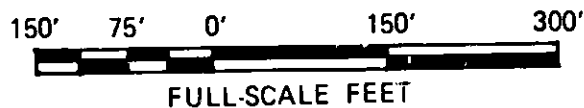−0.0
⊙

(

NOTE: NUMBERS IN
       BRACKETS ARE
       FOR EXTENDED
       STACK

(a) MODEL REFERENCE WIND VELOCITY, $U_{m_{ref}}$ = 5 fps

Figure 30   NEAR-FIELD TEMPERATURE RISE ABOVE AMBIENT, ΔT_f, FULL-SCALE °F
            STANDARD STACK, 240 deg WIND

113

150'   75'   0'   150'   300'

FULL-SCALE FEET

NORTH

RUN 57
WIND 240 DEGREES
U REF 7
COND. 1

0.0
⊙
⊙ 0.0
0.0
⊙

0.0   0.2
0   0

EXHAUST
0◄ STACK

-0.0   0.0   0.0   0.0
⊙   ⊙   0.0   ⊙
                          ⊙
                 0.0   0.0
                 ▷   ⊙
                                (INSIDE)

0.0
⊙

-0.0
⊙   -0.0
             ⊙
           -0.0
             ⊙

⊙

⊙

(b) MODEL REFERENCE WIND VELOCITY, $U_{m_{ref}}$ = 7 fps

Figure 30   NEAR-FIELD TEMPERATURE RISE ABOVE AMBIENT, ΔT_f, FULL-SCALE °F
STANDARD STACK, 240 deg WIND

114

150'   300'

FULL-SCALE FEET

RUN   73
WIND   270 DEGREES
U REF   3
COND.   1

NORTH

⊡.⊡
⊙
⊙ ⊡.⊡
⊡.⊡
⊙

⊡.⊡
⊡

EXHAUST
⊡◄ STACK

⊡.⊡   ⊡.⊡   ⊡.⊡   ⊡.⊡ (0.1)
⊙   ⊙   ⊙   ⊙

⊡.⊡   ⊡.⊡
[⊐►   ⊙
                                 (INSIDE)

⊡.⊡
⊙

SFV

⊡.⊡   ⊡.⊡
⊙   ⊙
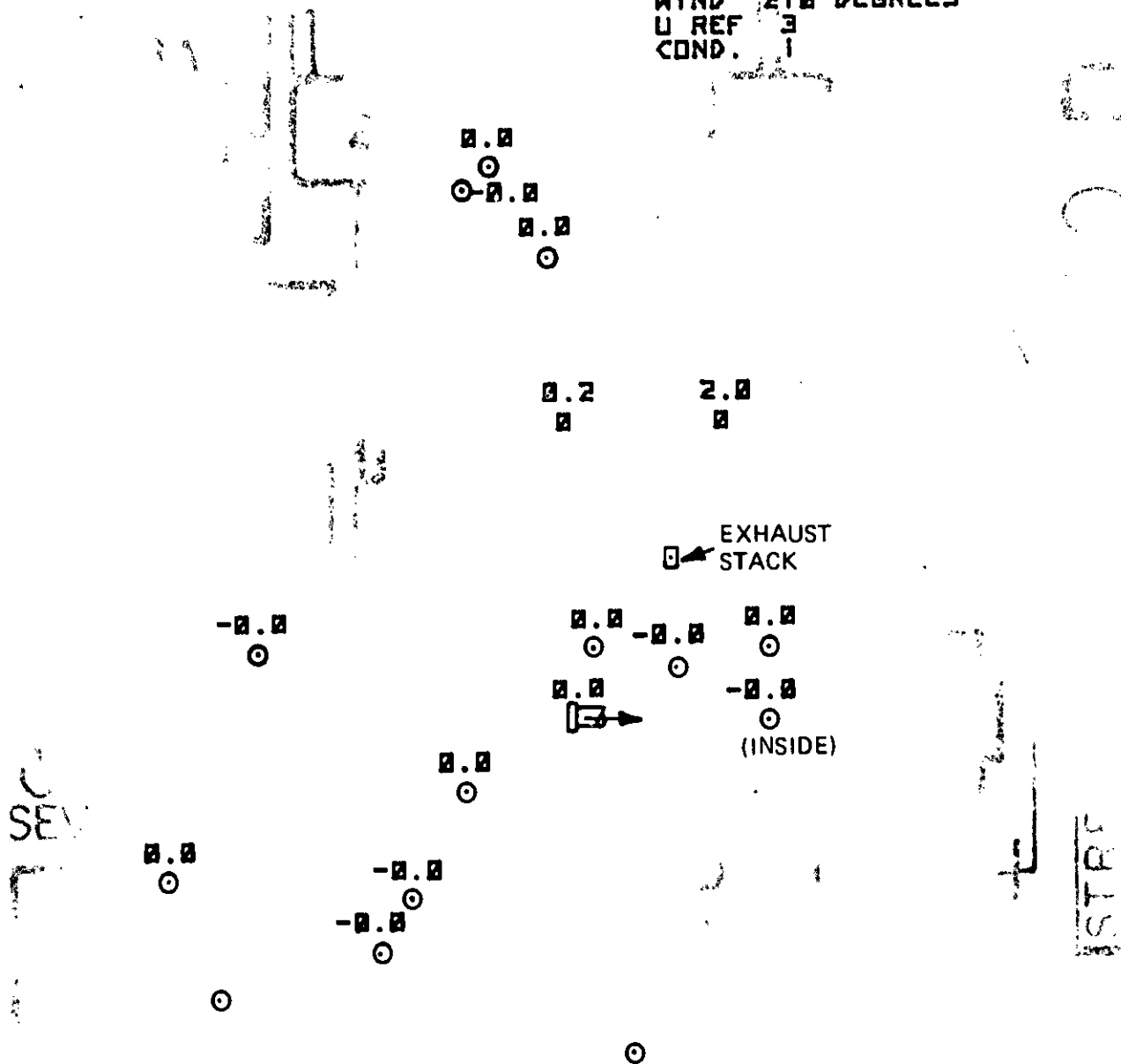   ⊡.⊡
        ⊙

⊙

⊙

STREET

NOTE: NUMBERS IN
        BRACKETS ARE
        FOR EXTENDED
        STACK

(a) MODEL REFERENCE WIND VELOCITY, $U_{m_{ref}}$ = 3 fps

Figure 31   NEAR-FIELD TEMPERATURE RISE ABOVE AMBIENT, ΔT_f, FULL-SCALE ^{o}F
STANDARD STACK, 270 deg WIND

115

NOTE: NUMBERS IN
         BRACKETS ARE
         FOR EXTENDED
         STACK

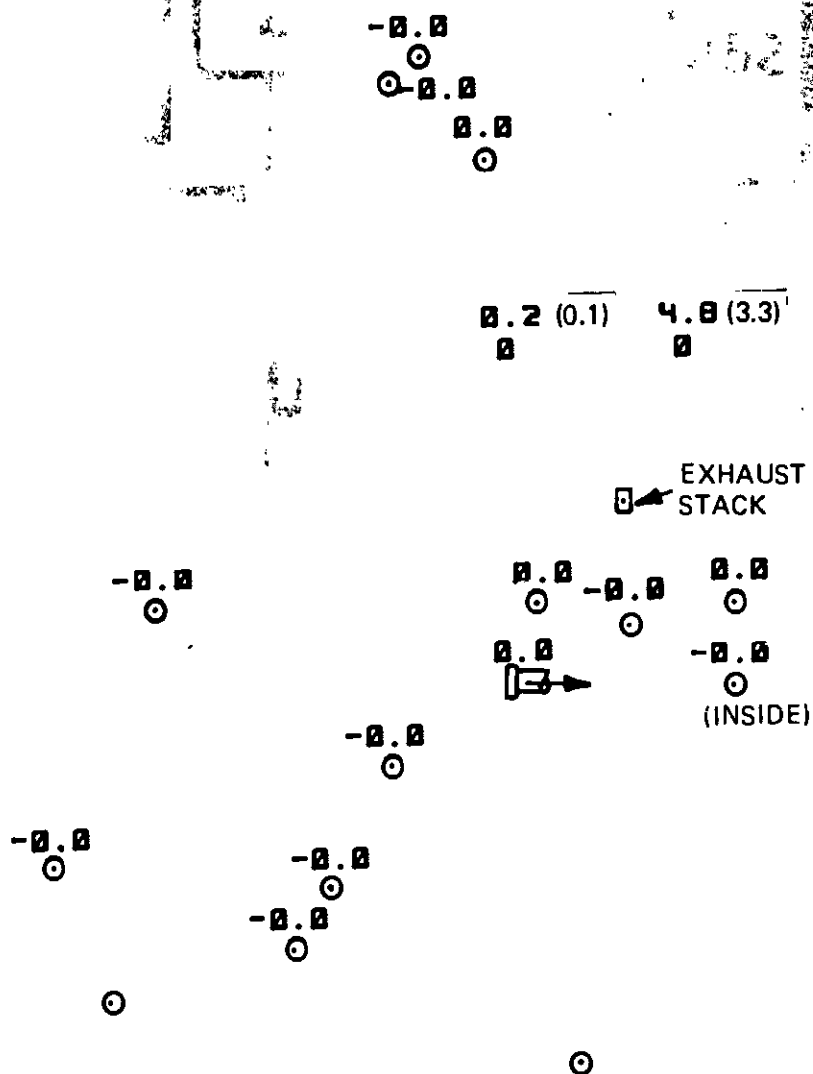(b) MODEL REFERENCE WIND VELOCITY, $U_{m_{ref}}$ = 5 fps

Figure 31   NEAR-FIELD TEMPERATURE RISE ABOVE AMBIENT, ΔT_f, FULL-SCALE °F
            STANDARD STACK, 270 deg WIND

116

FULL-SCALE FEET

RUN   75
WIND 270 DEGREES
U REF 7
COND. 1

NORTH

0.0
⊙
⊙─0.0
─0.0
⊙

─0.0
0

EXHAUST
STACK

─0.0
⊙

0.0
⊙

0.0
⊙

0.7 (0.3)
⊙

0.0
⊙

0.4 (0.1)
⊙
(INSIDE)

0.0
⊙

─0.0
⊙

0.0
⊙

0.0
⊙

⊙

⊙

NOTE: NUMBERS IN
BRACKETS ARE
FOR EXTENDED
STACK

(c) MODEL REFERENCE WIND VELOCITY, $U_{m_{ref}}$ = 7 fps

Figure 31   NEAR-FIELD TEMPERATURE RISE ABOVE AMBIENT, ΔT_f, FULL-SCALE °F
STANDARD STACK, 270 deg WIND

117

150' 75' 0' 150' 300'

FULL-SCALE FEET

NORTH

RUN 83
WIND 300 DEGREES
U REF 3
COND. 1

−0.0
⊙
⊙−0.0
−0.0
⊙

EXHAUST
◻⟵ STACK

−0.0
⊙

−0.0 (0.0) 3.0 (0.9)
⊙   0.1   ⊙
⊙

0.0   0.2 (0.0)
▯⟶   ⊙
(INSIDE)

−0.0
⊙

−0.0   −0.0
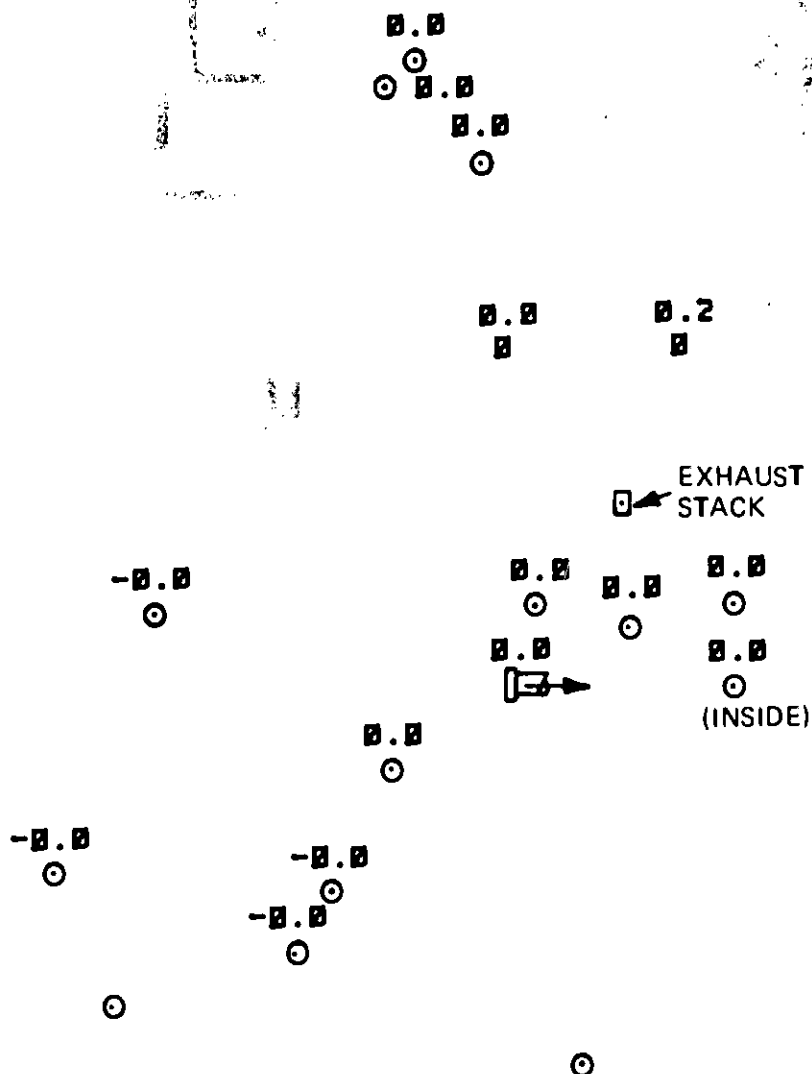⊙   ⊙

−0.0
⊙

−0.0
⊙

0.0
⊙

NOTE: NUMBERS IN
BRACKETS ARE
FOR EXTENDED
STACK

(a) MODEL REFERENCE WIND VELOCITY, $U_{m_{ref}}$ = 3 fps

Figure 32 NEAR-FIELD TEMPERATURE RISE ABOVE AMBIENT, ΔT_f, FULL-SCALE °F
STANDARD STACK, 300 deg WIND

118

150' 75' 0' 150' 300'
FULL-SCALE FEET

NORTH

RUN 84
WIND 300 DEGREES
U REF 5
COND. ,1

0.0
⊙
⊙ 0.0
0.0
⊙

EXHAUST
▯ STACK

0.0 (0.0) 6.3(2.4)
⊙ 0.2 ⊙
⊙

0.1 (0.0) 0.6(0.1)
▯▶ ⊙
(INSIDE)

0.0
⊙

0.0
⊙

0.0
⊙

0.0
⊙

0.0
⊙

0.0
⊙

0.0
⊙

NOTE: NUMBERS IN
BRACKETS ARE
FOR EXTENDED
STACK

(b) MODEL REFERENCE WIND VELOCITY, $U_{m_{ref}}$ = 5 fps

Figure 32 NEAR-FIELD TEMPERATURE RISE ABOVE AMBIENT, ΔT_f, FULL-SCALE °F
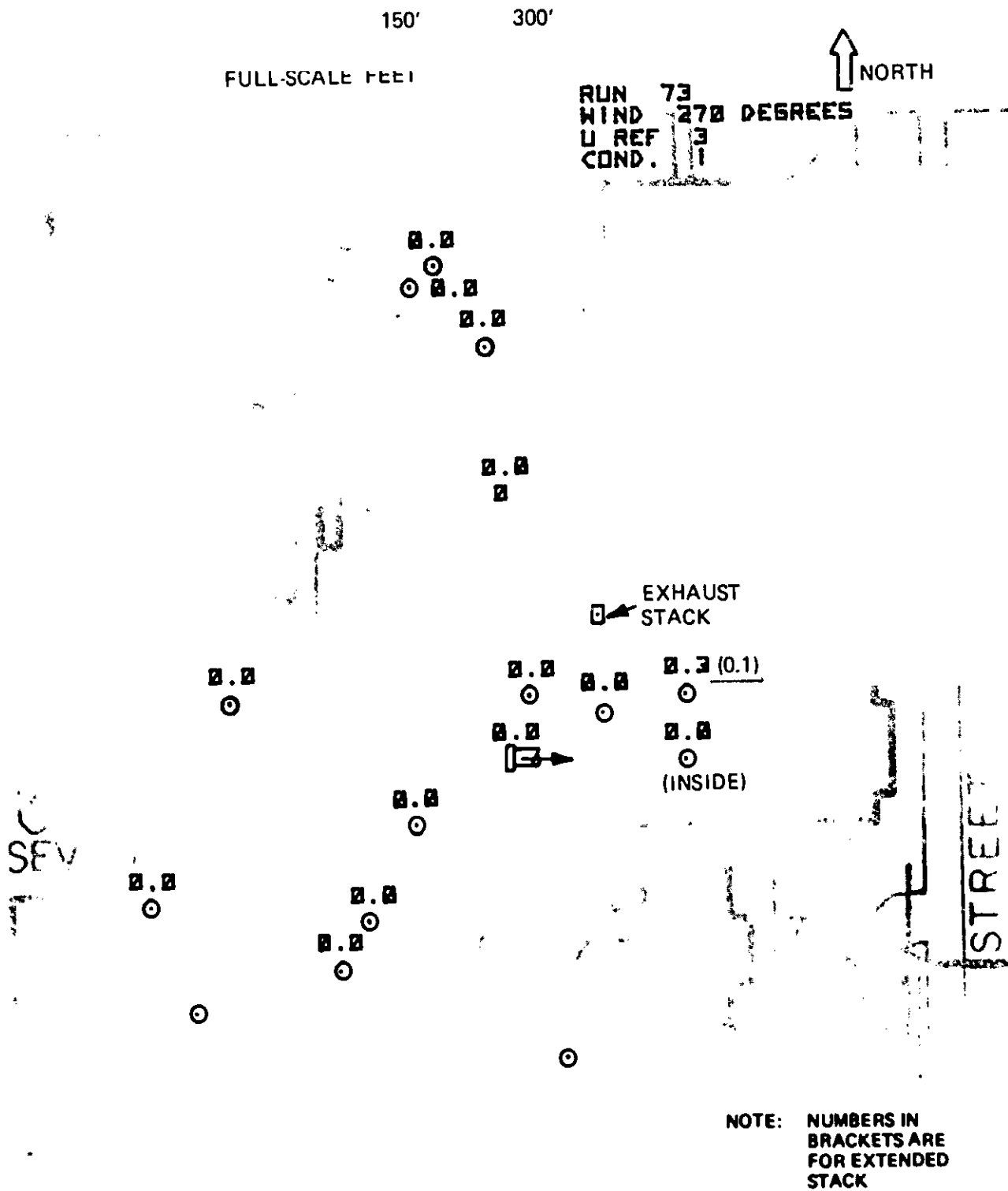STANDARD STACK, 300 deg WIND
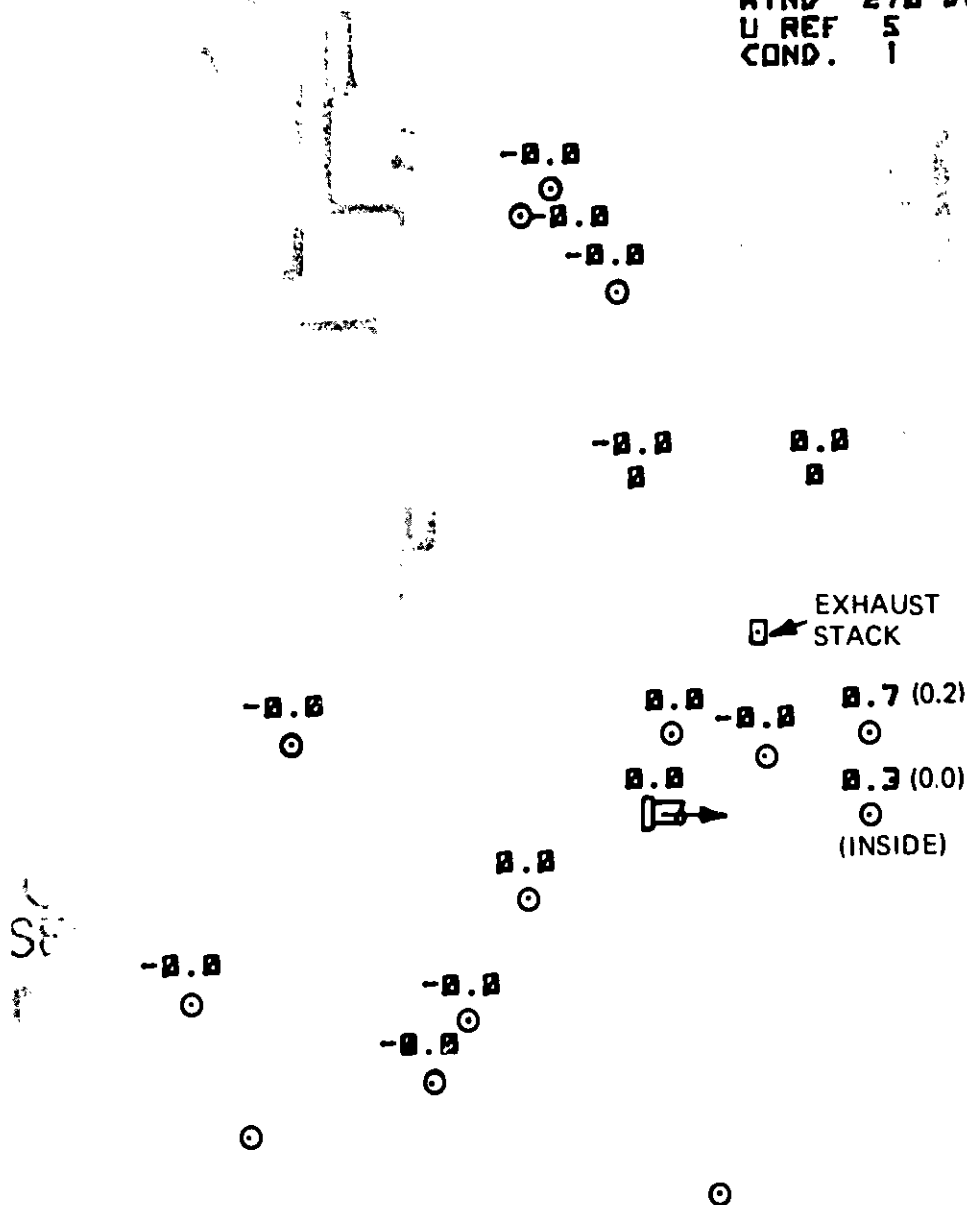
119

(a) MODEL REFERENCE WIND VELOCITY, $U_{m_{ref}}$ = 3 fps

Figure 33   NEAR-FIELD TEMPERATURE RISE ABOVE AMBIENT, ΔT_f, FULL-SCALE °F STANDARD STACK, 330 deg WIND

150' 75' 0' 150' 300'

FULL-SCALE FEET

RUN 91
WIND 330 DEGREES
U REF 5
COND. 1

↑ NORTH

-0.0
⊙
⊙-0.0
-0.0
⊙

EXHAUST
◻← STACK

-0.0
⊙

0.0   (0.8)   3.2 (1.0)
⊙   1.7   ⊙
         ⊙

0.2 (0.0)   0.7 (0.2)
🔲→   ⊙
                (INSIDE)

0.0
⊙

-0.0
⊙

0.0
⊙

-0.0
⊙

-0.0
⊙

0.1 (0.0)
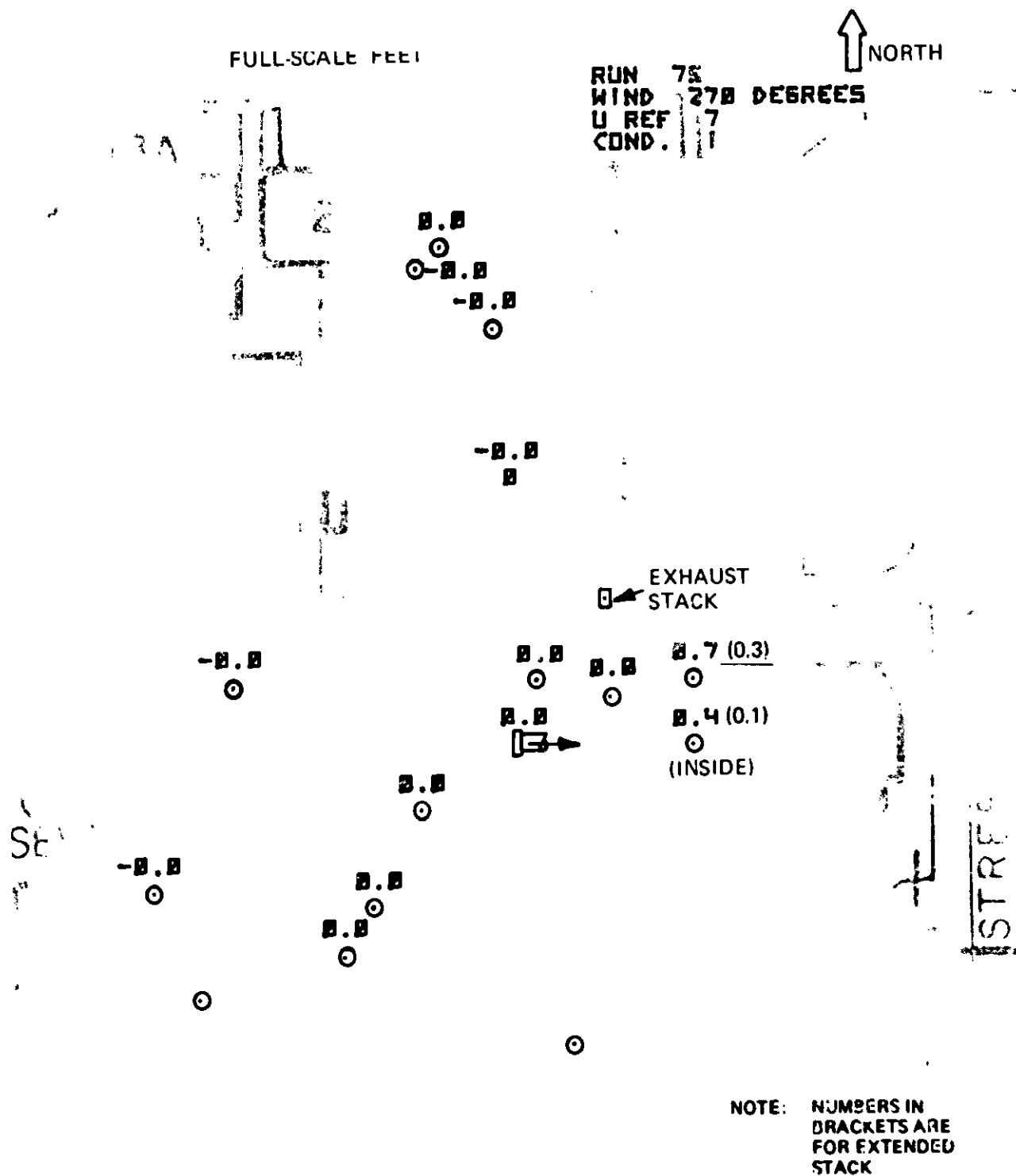⊙

NOTE: NUMBERS IN
       BRACKETS ARE
       FOR EXTENDED
       STACK

(b) MODEL REFERENCE WIND VELOCITY, $U_{m_{ref}}$ = 5 fps

Figure 33   NEAR-FIELD TEMPERATURE RISE ABOVE AMBIENT, ΔT_f, FULL-SCALE °F
STANDARD STACK, 330 deg WIND

122

NOTE: NUMBERS IN BRACKETS ARE FOR EXTENDED STACK

(c) MODEL REFERENCE WIND VELOCITY, $U_{m_{ref}}$ = 7 fps

Figure 33   NEAR-FIELD TEMPERATURE RISE ABOVE AMBIENT, ΔT_f, FULL-SCALE $^\circ$F STANDARD STACK, 330 deg WIND

123

RUN 2
WIND 0 DEGREES
U REF 3
COND. 1

NORTH ⬆

500' 250' 0' 500' 1000'

FULL-SCALE FEET

(a) MODEL REFERENCE WIND VELOCITY, $U_{m_{ref}}$ = 3 fps

Figure 34   FAR-FIELD TEMPERATURE RISE ABOVE AMBIENT, ΔT_f, FULL-SCALE °F
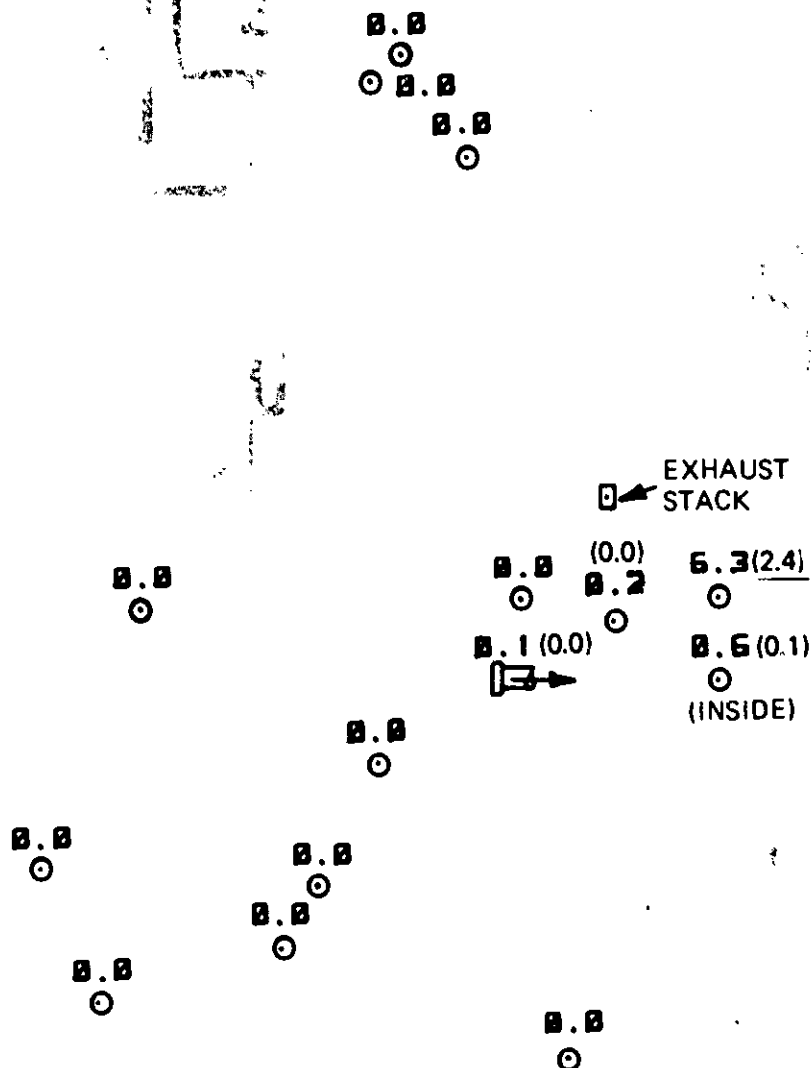STANDARD STACK, 0 deg WIND

RUN   3
WIND   0 DEGREES
U REF   5
COND .   1

NORTH ⬆

500'   250'   0'   500'   1000'

FULL-SCALE FEET

⊙ EXHAUST
  STACK

N
.
■

(b) MODEL REFERENCE WIND VELOCITY, $U_{m_{ref}}$ = 5 fps

Figure 34   FAR-FIELD TEMPERATURE RISE ABOVE AMBIENT, ΔT_f, FULL-SCALE $^\circ$F
STANDARD STACK, 0 deg WIND

RUN 4
WIND 0 DEGREES
U REF 7
COND. 1

NORTH ⇧

500'   250'   0'   500'   1000'
FULL-SCALE FEET

(c) MODEL REFERENCE WIND VELOCITY, $U_{m_{ref}}$ = 7 fps

Figure 34 FAR-FIELD TEMPERATURE RISE ABOVE AMBIENT, ΔT_f, FULL-SCALE °F
STANDARD STACK, 0 deg WIND

126

RUN 31
WIND 90 DEGREES
U REF 3
COND. 1

NORTH ⬆

500' 250' 0'   500'   1000'

FULL-SCALE FEET

+

(a) MODEL REFERENCE WIND VELOCITY, $U_{m_{ref}}$ = 3 fps

Figure 35   FAR-FIELD TEMPERATURE RISE ABOVE AMBIENT, ΔT_f, FULL-SCALE °F
STANDARD STACK, 90 deg WIND

RUN   32
WIND   90 DEGREES
U REF   5
COND.   1

NORTH ⬆

500'   250'   0'   500'   1000'

FULL-SCALE FEET

(b) MODEL REFERENCE WIND VELOCITY, $U_{m_{ref}}$ = 5 fps

Figure 35   FAR-FIELD TEMPERATURE RISE ABOVE AMBIENT, ΔT_f, FULL SCALE °F
STANDARD STACK, 90 deg WIND

RUN 33
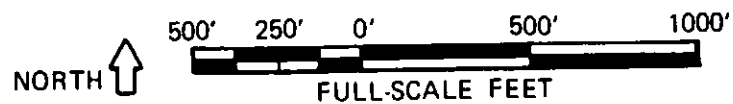WIND 90 DEGREES
U REF 7
COND. 1

NORTH ⇧   500'   250'   0'   1000'

FULL-SCALE FEET

+ 0.3

(c) MODEL REFERENCE WIND VELOCITY, $U_{m_{ref}}$ = 7 fps

Figure 35   FAR-FIELD TEMPERATURE RISE ABOVE AMBIENT, ΔT_f, FULL-SCALE °F
STANDARD STACK, 90 deg WIND

NORTH ⇧

500'   250'   0'   500'   1000'

FULL-SCALE FEET

⊙ EXHAUST
   STACK

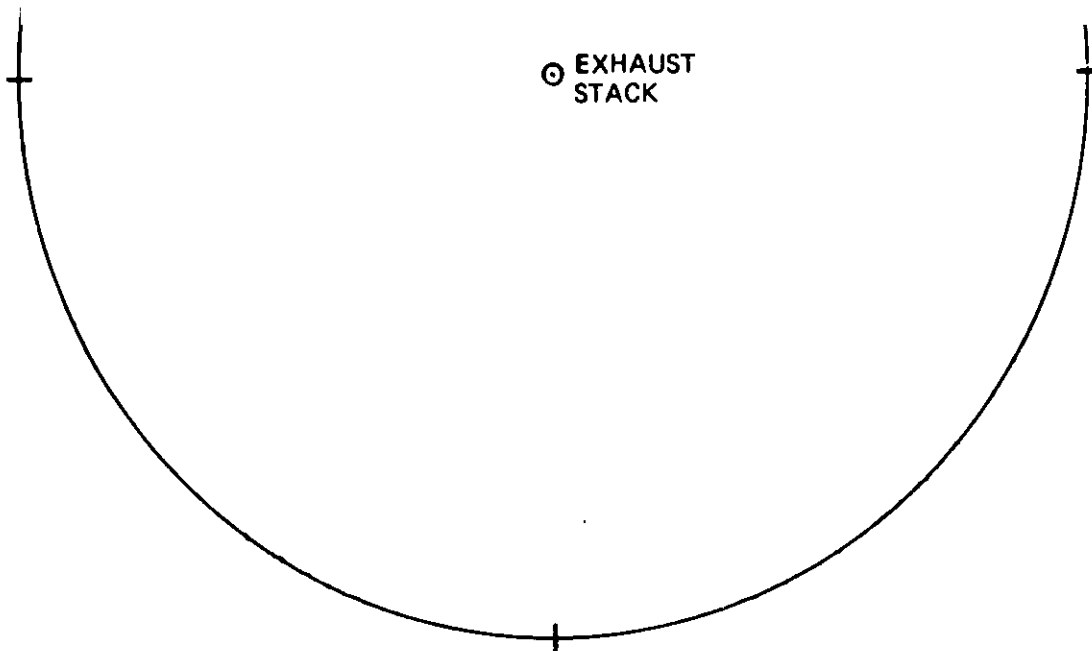(a) MODEL REFERENCE WIND VELOCITY, $U_{m_{ref}}$ = 3 fps

Figure 36   FAR-FIELD TEMPERATURE RISE ABOVE AMBIENT, ΔT_f, FULL-SCALE °F
STANDARD STACK, 180 deg WIND

130

RUN 51
WIND 180 DEGREES
U REF 5
COND. 1

NORTH ⇧

500' 250' 0' 500' 1000'

FULL-SCALE FEET

(b) MODEL REFERENCE WIND VELOCITY, $U_{m_{ref}}$ = 5 fps

Figure 36   FAR-FIELD TEMPERATURE RISE ABOVE AMBIENT, ΔT_f, FULL-SCALE ^{o}F
STANDARD STACK, 180 deg WIND

131

(c) MODEL REFERENCE WIND VELOCITY, $U_{m_{ref}}$ = 7 fps

Figure 36 FAR-FIELD TEMPERATURE RISE ABOVE AMBIENT, ΔT_f, FULL-SCALE °F STANDARD STACK, 180 deg WIND

RUN 73
WIND 270 DEGREES
U REF 3
COND. I

NORTH ⇧

500'   250'   0'   500'   1000'
FULL-SCALE FEET
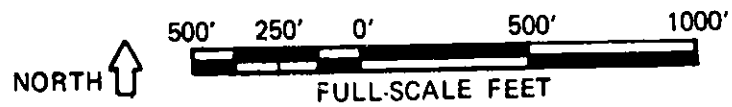
(a) MODEL REFERENCE WIND VELOCITY, U$_{m_{ref}}$ = 3 fps

Figure 37   FAR-FIELD TEMPERATURE RISE ABOVE AMBIENT, ΔT_f, FULL-SCALE °F
STANDARD STACK, 270 deg WIND

133

RUN 74
WIND 270 DEGREES
U REF 5
COND. 1

NORTH ⬆

500'   250'   0'   500'   1000'
FULL-SCALE FEET

(b) MODEL REFERENCE WIND VELOCITY, $U_{m_{ref}}$ = 5 fps

Figure 3/ FAR-FIELD TEMPERATURE RISE ABOVE AMBIENT, ΔT_f, FULL-SCALE °F
STANDARD STACK, 270 deg WIND

RUN 75
WIND 270 DEGREES
U REF 7
COND. 1

NORTH ⇧

500' 250' 0' 500' 1000'
FULL-SCALE FEET

(c) MODEL REFERENCE WIND VELOCITY, $U_{m_{ref}}$ = 7 fps

Figure 37   FAR-FIELD TEMPERATURE RISE ABOVE AMBIENT, ΔT_f, FULL-SCALE °F
STANDARD STACK, 270 deg WIND

135

STANDARD STACK
MODEL REFERENCE

SAMPLING POINT NO.		LOCATION (SEE FIGURE 8)
◯	1	CRF INLET
⊔	2	CRF INSIDE
◁	3	CRF RODF WEST
◇	5	CRF RDOF EAST
◇	6	BUILDING 62
●	14(b)	WHIRL TOWER WEST
◤	15(b)	WHIRL TOWER EAST

TEMPERATURE RISE ABOVE AMBIENT, ΔT, FULL SCALE °F

180   210   240   270   300   330

WIND DIRECTION, θ, degrees

Figure 38   FULL-SCALE TEMPERATURE VARIATION WITH WIND DIRECTION FOR CONSTANT WIND VELOCITY

TEMPERATURE RISE ABOVE AMBIENT, ΔT_f, FULL-SCALE °F

MODEL REFERENCE WIND VELOCITY, $U_{m_{ref}}$, fps

Figure 39   FULL-SCALE TEMPERATURE VARIATION WITH WIND VELOCITY IN CRF
INLET AND ON CRF ROOF FOR 30 deg WIND

TEMPERATURE RISE ABOVE
AMBIENT, ΔT_f, FULL-SCALE $^\circ$F

MODEL REFERENCE WIND VELOCITY, $U_{m_{ref}}$

Figure 40   FULL SCALE TEMPERATURE VARIATION WITH WIND VELOCITY
            NEAR BASE OF WHIRL TOWER FOR 180 deg WIND

MODEL REFERENCE WIND VELOCITY, $U_{m_{ref}}$

Figure 41   FULL SCALE TEMPERATURE VARIATION WITH WIND VELOCITY AT
            VENTILATION INTAKES NORTH OF CRF FOR 150 deg WIND

REFERENCES

1. McVehil, G.E., Ludwig, G.R. and Sundaram, T.R. "On the Feasibility of Modeling Small Scale Atmospheric Motions" Calspan Report No. ZB-2328-P-1 April 1967

2. Ludwig, G.R. and Sundaram, T.R. "On the Laboratory Simulation of Small-Scale Atmospheric Turbulence" Calspan Report No. VC-2740-S-1 December 1969

3. Ludwig, G.R., Sundaram, T.R. and Skinner, G.T. "Laboratory Modeling of the Atmospheric Surface Layer with Emphasis on Diffusion" Calspan Report No. VC-2740-S-2 July 1971

4. Sundaram, T.R., Ludwig, G.R. and Skinner, G.T. "Modeling of the Turbulence Structure of the Atmospheric Surface Layer" _AIAA Journal_ Vol. 10 No. 6 June 1972 (Originally presented as AIAA Paper No. 71-136 at the AIAA Aerospace Sciences Meeting, New York City, January 1971)

5. Ludwig, G.R. and Skinner, G.T. "Wind Tunnel Modeling Study of the Dispersion of Sulfur Dioxide in Southern Allegheny County, Pennsylvania" Environmental Protection Agency Report No. EPA 903/9-75-019 December 1976

6. Lumley, J.L. and Panofsky, H.A. _The Structure of Atmospheric Turbulence_ Interscience (John Wiley and Sons) New York pp. 42-43

7. Tomback, I.H. "An Evaluation of the Heat-Pulse Anemometer for Velocity Measurement in Inhomogeneous Turbulent Flow" _Rev. Sci. Instr._ Vol. 44 No. 2 pp. 141 February 1973